

**SYNTHESIS OF CHIRAL  
BIS(AMIDATE)BIS(AMIDO) TITANIUM AND ZIRCONIUM COMPLEXES  
FOR CATALYZED ASYMMETRIC ALKENE HYDROAMINATION**

by

MARK CHRISTOPHER WOOD

B. Sc. University of Victoria, 2003

A THESIS SUBMITTED IN PARTIAL FULFILLMENT OF  
THE REQUIREMENTS FOR THE DEGREE OF

MASTER OF SCIENCE

in

The Faculty of Graduate Studies

(Chemistry)

THE UNIVERSITY OF BRITISH COLUMBIA

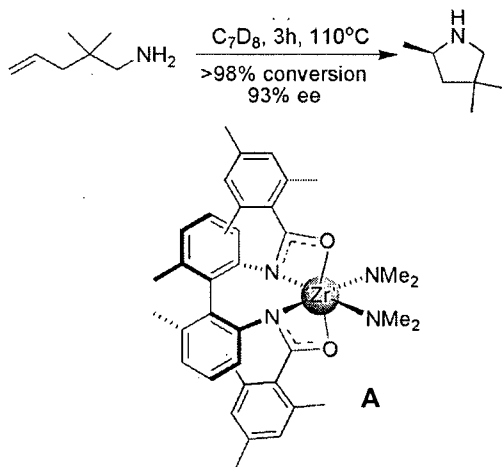
December 2006

© Mark Christopher Wood, 2006

## Abstract

---

Recent advances in transition metal and lanthanide catalyzed hydroamination have changed the way people think about the formation of C-N bonds. As a major contribution to this area of research, we have synthesized the first neutral group 4 precatalysts capable of enantioselective alkene hydroamination. We took advantage of a modular amidate ligand set to alter both the electronic and steric properties of the precatalysts. The amidate ligands employed in these catalysts were synthesized by reacting an axially chiral 2,2'-diamino-6,6'-dimethylbiphenyl diamine with a corresponding acyl chloride or anhydride. Further reaction of the chiral amide proligand with  $\text{Ti}(\text{NMe}_2)_4$  or  $\text{Zr}(\text{NMe}_2)_4$ , produced the bis(amidate)bis(amido) titanium and zirconium precatalysts in quantitative yields.



Enantioselectivity and reactivity investigations for aminoalkene hydroamination were conducted on the group 4 complexes prepared, and complex **A** produced the most excellent enantioselectivities. From this investigation, minor alterations to the electronic and steric properties of the ligand showed significant effects on reactivity and enantioselectivity. Further substrate scope investigations, using precatalyst **A**, displayed

high yields, moderate reaction times and enantioselectivities up to 93 % ee. Most importantly, the structural and substrate scope investigation provided a mechanistic rationale for observed trends in reactivity and enantioselectivity, yielding valuable insight for future catalyst development.

## Table of Contents

---

Abstract.....	ii
List of Tables.....	v
List of Figures.....	vi
List of Abbreviations and Symbols.....	ix
List of Compounds.....	xi
Acknowledgments and Dedication .....	xiv
CHAPTER 1 Introduction.....	1
1.1 Hydroamination.....	1
1.2 Amidate Complexes of Early Transition Metals.....	9
CHAPTER 2 Synthesis of Axially Chiral Group 4 Amidate Complexes as Hydroamination Precatalysts.....	12
2.1 Introduction.....	12
2.2 Synthesis of 6,6'-dimethylbiphenyl-2,2'-diamine and Amidate Proligands.....	15
2.3 Synthesis of Chiral Bis(amido)bis(amidate) Titanium(IV) and Zirconium(IV) Complexes.....	18
2.4 Summary and Conclusions.....	28
2.5 Experimental.....	29
CHAPTER 3 Asymmetric Aminoalkene Hydroamination Using Neutral Chiral Zirconium and Titanium Bis(amidate)Bis(amido) Precatalysts.....	36
3.1 Introduction.....	36
3.2 Precatalyst Reactivity.....	37
3.3 Asymmetric Hydroamination.....	43
3.4 Mechanistic Rationale.....	48
3.5 Substrate Scope Investigations.....	55
3.6 <i>In-situ</i> Hydroamination Reactions.....	63
3.7 Summary and Conclusions.....	65
3.8 Experimental.....	66
CHAPTER 4 Summary and Future Directions.....	73
4.1 Future Directions.....	73
4.1.1 Proposed Modification to Precatalysts (-)- <b>13b</b> and (+)- <b>13c</b> to enhance enantioselectivity and reactivity.....	73

4.12	Synthesis of a Chiral aniline; Progress Towards a Chiral Bidentate Amidate Ligand for Asymmetric Hydroamination.....	78
4.2	Summary and Conclusions.....	88
4.3	Experimental.....	91
BIBLIOGRAPHY.....		95
APPENDICES.....		99
Appendix I	Variable Temperature $^1\text{H}$ NMR Spectroscopic Analysis of Complex (-)- <b>13a</b> .....	99
Appendix II	DOSY NMR spectroscopy for complex (-)- <b>13a</b> .....	102
Appendix III	DOSY NMR spectroscopy for proligand (-)- <b>10</b> .....	103
Appendix IV	$^1\text{H}$ NMR and $^{13}\text{C}$ NMR spectra for complex (+)- <b>13c</b> .....	106
Appendix V	X-ray crystallographic data for complex (+)- <b>13c</b> .....	108

## List of Tables

---

<b>Table 2.1</b>	Synthesis of bis(amidate)bis(amido)titanium and zirconium precatalysts.....	18
<b>Table 3.1</b>	Investigation of reactivity for alkene hydroamination.....	38
<b>Table 3.2</b>	Investigation of enantioselectivity for alkene hydroamination.....	43
<b>Table 3.3</b>	Aminoalkene substrate scope investigations with precatalysts (-)- <b>13b</b> and (+)- <b>13c</b> .....	46
<b>Table 3.4</b>	Aminoalkene substrate scope investigations with precatalysts (-)- <b>13b</b> and (+)- <b>13c</b> .....	55
<b>Table 3.5</b>	Substrates that are Unreactive toward hydroamination.....	58
<b>Table 3.6</b>	Effects of tethered <i>gem</i> -dialkyl substituents on reactivity and enantioselectivity.....	61
<b>Table 3.7</b>	<i>In-situ</i> hydroamination reactions.....	63
<b>Table 3.8</b>	<sup>1</sup> H and <sup>19</sup> F NMR resonances for Mosher amide derivatives of pyrrolidine and piperidine products .....	71
<b>Table A-1.</b>	Crystal data and structure refinement for dimethylamine adduct of (+)- <b>13c</b> .....	108
<b>Table A-2</b>	Atomic coordinates (x 10 <sup>4</sup> ) and equivalent isotropic displacement parameters (Å <sup>2</sup> x 10 <sup>3</sup> ) for (+)- <b>13c</b> .....	109
<b>Table A-3</b>	Selected bond lengths and bond angles for (+)- <b>13c</b> .....	110
<b>Table A-4</b>	Anisotropic displacement parameters (Å <sup>2</sup> x 10 <sup>3</sup> ) for (+)- <b>13c</b> .....	113

## List of Figures

---

<b>Figure 1.1</b>	Hydroamination products as a result of alkyne, allene and alkene hydroamination.....	1
<b>Figure 1.2</b>	Examples of <i>N</i> -heterocyclic natural products isolated from various plant and insect species.....	3
<b>Figure 1.3</b>	Mechanism proposed by Bergman and coworkers for alkyne hydroamination catalyzed by zirconocene bisamides .....	5
<b>Figure 1.4</b>	Neutral titanium complexes for aminoalkene hydroamination by employed by Doye and coworkers.....	7
<b>Figure 1.5</b>	Amidate complexes that have displayed reactivity toward allene, alkyne and alkene hydroamination.....	9
<b>Figure 2.1</b>	Precatalyst progression from the non-tether complexes <b>3</b> and <b>4</b> to a $C_2$ symmetric non-racemic tethered complex.....	13
<b>Figure 2.2</b>	Possible geometric isomers for monomeric tethered and non-tethered 6-coordinate bis(amidate)bis(amide) titanium or zirconium complexes.....	13
<b>Figure 2.3</b>	Investigation into the racemization of proligand (+)- <b>10</b> under conditions used for hydroamination in Chapter 3.....	17
<b>Figure 2.4</b>	Two views of an ORTEP diagram for the dimethylamine adduct of (+)- <b>13c</b> .....	21
<b>Figure 2.5</b>	Bis(sulfonamide) zirconium complex reported by Bergman <i>et al.</i> .....	22
<b>Figure 2.6</b>	$^1\text{H}$ NMR spectra of complex (-)- <b>14</b> .....	25
<b>Figure 2.7</b>	Comparison of $^1\text{H}$ NMR spectra for titanium (-)- <b>15a</b> and (+)- <b>16a</b> vs. the zirconium analogues (-)- <b>15b</b> and (+)- <b>16b</b> .....	26
<b>Figure 3.1</b>	Summary of the titanium and zirconium precatalysts screened for alkene hydroamination catalysis.....	37
<b>Figure 3.2</b>	GC-MS analysis of products obtained from the stoichiometric reaction of <b>17b</b> with precatalyst (-)- <b>14</b> .....	40
<b>Figure 3.3</b>	$^1\text{H}$ NMR spectrum for Mosher amide derivatives of the (S)- and (R)-pyrrolidine products ( <b>18</b> ). .....	44

<b>Figure 3.4</b>	Proposed catalytic cycle for bis(amidate)bis(amido) group 4 metal catalyzed hydroamination of <i>gem</i> -disubstituted aminoalkenes.....	48
<b>Figure 3.5</b>	Plot of ln[substrate <b>17</b> ] vs time for hydroamination of <b>17</b> at 140 °C in <i>d</i> <sub>8</sub> -toluene using precatalyst (+)- <b>13c</b> .....	50
<b>Figure 3.6</b>	Plot of <i>k</i> <sub>obs</sub> vs [(+)- <b>13c</b> ] for hydroamination of <b>17</b> .....	51
<b>Figure 3.7</b>	Plot of ln[substrate <b>17</b> ] vs time for hydroamination of <b>17</b> at 110 °C in <i>d</i> <sub>8</sub> -toluene using precatalyst (+)- <b>13c</b> .....	51
<b>Figure 3.8</b>	Illustration that is representative of the X-ray solid state structure for an imido complex recently prepared by our group.....	53
<b>Figure 3.9:</b>	Proposed mechanism for enantioselectivity of aminoalkene <b>17</b> using precatalyst (+)- <b>13c</b> .....	54
<b>Figure 3.10</b>	Proposed mechanism for enantioselectivity of aminoalkene <b>23</b> using precatalyst (+)- <b>13c</b> .....	57
<b>Figure 3.11</b>	Proposed mechanism for enantioselectivity of aminoalkene <b>24</b> using precatalyst (-)- <b>13b</b> .....	57
<b>Figure 3.12</b>	<i>Gem</i> -disubstituent effect.....	59
<b>Figure 3.13</b>	Example of the relative reaction rates for <i>gem</i> -disubstituted 4-bromoalkylamines versus unsubstituted 4-bromoalkylamine.....	60
<b>Figure 3.14</b>	The effect different size tethered <i>gem</i> -dialkyl ring systems have on the rate of aminoalkene hydroamination.....	62
<b>Figure 4.1</b>	Suggested modifications to proligand <b>12</b> to enhance reactivity and/or enantioselectivity.....	74
<b>Figure 4.2</b>	Retrosynthetic approach to the synthesis of the 2,4,6-triisopropylphenyl analog of proligand <b>12</b> .....	75
<b>Figure 4.3</b>	Proposed synthesis of an ortho substituted biphenyl diamine proligand precursor.....	75
<b>Figure 4.4</b>	Proposed modifications to proligand <b>10</b> to alter the electronic properties of the biphenyl diamine backbone.....	76

<b>Figure 4.5</b>	A) Side view of precatalyst <b>3</b> <sup>2</sup> , and B) Proposed incorporation of the 2,6-substituted chiral aniline in precatalyst <b>3</b> .....	78
<b>Figure 4.6</b>	Application of chiral aniline <b>37</b> incorporated into $\alpha$ -diimine nickel catalyst for isoselective 2-butene polymerization.....	79
<b>Figure 4.7</b>	GC-MS analysis of the reaction mixture in the synthesis of compound <b>38</b> .....	80
<b>Figure 4.8</b>	GC-MS chromatograph for compound <b>38</b> .....	83
<b>Figure 4.9</b>	GC-MS chromatograph for the hydrogenation products of compound <b>43</b> .....	86
<b>Figure A-1</b>	Variable temperature <sup>1</sup> H NMR of complex (-)- <b>13c</b> .....	100



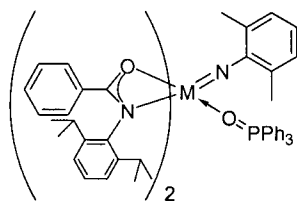
## List of Abbreviations and Symbols

---

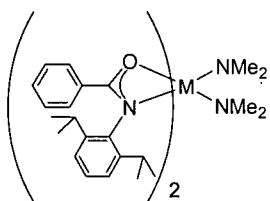
Å	angstrom
Ac	acetyl
<i>ansa</i>	latin for 'handle'
APT	attached proton test (NMR)
Ar	aryl
atm	atmosphere
br	broad (NMR)
Bu	butyl
Calcd.	calculated
cat.	catalyst
cm	centimeter
Cp	cyclopentadienyl
d	doublet (NMR)
δ	delta (NMR chemical shift)
dd	doublet of doublets (NMR)
DMAP	4-( <i>N,N</i> -dimethylamino)pyridine
DMF	<i>N,N</i> -dimethylformamide
D	Diffusion coefficient (m <sup>2</sup> /s)
d <sub>x</sub>	deuterated solvent (x = number of deuterium atoms)
EA	elemental analysis
ee	enantiomeric excess
EI	electron ionization / electron impact (MS)
equiv.	equivalents
ESI	electrospray ionization
Et	ethyl
EtOAc	ethyl acetate
g	gram
GC	gas chromatography
<i>gem</i>	geminal
h	hour
HPLC	high pressure / high performance liquid chromatography
HR	high resolution
Hz	hertz
I.D.	inner diameter
iPr	isopropyl
IR	infrared
J	coupling constant (NMR)
K	degrees Kelvin
kJ	kilojoule
k <sub>obs</sub>	observed rate constant
L	liter

LAH	lithium aluminum hydride
LDA	lithium diisopropylamide
<i>m</i>	meta
M	molar or metal
m	multiplet (NMR)
<i>m/z</i>	mass / charge ratio
M <sup>+</sup>	molecular ion
Me	methyl
mg	milligram
MHz	megahertz
min	minute
mL	milliliter
MMAO	modified methylaminoxane
mmol	millimole
mol	mole
Mosher's acid chloride	( <i>S</i> )-(+)- $\alpha$ -methoxy- $\alpha$ -(trifluoromethyl)phenylacetyl chloride
MS	mass spectrometry
nm	nanometers
NMR	nuclear magnetic resonance
NR	No Reaction
°	degree
°C	degrees Celsius
ORTEP	Oak Ridge Thermal Ellipsoid Plot
<i>p</i>	para
Pd-C	palladium on activated carbon
Ph	phenyl
ppm	parts per million
q	quartet (NMR)
r.t.	room temperature
rac	racemic
SMB	simulated moving bed
t	time or triplet (NMR)
<i>t</i> <sub>1/2</sub>	half life
<i>tert</i>	tertiary
TFAA	trifluoroacetic anhydride
THF	tetrahydrofuran
TPPO	triphenylphosphine oxide
VT	variable temperature (NMR)
wt	weight (mass)
$\alpha$	alpha (specific rotation / $\alpha$ -carbon)
$\theta$	Theta (angle in degrees)
$\kappa$	kappa

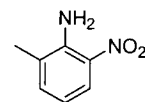
# List of Compounds



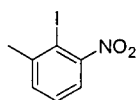
1, M = Ti  
2, M = Zr



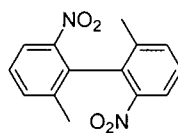
3, M = Ti  
4, M = Zr



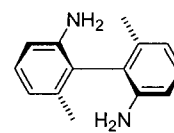
5



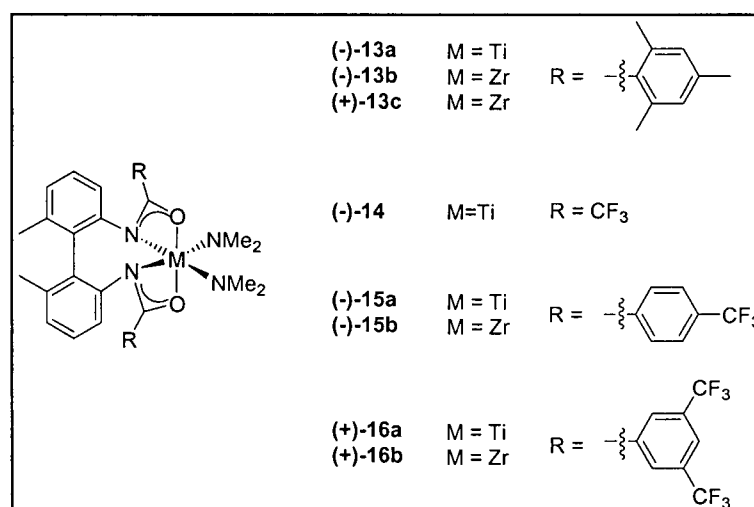
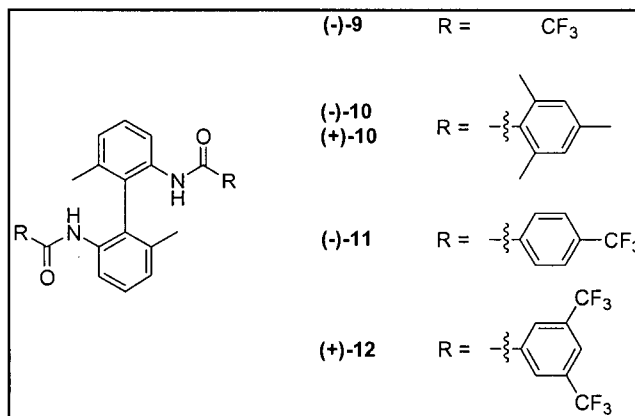
6

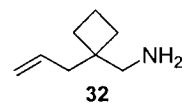
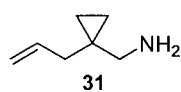
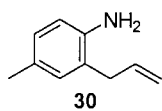
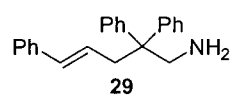
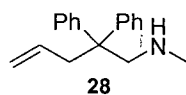
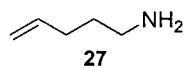
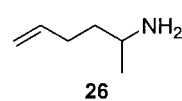
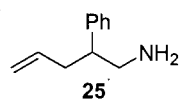
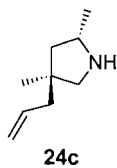
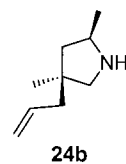
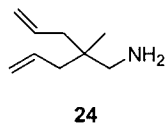
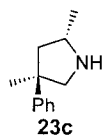
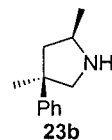
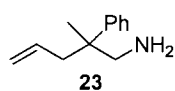
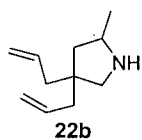
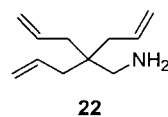
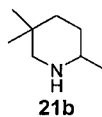
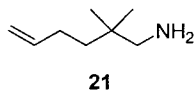
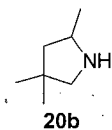
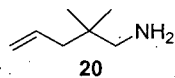
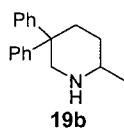
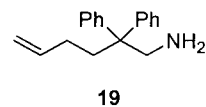
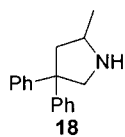
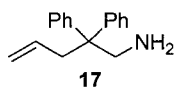
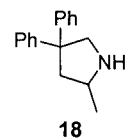
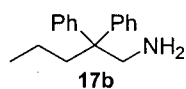
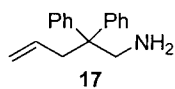


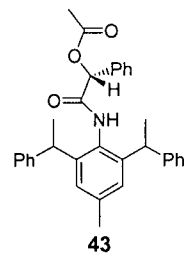
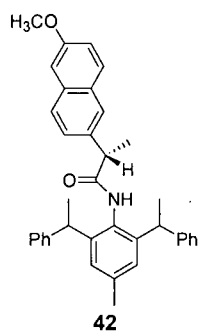
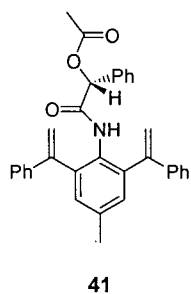
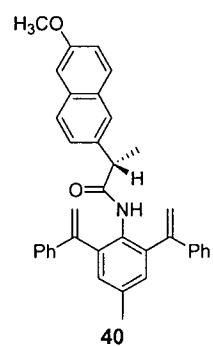
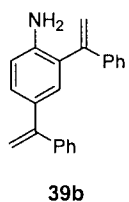
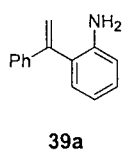
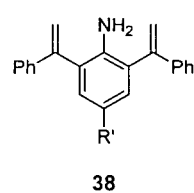
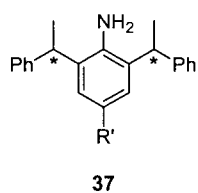
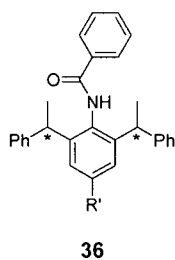
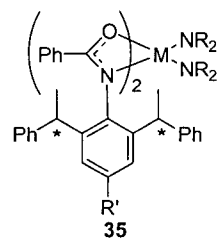
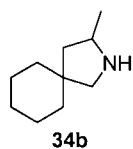
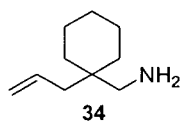
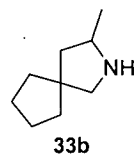
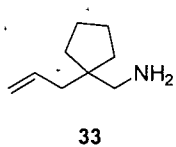
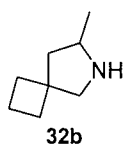
7



8







## Acknowledgments and Dedication

---

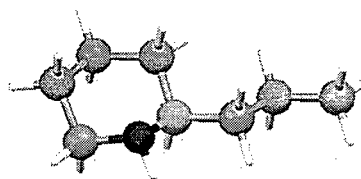
I would like to thank Professor Laurel L. Schafer for her support and guidance throughout the progress of my Masters thesis. I am indebted to my many student colleagues for providing a stimulating and fun environment in which to learn and grow. I am especially grateful to Louisa Stanlake, Alison Lee, Robert Thomson, Jason Bexrud, David Leitch, Rashidat Ayinla, Charles Yeung, Jennifer Kozak, Scott Lawson, Courtney Turner and Neal Yonson. Robert Thomson and David Leitch were particularly helpful in processing and solving X-ray crystallographic data. I would also like to thank David Leitch and Jason Bexrud for the synthesis of a number of aminoalkene substrates used throughout this thesis.

I would also like to give my thanks to Prof. Marco Ciufolini and Prof. Glenn Sammis for taking time out of there busy days to sit in as my defense committee. I would also like to thank the UBC support staff especially Minaz and Marshall from the analytical services department, Maria and Zorana from the NMR facility, and Brian Patrick from the X-ray crystallography laboratory.

I wish to thank my parents, Gary and Janis Wood. They bore me, raised me, supported me, taught me and loved me. I wish to thank my entire extended family including my brothers and grandparents who were particularly supportive. I would also like to thank Kathleen's parents who accepted me into their family earlier this year.

Lastly, and most importantly, I would like to thank my wife Kathleen for her love, support and for putting up with me throughout my undergraduate and graduate studies. Without her I would not have been able to get through this. To her I dedicate this thesis.

# Chapter 1



## Introduction

### 1.1 Hydroamination

Hydroamination is an atom-economical process in which N-H is formally added across a carbon-carbon multiple bond resulting in the formation of a new C-N bond. As an alternative to classical methods, hydroamination is a synthetically appealing and efficient route for the preparation amines, imines, enamines and *N*-heterocyclic compounds from readily accessible starting materials (Figure 1.1).

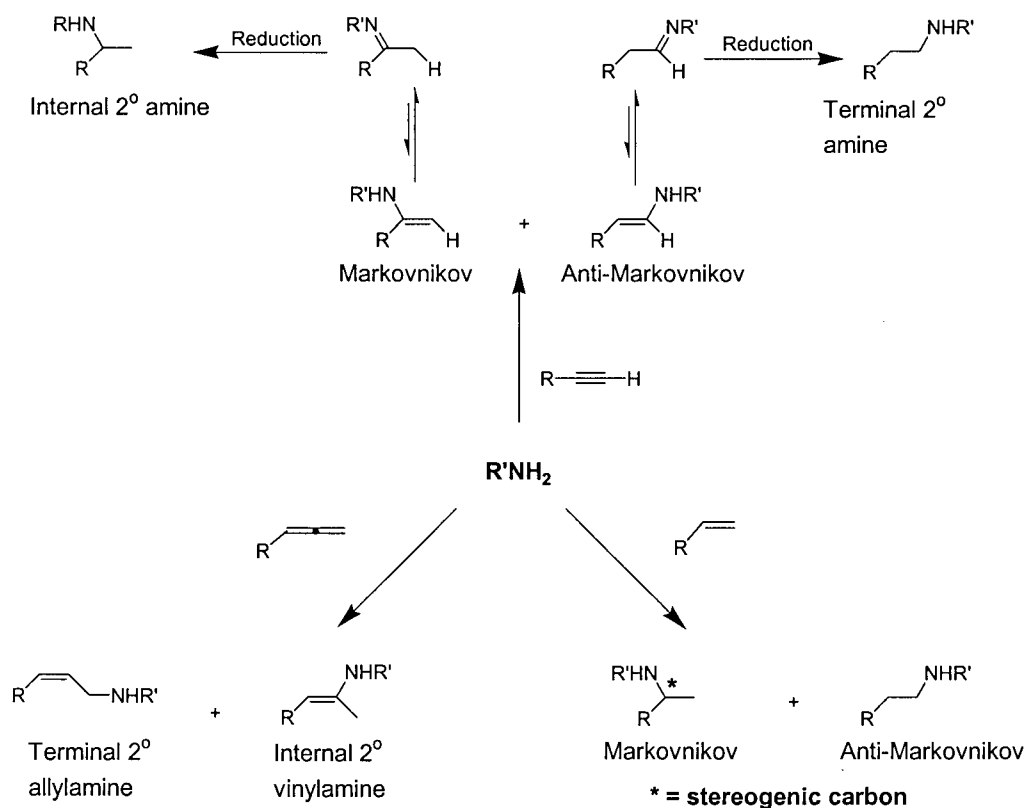


Figure 1.1 Hydroamination products as a result of alkyne, allene and alkene hydroamination

In considering the thermodynamics of the reaction, hydroamination is both exergonic and exothermic under standard conditions.<sup>1</sup> However, hydroamination is hindered by two factors: first, there is an electrostatic repulsion between the lone pair of electrons on the nitrogen and the electron rich C-C  $\pi$ -bonds. Secondly, for intermolecular hydroamination, there is negative entropy of reaction that results in the equilibrium shifting to the reactants at higher temperatures. Unfortunately, higher temperatures are required to overcome the high energy barrier, and hence, non-catalyzed hydroamination reactions proceed in only a few select circumstances.<sup>2</sup> Since intermolecular hydroamination is not entropically favored, there are many examples of intramolecular hydroamination, particularly for alkene hydroamination. These substrates are used as models to probe catalyst reactivity in the development of more general catalysts for intermolecular transformations which.

Hydroamination has attracted significant attention over the past decade and a great deal of progress has been made.<sup>1,3-7</sup> Numerous advances for alkyne and allene hydroamination include lanthanide<sup>8-12</sup>, early<sup>13-15</sup> and late<sup>16</sup> transition metal catalysts, however, the search for a general alkene hydroamination catalyst is still ongoing. The advantage of alkene hydroamination is that the addition of an amine to an alkene results in the direct formation of a more functionalized amine (Figure 1.1). Though alkene hydroamination is approximately thermoneutral, calculations by Eisen and coworkers illustrated that alkyne hydroamination is more favorable than alkene hydroamination.<sup>5b</sup> They estimated that the addition of ammonia to acetylene was 63 kJ/mol more exothermic than the addition of ammonia to ethylene. The greater precedence of alkyne versus alkene hydroamination catalysts is in accord with these calculations.

To date, lanthanide and group 3 catalysts have shown the greatest promise for inter- and intramolecular hydroamination of alkenes. Cyclopentadienyl based complexes of lanthanides and group 3 metals for intramolecular hydroamination of aminoalkenes was pioneered by Marks and coworkers in the early 1990's.<sup>5a,6</sup> More recently, non-cyclopentadienyl catalysts have been investigated and show similar efficacy.<sup>17</sup> Our group has also shown that cationic  $\beta$ -diketaminato scandium complexes are active aminoalkene hydroamination catalysts.<sup>18-24</sup> Unfortunately, the lanthanide and group 3 catalysts are unattractive from an industrial point of view, due to their limited functional group



tolerance and increased sensitivity to moisture. Late transition metal catalysts have also been employed for alkene hydroamination.<sup>25</sup> Although late transition metal catalysts show moderate reactivity and functional group tolerance, they have been limited to only activated alkene substrates. Furthermore, recent contributions suggest that many of these transformations likely proceed via an *in-situ* generated proton.<sup>5,6,26-37</sup> Consequently, asymmetric versions of these reactions will be challenging to optimize.

Asymmetric synthesis has been a topic of interest that has escalated over the past two decades, and is now the focus of many research groups around the world. Chiral compounds are very important in both the academic world as well as in industry. The focus of this thesis will be the synthesis of  $\alpha$ -chiral *N*-heterocyclic compounds through asymmetric hydroamination. A few examples of naturally occurring *N*-heterocyclic compounds are illustrated in Figure 1.2.

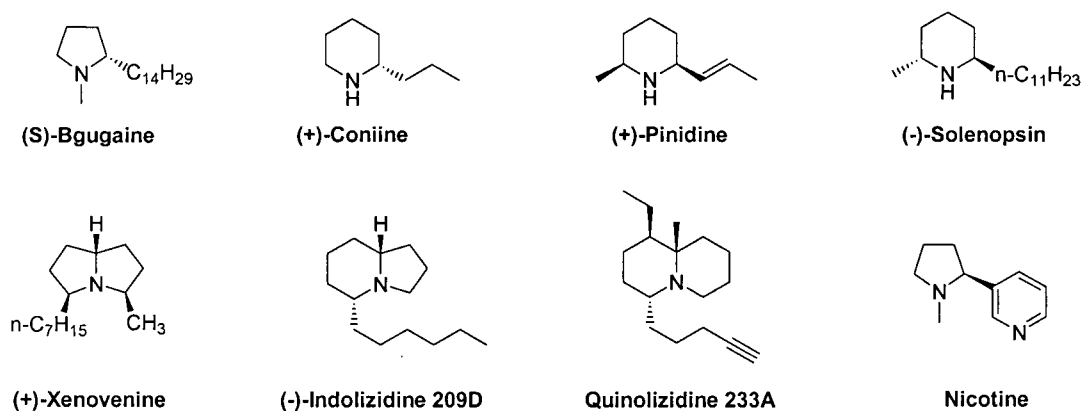


**Figure 1.2** Examples of *N*-heterocyclic natural products isolated from various plant and insect species.

Before the extensive exploration into catalytic asymmetric synthesis, researchers had to rely on enantiomerically pure starting materials or chiral auxiliaries to introduce chirality. This limited the scope of asymmetric synthesis, and therefore research into catalytic methods marked the beginning of a new area in synthetic chemistry. One of the major challenges in asymmetric catalysis has been enantioselective hydroamination. Increasing research efforts over the past 2 decades have led to a number of catalysts capable of this transformation.<sup>29,38</sup> Although many efforts have arisen from group 3 and lanthanide metal catalysts, enantioselectivities exceeding 90 % have been rarely reported.

The first asymmetric hydroamination catalysts were C<sub>1</sub> symmetric organolanthanide *ansa*-metallocene cyclopentadienyl complexes developed in the early 1990's by Marks and coworkers.<sup>12</sup> These precatalysts produced enantiomeric excesses (ee's) upwards of 74 % for intramolecular hydroamination of 2,2-dimethyl-1-aminopent-4-ene. These moderate enantioselectivities were limited to pyrrolidine  $\alpha$ -methyl *N*-heterocycles, and attempts at asymmetric  $\alpha$ -methyl piperidine synthesis resulted in low ee's ranging from 15 – 17 %. Recent modifications to the chiral C<sub>1</sub> organolanthanide catalysts by incorporating an electron donating octahydrofluorenyl group have exhibited greater activity in the formation of 6-membered cyclohydroamination products (ee's up to 67 %).<sup>5</sup> In recent years non-cyclopentadienyl based catalysts have become more prominent in the literature. These non-cyclopentadienyl type catalysts have been getting more attention in recent years due to the instability of the metallocene cyclopentadienyl complexes in the presence of protic amines.<sup>39</sup> Epimerization of these catalysts to one preferred enantiomer lowered enantioselectivity and reduced the possibility of obtaining both enantiomeric products from each isomer of the catalyst. To solve this problem, Marks and coworker have reported chiral bis(oxazoline) complexes which show similar enantioselectivities to the metallocene cyclopentadienyl complexes prepared previously, but without the problem of catalyst epimerization.<sup>40,41</sup>

Non-cyclopentadienyl complexes reported by Hultsch and coworkers have shown some of the highest enantioselectivities for alkene hydroamination reported to date. Early reports included axially chiral biphenolate and binaphtholate rare earth metal complexes produces ee's up to 83 % for the cyclohydroamination of 1-aminopent-4-ene.<sup>32</sup> In a recent report, increasing the steric bulk at the 3 and 3' positions of the binaphtholate ligands has now produced ee's upward of 95 % for the hydroamination of 2,2-diphenylpent-4-ene-1-amine.<sup>42</sup> This is the highest ee reported to date for intramolecular alkene hydroamination. These catalysts were also capable of intermolecular hydroamination with activated alkenes, but unfortunately, the anti-Markovnikov product was obtained (ie. no  $\alpha$ -chiral amine produced). Livinghouse and coworkers have contributed an axially chiral bis(thiolato) complex of yttrium(III) for aminoalkene hydroamination. This catalyst was prepared *in-situ*, and produced ee's up to

89 % with high conversions.<sup>43</sup> Scott and coworkers also showed enantioselectivities up to 61% for axially chiral Schiff-base complexes of lanthanum(III) and yttrium(III).<sup>44</sup>

Group 4 catalysts have several advantages over many of the lanthanoid and late transition metals. First, titanium is the second most abundant metal (ninth most abundant element) in the earth's crust<sup>2</sup> and is inexpensive compared to many of the late transition metals, thus greater catalyst loadings are not as significant in terms of cost. Secondly, upon hydrolysis of the complexes, the  $\text{TiO}_2$  and  $\text{ZrO}_2$  byproducts are non toxic and insoluble, thus they can easily be removed from reaction products by filtration.

The earliest reports of group 4 hydroamination are from Bergman<sup>45</sup> and Livinghouse.<sup>2</sup> In 1992 Bergman and coworkers reported the addition of 2,6-dimethylaniline to alkynes and allenes catalyzed by  $\text{Cp}_2\text{Zr}(\text{NHR})_2$ . Also in 1992, Livinghouse reported a titanium cyclopentadienyl complex,  $[\text{CpTiCl}_3]$ , for intramolecular hydroamination of aminoalkynes. The most thorough investigations of group 4 catalysts have been from groups such as Bergman,<sup>45</sup> Livinghouse,<sup>46-48</sup> and Doye,<sup>49</sup> where they employed cyclopentadienyl ancillary ligands. Our research group and others<sup>2</sup> have focused on the preparation of non-cyclopentadienyl based ligands for alkyne, allene and alkene hydroamination.

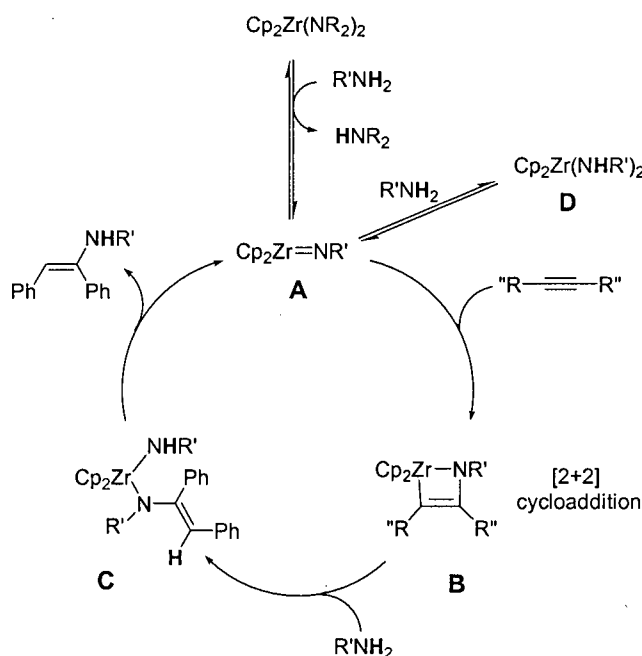
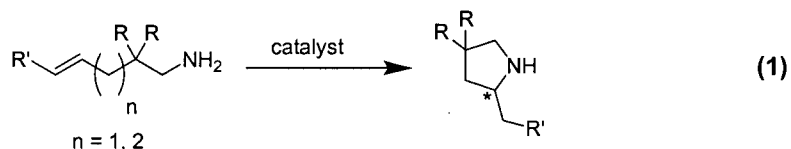


**Figure 1.3** Mechanism proposed by Bergman and coworkers for alkyne hydroamination catalyzed by zirconocene bisamides<sup>2</sup>

The mechanism for group 4 hydroamination was originally proposed by Bergman and coworkers for hydroamination of alkynes catalyzed by zirconocene bis(amido) complexes (Figure 1.3).<sup>47,50-53</sup> The zirconocene bis(amido) undergoes transamination with the amine reactant ( $R'NH_2$ ) to form the zirconocene imido complex **A**. At this point, the alkyne reactant and the amine reactant ( $R'NH_2$ ) will compete for reaction with the imido complex. The imido complex can either undergo a [2+2] cycloaddition with the alkyne to form an azametallocyclobutene intermediate **B** or the amine will react to form a catalytically unproductive  $Cp_2Zr(NHR')_2$  zirconocene bis(amido) **D**. For this cyclopentadienyl complex, the cycloaddition is believed to be the rate limiting step due to this unproductive competitive pathway. Upon formation of the azametallocyclobutene **B**, another equivalent of amine reactant ( $R'NH_2$ ) will undergo a protonolysis reaction with the metallocycle **B** to form the mixed amido species **C**. A proton transfer from the reactant amido ligand to the vinyl amido yields the enamine product and regenerates the imido intermediate. Our group and others have also supported this imido / cycloaddition mechanism for hydroamination of alkynes, allenes and alkenes employing both cyclopentadienyl and non-cyclopentadienyl group 4 catalysts.<sup>53-58</sup>

Until recently, group 4 metal hydroamination catalysts in the literature were limited to the hydroamination of alkynes and allenes. Recent advances have shown that group 4 catalysts are also capable of alkene hydroamination.<sup>59</sup> The first example of group 4 catalyzed alkene hydroamination was reported by Ackermann and co-workers in 2004.<sup>60</sup>  $TiCl_4$  was used to catalyze the reaction between norbornene and a number of aryl functionalized anilines. The method tolerated many functionalized anilines, but unfortunately gave rise to an undesirable *ortho* hydroarylation byproduct. Not long after, Ackermann complimented his earlier results with  $TiCl_4$  catalyzed hydroamination of vinyl arene derivatives with aryl anilines.<sup>61</sup> Recent results by Bergman and coworkers have suggested that these  $TiCl_4$  catalyzed reactions are likely proceeding via a proton formed in situ rather than a metal catalyzed mechanism.<sup>54</sup>



Our group recently reported that commercially available  $\text{Ti}(\text{NEt}_2)_4$  is an efficient catalyst for aminoalkene hydroamination (Equation 1). These intramolecular hydroamination reactions were accomplished with high conversion and isolated yields up to 92 %. This was the first report of a neutral group 4 alkene hydroamination catalyst that was suggested to proceed via an imido based mechanism. Shortly thereafter, Livinghouse and coworkers reported a neutral bis(thiophosphinic amidate) zirconium(IV) hydroamination precatalyst.<sup>56</sup> The bis(thiophosphinic amidate) system has proven successful for a number of intramolecular hydroamination reactions with substrates of the general structure in equation 1. Doye and coworkers have also investigated a variety of previously reported neutral titanium complexes for alkene hydroamination (Figure 1.4).<sup>56</sup> All the complexes in Figure 1.4 displayed reactivity for the cyclization of 2,2-diphenylpent-4-ene-1-amine **19**, however  $\text{Ti}(\text{NMe}_2)_4$  gave the best result.

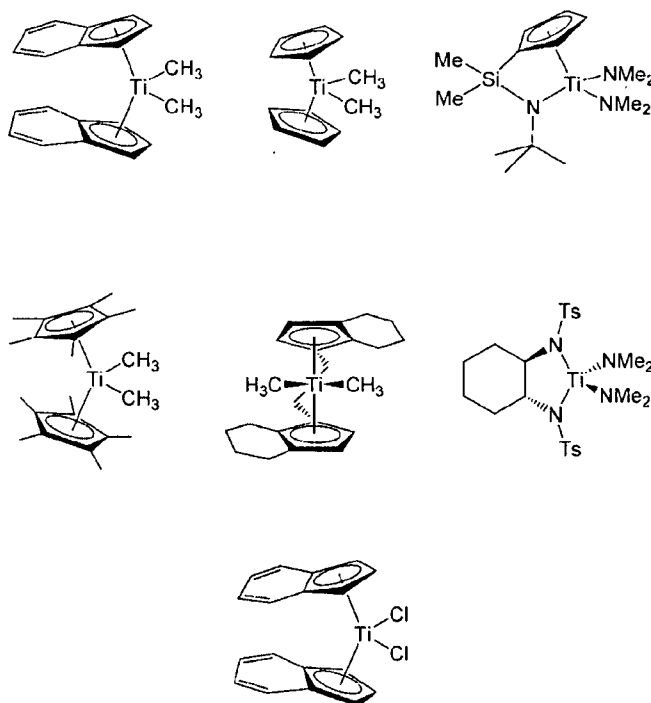


**Figure 1.4** Neutral titanium complexes for aminoalkene hydroamination by employed by Doye and coworkers.<sup>26</sup>

Cationic group 4 catalysts have also been established for group 4 alkene hydroamination. Hultzsich and coworkers reported the first cationic zirconocene and titanocene alkene hydroamination catalysts.<sup>36</sup> These were capable of cyclizing *N*-substituted aminoalkenes with high yield and moderate reaction times. Though these complexes were efficient alkene hydroamination catalysts, cationic zirconocene and titanocene complexes are not capable of primary aminoalkene hydroamination. It is postulated that cationic complexes proceed through alkene insertion into a metal amido bond<sup>2</sup> rather than the imido / cycloaddition mechanism proposed by Bergman.<sup>26,36</sup> When primary amines are employed with these catalysts, it is suggested that the metal amido intermediate formed can undergo  $\alpha$ -proton abstraction to render a catalytically inactive imido complex.<sup>62</sup>

In the Schafer research group, we have become interested in exploiting our modular amidate ligands for group 4 metal catalyzed alkene hydroamination. Section 1.2 will focus on early transition metal amidate complexes employed by our group for alkene hydroamination.

## 1.2 Amidate Complexes of Early Transition Metals

N,O chelating amidate ligands, which are prepared from amide proligands, have rarely been employed in early-transition metal complexes. Arnold and coworkers prepared the first bimetallic titanium amidate complexes that were used as ethylene polymerization catalysts in 2001.<sup>53,57,63-66</sup> Our research group has exploited these amidate ligands for group 4 complexes of titanium, zirconium and hafnium.<sup>65</sup> Amide ligands are easily synthesized from a wide range of commercially available starting materials and are easily modified at both the carbonyl carbon and the nitrogen to alter the electronic and steric properties. The electronic and steric effects of the amidate ligand have displayed significant influences on the reactivity of the resultant complexes toward alkyne hydroamination.<sup>67</sup> Similar to the amidate ligands that we employed in our complexes, guanidates have been reported as ligands for group 4 hydroamination catalysts.<sup>68-70</sup> While amidinate<sup>71</sup>, ureate<sup>72</sup> and carboxylate<sup>65,66,73,74</sup> complexes of titanium have been prepared, to date, none have been employed as hydroamination catalysts.

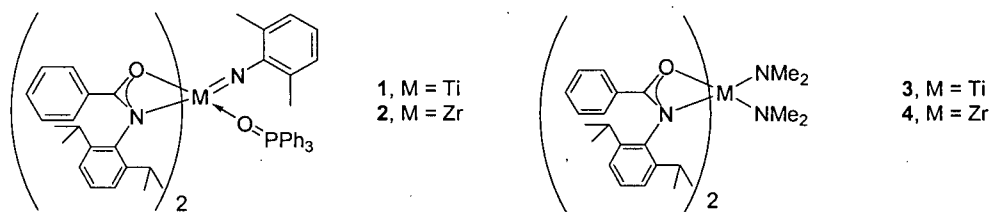


**Figure 1.5:** Amidate complexes that have displayed reactivity toward allene, alkyne and alkene hydroamination

Following our discovery that commercially available  $\text{Ti}(\text{NET}_2)_4$  is an efficient precatalyst for primary aminoalkene hydroamination (Equation 1), we decided to employ our bis(amidate)bis(amido) complexes for aminoalkene hydroamination. Our earlier investigations showed that bis(amidate)bis(amido) titanium complex **3** was an effective precatalyst for the intermolecular hydroamination of alkynes and allenes.<sup>53</sup> Recent experiments have revealed that the hydroamination of aminoalkenes was also possible with these bis(amidate)bis(amido) group 4 precatalysts (Figure 1.5).<sup>65</sup> When 2,2-diphenylpent-4-ene-1-amine **20** was used as the test substrate, titanium complex **3** (Figure

1.5) showed much lower reactivity ( $t_{1/2}$  = 195 min) than the zirconium analog **4** ( $t_{1/2}$  = 75 min). The opposite trend is observed for bis(amidate)bis(amido) complexes for alkyne hydroamination where the titanium complexes have shown higher reactivity.<sup>36</sup> Precatalysts **3** and **4** are not as reactive as the starting materials  $\text{Ti}(\text{NEt}_2)_4$  or  $\text{Zr}(\text{NMe}_2)_4$ , however, employing amidate ligands allows us to tune the reactivity by altering the sterics and electronics of the system. Interestingly, titanium and zirconium imido complexes **1** and **2** also showed catalytic activity toward hydroamination of 2,2-diphenylpent-4-ene-1-amine. This suggests bis(amidate) metal imido intermediates are catalytically active unlike the cyclopentadienyl cationic zirconium complexes mentioned previously. Overall, this is supportive of our complexes proceeding through an imido type mechanism rather than a sigma bond insertion mechanism. These tunable metal-catalyzed systems for hydroamination provided an ideal starting point for the development of an enantioselective catalyst.

Until 2006, the only asymmetric group 4 hydroamination catalyst reported was a cationic chiral non-racemic zirconium complex prepared by Scott and coworkers.<sup>58</sup> With this hydroamination catalyst, they cyclized a variety of *N*-methylaminoalkenes with high conversion and ee's up to 82 %. Although a group 4 metal is being employed in this reaction, a cationic zirconium complex is isoelectronic with the group 3 metals and therefore is a different class of catalyst that proceeds via an alternate reaction mechanism. Also as mentioned before, this catalyst is limited to *N*-substituted aminoalkenes and does not show any reactivity toward primary amines for hydroamination.

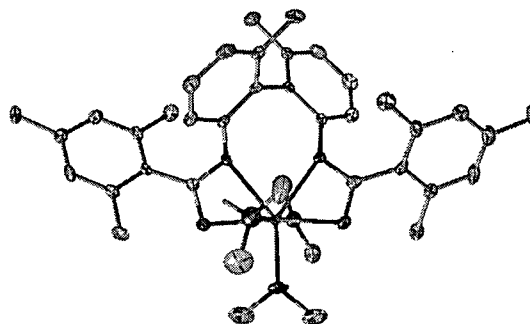
The first neutral asymmetric group 4 catalysts for intramolecular alkene hydroamination were submitted by the Schafer group and the Bergman group within days of one another during the summer of 2006. Bergman and coworkers reported a variety titanium, zirconium and hafnium bis(amido) hydroamination catalysts that were prepared *in-situ* from  $\text{M}(\text{NMe}_2)_4$  ( $\text{M} = \text{Ti}, \text{Zr}, \text{Hf}$ ) and a variety of chiral ligands that already had literature precedence. Of the three metals used, zirconium showed the highest conversions and enantioselectivities. The tetradentate diphosphinic amide proligand employed showed the highest enantioselectivity and was utilized for aminoalkene hydroamination substrate scope investigations. Enantioselectivities up to 80 % were observed for the cyclization of 2,2-dimethyl-1-aminopent-4-ene. Although these were



very important results for group 4 hydroamination, only moderate ee's were obtained, and attempts to characterize these *in-situ* prepared catalysts were unsuccessful.

Our group has recently become interested in applying our bis(amidate)bis(amido) group 4 complexes for asymmetric hydroamination of alkenes. We believe we can exploit our highly modular amidate ligands to synthesize a group 4 precatalyst that displays excellent enantioselectivity and reactivity. Having shown that complexes 1 through 4 are catalytically active toward the cyclohydroamination of aminoalkenes, modifications were made to these precatalysts to introduce chirality into the amidate ligands. These efforts resulted in a structure activity relationship for a number of titanium and zirconium amidate complexes, and helped to identify the most selective and reactive catalyst. Ultimately, we succeeded in the synthesis and characterization of the first neutral, chiral non-racemic, group 4 complex for enantioselective aminoalkene hydroamination.

## Chapter 2



### Synthesis of Axially Chiral Group 4 Amidate Complexes as Hydroamination Precatalysts

---

#### 2.1 Introduction

Over the past thirty years, catalysts containing axially chiral ligands have become prominent in the literature and have produced a number of ground breaking results for asymmetric catalysis.<sup>75</sup> Axial chirality is a special case where a molecule has an axis of chirality rather than a stereogenic carbon center.<sup>76</sup> It is most common in biaryl compounds where steric strain causes restricted rotation about the C-C single bond that joins the two aryl groups. If the energy barrier for rotation around this bond is high, the different atropisomers (conformational isomers) can be isolated as separate compounds. Axially chiral compounds can also be racemized thermally, whereas molecules containing a stereogenic carbon can only be racemized through a chemical reaction. Some common examples include bis(anthracenyl), binaphthyl, 2,2'-disubstituted biphenyl, and others. Since the late 90's, incorporation of axial chirality into hydroamination catalysts has been investigated by a number of research groups.<sup>27,32,36,37,40-42,58,77-80</sup> Recent reports by Livinghouse<sup>42</sup> and Hultsch<sup>32</sup> and have shown enantioselectivities up to 95 % ee for select examples of intramolecular hydroamination.

Group 4 catalysts for alkene hydroamination have been limited to a few reported cases. Most recently, Bergman and coworkers reported a series of bis(amido) group 4 precatalysts where enantioselectivities up to 80 % were obtained for primary aminoalkene substrates.<sup>58</sup> Scott and coworkers reported an axially chiral cationic

zirconium complex capable of enantioselectivities up to 82 % for secondary aminoalkene substrates.<sup>36</sup> Until this year, this was the highest recorded enantiomeric excess for a group 4 metal hydroamination catalyst.<sup>57</sup> With the recent success of asymmetric hydroamination by group 4 catalysts containing axially chiral ligands, we sought to develop a neutral group 4 hydroamination catalyst that would incorporate an axially chiral backbone into an amidate ligand (Figure 2.1).

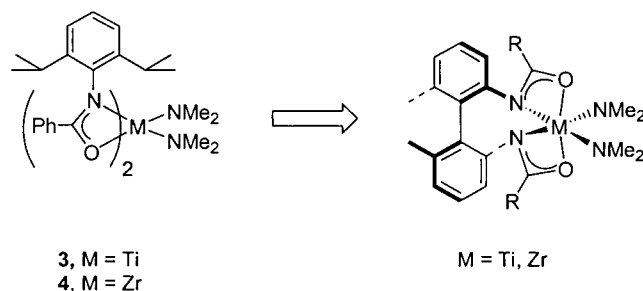


**Figure 2.1** Precatalyst progression from the non-tether complexes **3** and **4** to a C<sub>2</sub> symmetric non-racemic tethered complex.

Our group has reported complexes **3** and **4** as efficient and regioselective catalysts for the intermolecular hydroamination of alkynes and allenes with primary amines (Figure 2.1).<sup>66,73,74</sup> Early results suggested that complexes **3** and **4** were unreactive towards alkene hydroamination, but further investigations have shown that aminoalkene hydroamination does proceed at higher temperatures.<sup>53</sup> Because we have shown alkene hydroamination is achievable with our bis(amidate)bis(amido) titanium and zirconium catalysts, asymmetric versions of the amidate ligands were pursued.

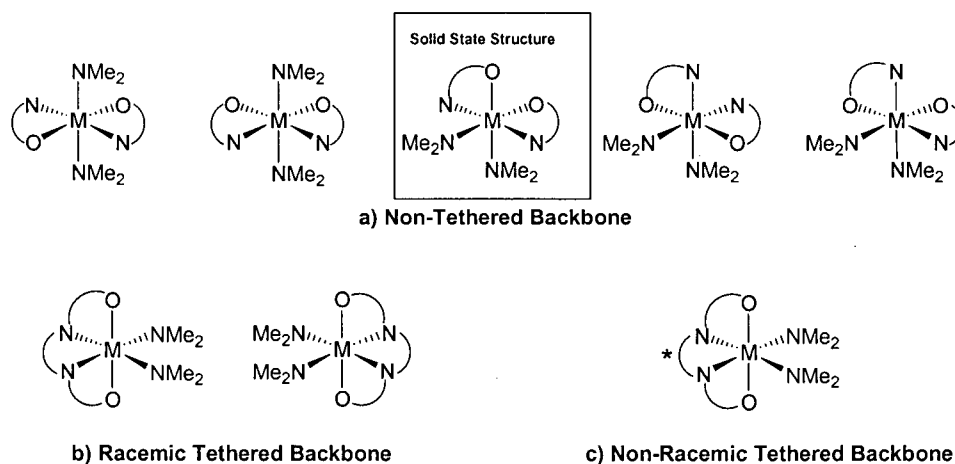


**Figure 2.2** Possible geometric isomers for monomeric tethered and non-tethered 6-coordinate bis(amidate)bis(amido) titanium or zirconium complexes.

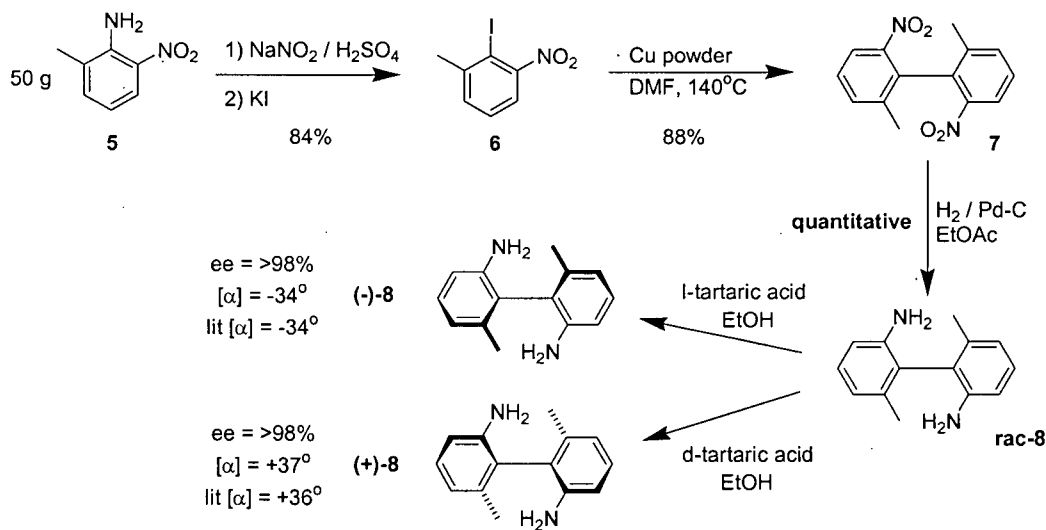
One challenge with six-coordinate amidate complexes similar to **3** and **4** is the possibility of multiple coordination geometries.<sup>64</sup> The five potential monomeric geometric isomers for complexes **3** and **4** are illustrated in Figure 2.2a, where the observed solid state geometry is highlighted.<sup>73</sup> In an octahedral complex, a tethered tetradentate amidate ligand would reduce the number of expected geometric isomers to two for a racemate (Figure 2.2b), and one for a homochiral complex (Figure 2.2c). The forced coordination geometry is another attractive feature when a rigid tethered ligand is employed. The amidate nitrogens should be forced into a *cis* conformation leaving the oxygens *trans* to one another.

For the new bis(amidate) precatalysts, we selected the 6,6'-dimethylbiphenyl-2,2'-diamine axially chiral backbone that Scott and coworkers used in their cationic zirconium complex for asymmetric alkene hydroamination.<sup>36</sup> We hypothesized that a rigid tethered ligand backbone would expose the catalytically active site on the metal by forcing the amidate ligands to be pulled back. Opening up the reactive site on the precatalyst should allow for increased reactivity. Another benefit of using 6,6'-dimethylbiphenyl-2,2'-diamine is the ease with which the diamine can be resolved before further elaboration to an amide proligand.<sup>57,81</sup>

This chapter will describe the design and the synthesis of homochiral titanium(IV) and zirconium(IV) complexes as potential asymmetric alkene hydroamination precatalysts. The modular design of the amide proligand allows us to easily change the steric and electronic effects imposed by the ligands. To probe the effects that electron withdrawing substituents have on hydroamination reactivity, four amide proligands were investigated, where three proligands contain electron withdrawing trifluoromethyl substituents (Scheme 2.2). Herein, we will investigate the stability of titanium and zirconium bis(amidate)bis(amido) complexes containing different axially chiral tetradentate amidate ligands.

## 2.2 Synthesis of 6,6'-Dimethylbiphenyl-2,2'-diamine and Amidate Proligands

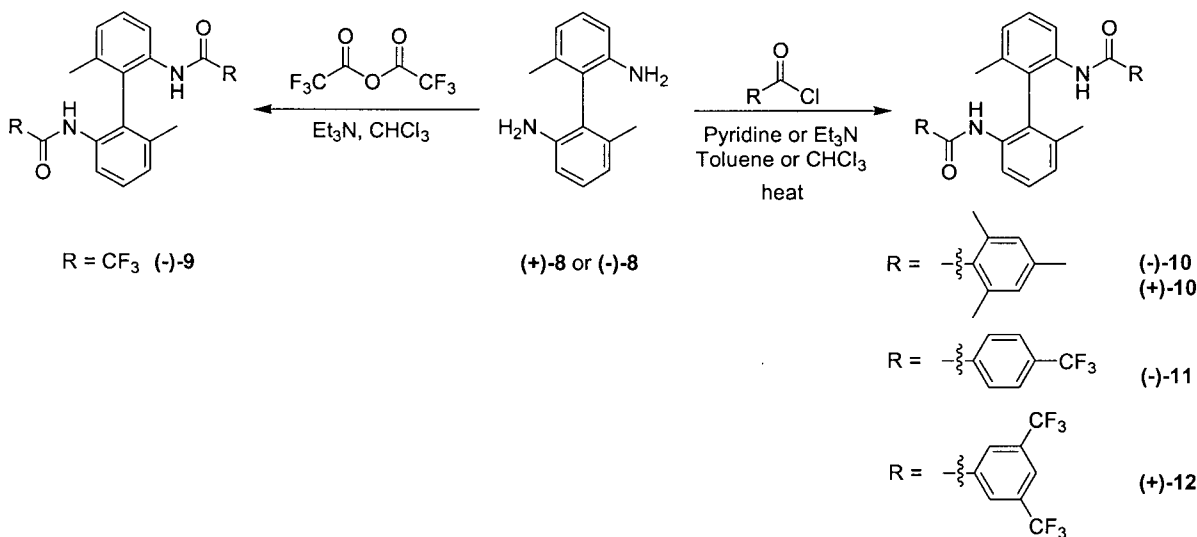
Prior to the preparation of the tethered amide proligands, the axially chiral biphenyl amine, 6,6'-dimethylbiphenyl-2,2'-diamine (**8**) had to be synthesized and resolved. Diamine rac-**8** was prepared in 3 steps from commercially available 2-methyl-6-nitroaniline (**5**) according to a modified literature procedure (Scheme 2.1).<sup>82</sup> The resolution of rac-**8** was achieved through successive recrystallization of the D- or L-tartrate salt producing (-)-**8** from L-tartaric acid, and (+)-**8** from D-tartaric acid.<sup>81</sup>



**Scheme 2.1** Synthesis of chiral 6,6'-dimethylbiphenyl-2,2'-diamine (**8**)

The diamine (+)-**8** or (-)-**8** tartrate salts were treated with 1 M NaOH to isolate the free diamine. The enantiopurity was then determined by optical rotation relative to literature values.<sup>81</sup> Compound (-)-**8**, for example, was isolated from the L-tartrate recrystallization with a specific rotation of  $[\alpha] = -25^\circ$ , which was lower than the literature value  $[\alpha] = -34^\circ$ . The enantiopurity of diamines (+)-**8** or (-)-**8** was further enhanced through diffusion recrystallization of the neutral amine from a biphasic system of dichloromethane and hexanes. The resulting neutral diamines (+)-**8** and (-)-**8** had specific rotations of  $[\alpha] = +37^\circ$  (literature:  $+35^\circ$ ) and  $[\alpha] = -34^\circ$  (literature:  $-34^\circ$ ) respectively. The

enantiopurity of the diamines was also confirmed by GC-MS analysis of the bis((+)-(S)- $\alpha$ -methoxy- $\alpha$ -trifluoromethylphenylacetamide) derivative; enantiomeric excess greater than 98 % was achieved for each enantiomer. The overall yield from this resolution was 50 % ((+) and (-) combined) from 24 g of unresolved diamine **8**. The remaining 12 g of diamine recovered from the recrystallization were combined and resolved again using the same method. This method proved less laborious than the chiral resolution performed by Scott and co-workers involving a method known as simulated moving bed chromatography (SMB).<sup>82</sup>



**Scheme 2.2** Synthesis of chiral bis(amide) proligands **9** - **12**

Proligands **9** through **12** were synthesized to probe both the steric and electronic effects on reactivity and enantioselectivity for group 4 alkene hydroamination (Scheme 2.2). Proligand (-)-**9** was easily synthesized in 94 % yield from diamine (-)-**8** and 2.1 equivalents of trifluoroacetic anhydride. Alternatively, compounds (-)-**10**, (+)-**10**, (-)-**11** and (+)-**12** were synthesized in moderate yields from commercially available acid chlorides: 2,4,6-trimethylbenzoyl chloride, 4-trifluoromethylbenzoyl chloride and 3,5-bis(trifluoromethyl) benzoyl chloride respectively. Proligands (-)-**10** and (+)-**10** proved the most difficult to synthesize. They required elevated temperatures (90 °C), excess mesitoyl chloride (3 equiv.) and pyridine as a base in order to achieve complete conversion to the bis(amide).<sup>57</sup> The reaction was attempted at room temperature with dichloromethane as the solvent and triethylamine as a base, but no reaction was observed.

Heating the same reaction mixture to reflux still only resulted in conversion to the mono(amide). This lack of reactivity for the preparation of proligand **10** was not observed for proligands (-)-**9**, (-)-**11** or (+)-**12** and is likely attributed to the steric bulk at the 2,6-position of the mesitoyl chloride. Each proligand was purified by recrystallization prior to full characterization by NMR spectroscopy, mass spectrometry and elemental analysis. The compounds were thoroughly milled, and dried vigorously under vacuum (overnight at 60 °C) before reaction with either Ti(NMe<sub>2</sub>)<sub>4</sub> or Zr(NMe<sub>2</sub>)<sub>4</sub>.

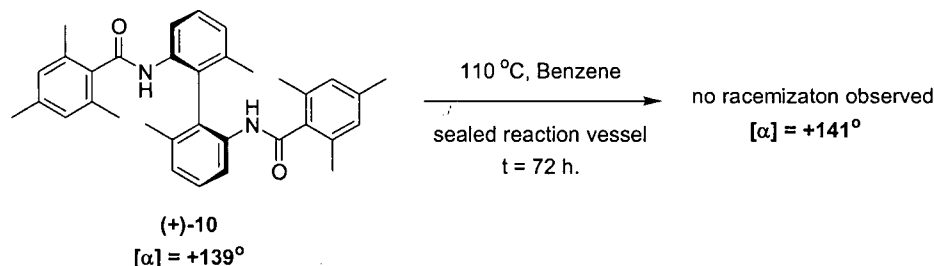


**Figure 2.3** Investigation into the racemization of proligand (+)-**10** under conditions used for hydroamination in Chapter 3.

The possibility of ligand racemization (Figure 2.3) was a concern at the high temperatures employed during preparation of the ligand (90 °C) and under catalytic hydroamination conditions (*vide infra*). A control experiment was performed in which the proligand was heated in benzene at 110 °C for 72 h in a sealed reaction vessel. The specific rotation of the proligand (+)-**10** was recorded as  $[\alpha] = +139^\circ$  prior to heating and  $[\alpha] = +141^\circ$  after heating, indicative of no thermally induced racemization.

Overall, ligand synthesis was complete in five steps from commercially available 2-methyl-6-nitroaniline with overall yields ranging from 47 to 71 %. The unresolved 6,6'-dimethylbiphenyl-2,2'-diamine **8** was synthesized with an overall yield of 74 %. Resolution of the diamine resulted in minimal loss of material because all discarded diamine could be easily recovered from the recrystallization supernatants. Synthesis of the proligands and purification by recrystallization resulted in the most significant loss in material, but ultimately the reactions were quantitative, and the lost proligand need not be discarded. In particular, the synthesis of proligands **9-12** was straightforward, efficient and could be completed on multigram scale.

### 2.3 Synthesis of Chiral Bis(amido)bis(amidate) Titanium(IV) and Zirconium(IV) Complexes.

With the synthesis of proligands **9** through **12** complete, zirconium and titanium complexes were prepared as hydroamination precatalysts. We anticipated that the rigid biphenyl backbone, as well as the steric bulk imposed by the substituents on the amide carbonyl substituents, would generate a well defined chiral environment around the metal center. This section will focus on the synthesis and characterization of the titanium and zirconium complexes using such axially chiral amide proligands.

**Table 2.1** Synthesis of bis(amidate)bis(amido)titanium and zirconium precatalysts

Entry	Complex	Proligand	Metal	R
1	(-)-13a	(-)-10	Ti	
2	(-)-13b	(-)-10	Zr	
3	(+)-13c	(+)-10	Zr	
4	(-)-14	(-)-9	Ti	R = -CF <sub>3</sub>
5	(-)-15a	(-)-11	Ti	
6	(-)-15b	(-)-11	Zr	
7	(+)-16a	(+)-12	Ti	
8	(+)-16b	(+)-12	Zr	



The synthesis of the complexes **13** - **16** (Table 2.1, entries 1-8) were completed in high yield through a protonolysis reaction between the corresponding bis(amide) and commercially available  $\text{Ti}(\text{NMe}_2)_4$  or  $\text{Zr}(\text{NMe}_2)_4$ . The reactions were completed in a non-coordinating solvent and stirred at room temperature until complete dissolution of the poorly soluble proligands was observed. The color of the solution changed instantly to an intense red color for the titanium(IV) complexes (Table 2.1, entries 1, 4, 5 and 7) and yellow for the zirconium(IV) complexes (Table 2.1, entries 2, 3, 6 and 8). The resulting complexes were isolated in quantitative yields as either an orange/red solid for titanium, or a pale yellow solid for zirconium. Complexes were typically synthesized on 300-400 mg scale in a nitrogen filled glove box using benzene as the solvent. Small scale synthesis was required since catalyst decomposition was observed upon long term storage (>1 month). The intensity of the color was greatest when electron withdrawing proligands were used ((-)-**9**, (-)-**11** and (+)-**12**). All complexes were highly soluble in most solvents, including hexanes, pentanes, benzene, toluene and *m*-xylene. The high solubility of these complexes proved challenging for purification by recrystallization, so catalytic screens employed crude products.

Titanium complex (-)-**13a** was characterized by  $^1\text{H}$  and  $^{13}\text{C}$  NMR spectroscopy, EI mass spectrometry and elemental analysis. Although mass spectrometry and elemental analysis were both consistent with the chemical formula  $\text{C}_{38}\text{H}_{46}\text{N}_4\text{O}_2\text{Ti}$ ,  $^1\text{H}$  NMR and  $^{13}\text{C}$  NMR for this complex were very difficult to interpret, and a proposed structure could not be assigned. Variable temperature (VT)  $^1\text{H}$  NMR analysis was also performed on complex (-)-**13a** but the data did not give conclusive evidence of structure (see Appendix I). The only information that could be obtained from the VT NMR was that a complicated oligomer / monomer equilibrium is taking place. A DOSY NMR experiment of (-)-**13a** was also conducted to determine if the solution phase structure could be established (see Appendix). Diffusion-ordered spectroscopy (DOSY) separates NMR signals of different compounds according to their diffusion coefficients, and is displayed as a 2-D NMR spectrum where the  $^1\text{H}$  NMR is plotted versus  $\log(D)$ . If compound (-)-**13a** exists as two compounds in solution, such as a dimer / monomer mixture, the  $^1\text{H}$  NMR spectrum would be divided into two separate diffusion coefficients. However, the DOSY spectrum of compound (-)-**13a** only shows one diffusion coefficient

( $D = 4.3 \times 10^{-10} \text{ m}^2/\text{s}$ , Solvent = Benzene); therefore the solution phase structure is one discrete compound. A DOSY NMR experiment was also carried out for ligand (-)-10 and also showed a single compound with a similar diffusion coefficient ( $D = 4.6 \times 10^{-10} \text{ m}^2/\text{s}$ , Solvent = 5:1 Benzene/ $\text{CDCl}_3$ ). A relationship for two molecular species in the same solvent allows for a rough estimation of molecular weight if one compound is known. The equation that relates molecular weight to the diffusion coefficient ( $D$ ) is presented below (equation 1).<sup>83</sup>

$$\text{MW}_A / \text{MW}_B = [D_B/D_A]^3 \quad (1)$$

This relationship is an estimation based on roughly spherical molecules in solution, and only gives an approximation of the molecular weight (MW) for the unknown compound (-)-13a. From this equation, the solution phase molecular weight for (-)-13a was calculated to be 617 g/mol. The actual molecular weight of (-)-13a based on EI-MS was 638 g/mol. Though the molecular weight of complex (-)-13a is not identical to the calculated value of 617 g/mol, the monomer molecular weight is much closer to this calculated value than the dimer molecular weight ( $\text{MW}_{\text{dimer}} = 1276 \text{ g/mol}$ ). Thus, fluxional behaviour of the monomer complex is a likely explanation for the complicated solution state structure.

The zirconium complexes (-)-13b and (+)-13c were also prepared using the mesityl substituted proligands (-)-10 and (+)-10. The solution state structure of these zirconium complexes were not complicated. Based on the simplicity of the  $^1\text{H}$  and  $^{13}\text{C}$  NMR spectra, the structure was proposed to be  $C_2$  symmetric, with the tethered bis(amidate) ligand coordinated in a tetradentate fashion along with two dimethylamido ligands. Mass spectrometry and elemental analysis were also consistent with the predicted structure. The change in size of zirconium(IV) in comparison to titanium(IV) appears to have altered the coordination environment sufficiently to give a discrete monomeric species rather than the complicated structure for complex (-)-13a. Confirmation of structure was later obtained by X-ray crystallography (Figure 2.4). Though (+)-13c was characterized as a 6-coordinate bis(amidate)bis(amido) complex by  $^1\text{H}$  and  $^{13}\text{C}$  NMR spectra, EI mass spectrometry and elemental analysis, the solid state molecular structure obtained was a 7 coordinate pseudo-pentagonal bipyramidal complex with a neutrally bound dimethylamine axial to the amidate ligands. As anticipated, the

tethered backbone forces the amidate nitrogens to be *cis* and the oxygens to be *trans*. The amidate C1-N1 and C1-O1 bond lengths are 1.320 Å and 1.278 Å respectively, which is consistent with limited delocalization throughout the N1-C1-O1 bonds. Due to the rigidity of the biphenyl backbone, the  $\kappa^4$  bis(amidate) ligand is pulled back with an [O-Zr-O] bond angle of 166.7° in the equatorial plane.

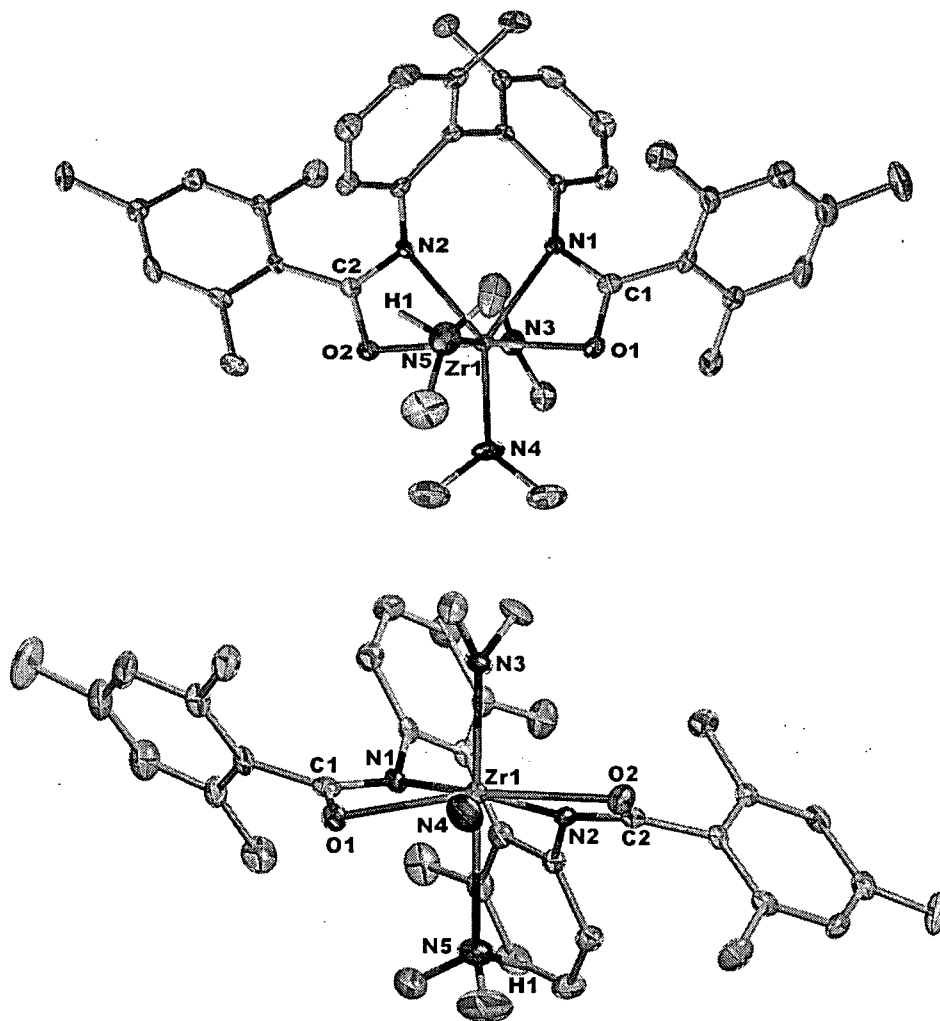


**Figure 2.4:** Two views of an ORTEP diagram for the dimethylamine adduct of (+)-13c (CH<sub>3</sub> substituents omitted from N4 dimethylamido ligand for clarity in bottom view. Ellipsoids shown at 50 % probability level). Selected interatomic distances [Å] and angles [°]: Zr1 - O1 2.2802(35), Zr1 - O2 2.2890(37), Zr1 - N1 2.3134(43), Zr1 - N2 2.3468(33), Zr1 - N3 2.0651(41), Zr1 - N4 2.0694(43), Zr1 - N5 2.5357(53); O1 - Zr1 - O2 166.68(0.13), N1 - Zr1 - N2 74.87(0.16), O1 - Zr1 - N1 56.81(0.13), O2 - Zr1 - N2 56.21(0.13), N3 - Zr1 - N5 177.95(0.17), O1 - C1 - N1 144.52(0.41), O2 - C2 - N2 113.47(0.42). biphenyl torsion angle [°]: 68.28(0.65).

The neutrally bound dimethylamine, which is a byproduct of the protonolysis reaction between  $\text{Zr}(\text{NMe}_2)_4$  and the amide proligand, was not observed in any of the characterization techniques used except X-ray crystallography. The dimethylamine appears to stabilize a 7 coordinate complex that produced X-ray quality crystals. Based on a small collection of group 4 complexes in the literature, the methyl groups on dimethylamine ligands are typically observed as a broad singlets or doublets between 1.5 to 3.1 ppm in the  $^1\text{H}$  NMR spectrum.<sup>84-88</sup> However, no dimethylamine resonances were identified in the  $^1\text{H}$  NMR spectrum of (+)-**13c**. The closest related complexes to (+)-**13c** found in the literature were the bis(sulfonamide) zirconium complexes reported by Bergman and coworkers in 2003 (Figure 2.5).<sup>88</sup>

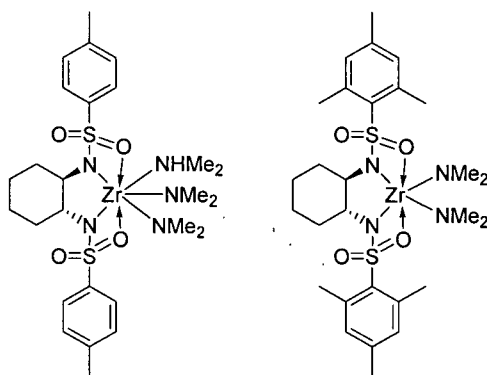


**Figure 2.5:** Bis(sulfonamide) zirconium complex reported by Bergman *et al.*<sup>88</sup>

Infrared spectroscopy was also completed for the complex (+)-**13c**; no N-H stretch was observed at around  $3400\text{ cm}^{-1}$ .<sup>85</sup> It is probable that the adduct crystals formed as a result of trace amounts of dimethylamine that were not entirely removed before recrystallization. Further investigation with the addition of donors such as THF, diethylether and triphenylphosphine oxide (TPPO) did not result in X-ray quality crystals. However,  $^{31}\text{P}$  NMR of the TPPO adduct shows bound triphenylphosphine oxide at 44.6 ppm which is consistent with literature values.<sup>53</sup> Furthermore, poor reactivity in the intramolecular hydroamination of aminoalkenes was observed with these particular adducts.

With the intention of investigating the effects of electronics and sterics on the reactivity of alkene hydroamination catalysts, electron withdrawing groups were incorporated into the tetradentate bis(amidate) ligands. Typical aryl electron

withdrawing substituents that contain heteroatoms, such as nitrogen and oxygen, can act as metal donor atoms and be problematic when preparing metal complexes that are oxo- and azaphilic (example: -CN, -NO<sub>2</sub>, -SO<sub>2</sub>CF<sub>3</sub>, etc.). We wanted to investigate the effects that fluorine would have on reactivity compared to non-fluorinated counterparts. Although a fluorine substituted amidate ligand would likely influence electronic behaviour, little has been investigated concerning the size of fluoroalkyl constituents compared to their hydrocarbon counterparts. The relative size of a fluorine compared to hydrogen is 1.35 Å to 1.20 Å (van der Waals radii), where the relative electronegativity is 4.0 for fluorine and 2.1 for hydrogen (Pauling scale).<sup>89</sup> Based on this scale you would predict that incorporating fluorine into the ligand would increase the overall size of the ligand as well as significantly affect the electronic properties of the system. A recent publication by Timperley *et al.* discusses the effects that fluorine atoms exert on both volume and electronics.<sup>89</sup> According to their calculations, a -CF<sub>3</sub> substituent is approximately 1.25 times larger than a -CH<sub>3</sub>. Overall, one would expect to see different steric effects when trifluoromethyl substituents are incorporated into the bis(amidate) ligand. Similarly, the electronegativity of the trifluoromethyl group should influence the charge distribution in the complexes.

Based on Hammett sigma constants, the electron withdrawing power of *m*-CF<sub>3</sub> or *p*-CF<sub>3</sub> substituted benzoic acid is similar to that of a -CN substituted benzoic acid. Although this estimation does not include disubstituted benzoic acid derivatives, it would be expected that two trifluoromethyl groups would have a larger electron withdrawing effect than one. Previous work by our group has shown that -CN and -CF<sub>3</sub> substituted amidate ligands are equally reactive toward aminoalkene hydroamination which is consistent with the Hammett approximation.<sup>90</sup>

The Schafer group also investigated pentafluorophenyl substituted amidate ligands, however, aryl C-F activation occurred as a side-reaction at the temperatures required for alkene hydroamination (110°C).<sup>91</sup> Replacing a pentafluorophenyl substituent with a trifluoromethyl substituted phenyl may address the C-F activation difficulty observed. To probe the effects of trifluoromethyl substituents on group 4 bis(amidate) complexes, we prepared complexes (-)-14, (-)-15 and (+)-16 (Table 2.1). The main focus

of making these alterations to the ligand was to increase the reactivity without varying the observed enantioselectivity seen for complexes (-)-**13b** and (+)-**13c** (Chapter 3).

Complex (-)-**14** was the first trifluoromethyl substituted compound prepared. This complex contained less steric bulk on the amide carbon in comparison to the mesityl substituted catalysts **13a-c**. Preliminary synthesis of complex (-)-**14** was completed on NMR scale in J. Young Teflon sealed NMR tube. Proligand (-)-**9** was reacted with one equivalent of  $\text{Ti}(\text{NMe}_2)_4$  to produce a single compound with a simple  $^1\text{H}$  NMR spectrum (Figure 2.6a). Close examination of the  $^1\text{H}$  NMR spectrum showed a broad singlet at 1.84 ppm, which could correspond to the methyl groups from a bound dimethylamine ligand. The broad singlet at -0.14 ppm may also be the dimethylamine N-*H* signal. Because the reaction was conducted in a closed system, the dimethylamine byproduct remains to stabilize a  $C_1$  symmetric complex. However, when the volatiles are removed under vacuum, the  $^1\text{H}$  NMR spectrum becomes very complicated consistent with the removal of a stabilizing donor (Figure 2.6b). It appears that the complex is stabilized by the presence of an external donor, and that the trifluoromethyl substituents are not bulky enough to stabilize a discrete species in solution in the absence of such a donor. The crude product observed in Figure 2.6b was used for hydroamination reactions in Chapter 3; however the complex stability proved to be poor under the reaction conditions. Further structural elucidation of this metal complex was not performed due to the poor stability observed.

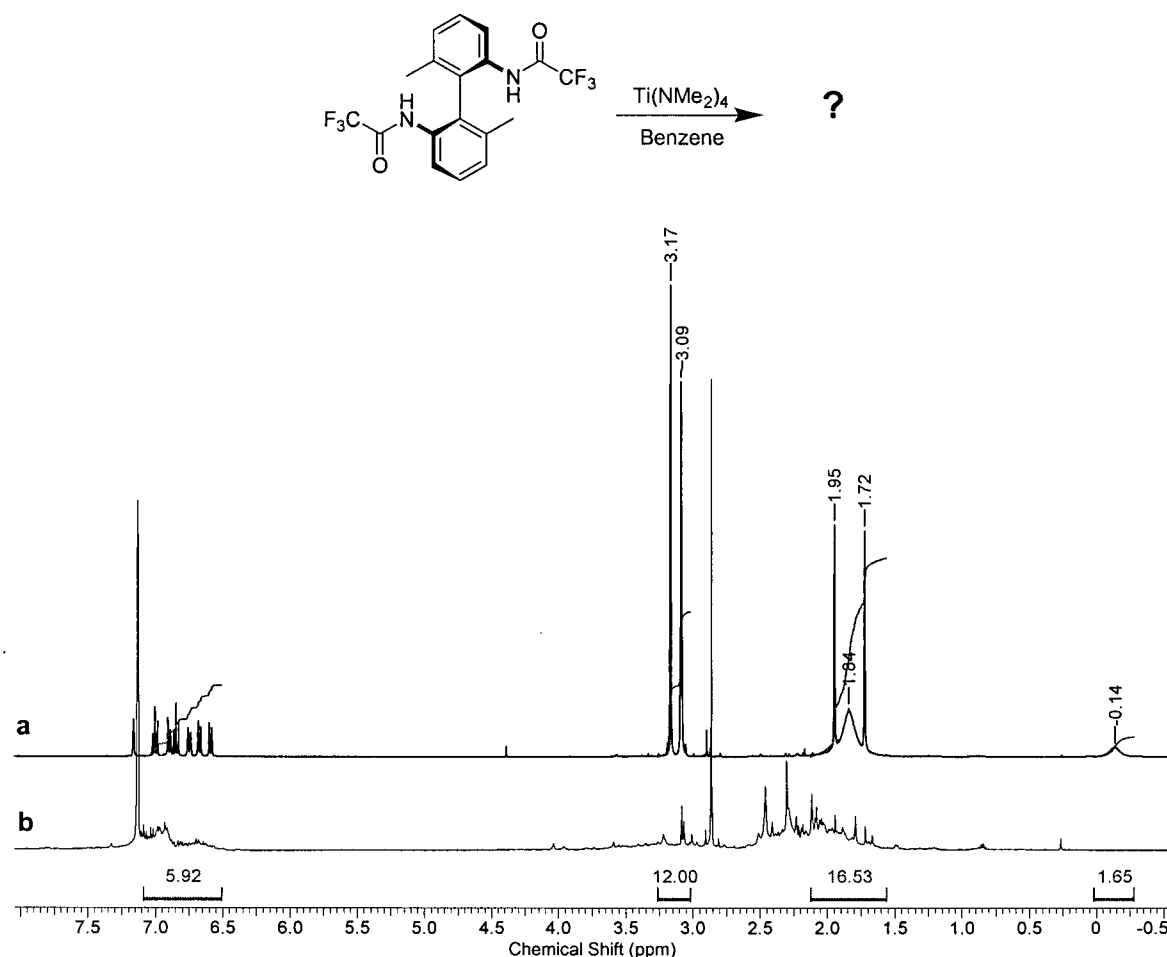


**Figure 2.6**  $^1\text{H}$  NMR spectra of complex **(-)-14** prepared in  $d_6$ -benzene in a Teflon sealed NMR tube: a) before solvent and dimethylamine removed and b) after solvent removed under high vacuum and redissolved in  $d_6$ -benzene.

Considering the complications that occurred for complex **(-)-14**, attention was focused on a fluorinated ligand that contained enough steric bulk to disfavor the formation of complicated oligomeric species, and also be less prone to decomposition under typical conditions for aminoalkene hydroamination. To accomplish this, *p*-trifluoromethylphenyl and 3,5-bis(trifluoromethyl)phenyl bis(amide) proligands **(-)-11** and **(+)-12** were prepared. Titanium complexes **(-)-15a** and **(+)-16a** were synthesized from these proligands cleanly and isolated in a quantitative yields. Full characterization by  $^1\text{H}$ ,  $^{19}\text{F}$ , and  $^{13}\text{C}$  NMR spectroscopy, elemental analysis and EI mass spectrometry were completed on both complexes. The NMR spectroscopy suggests a  $C_2$  symmetric complex in solution.

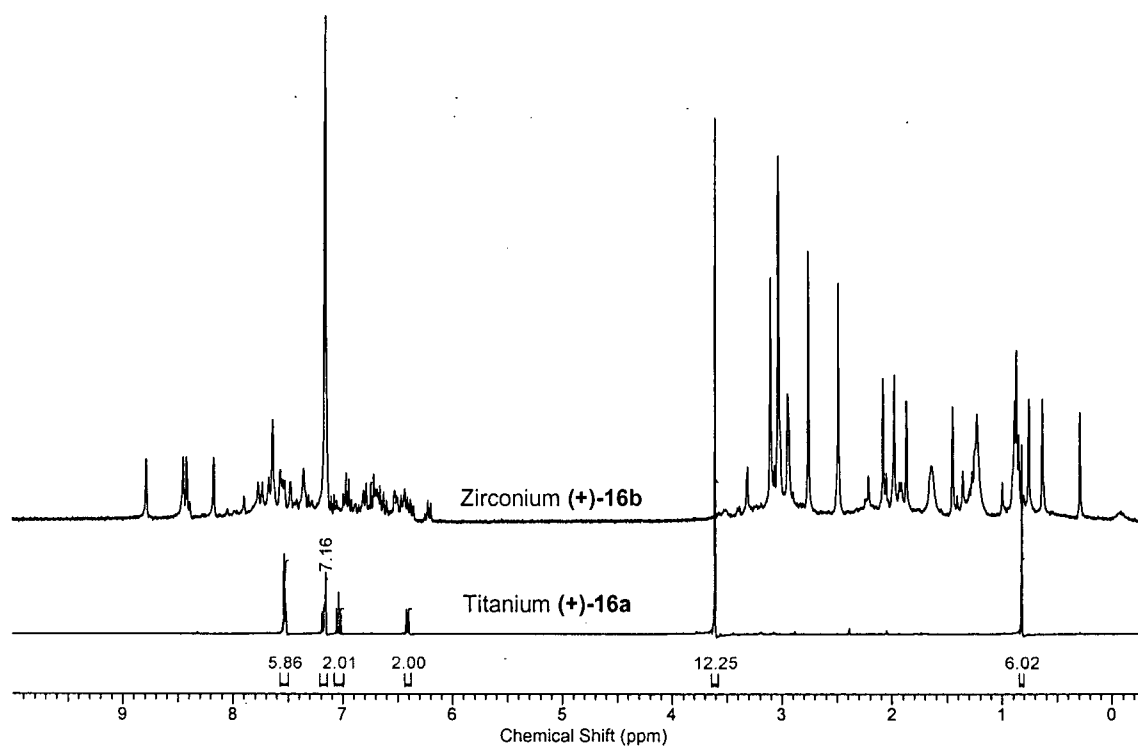
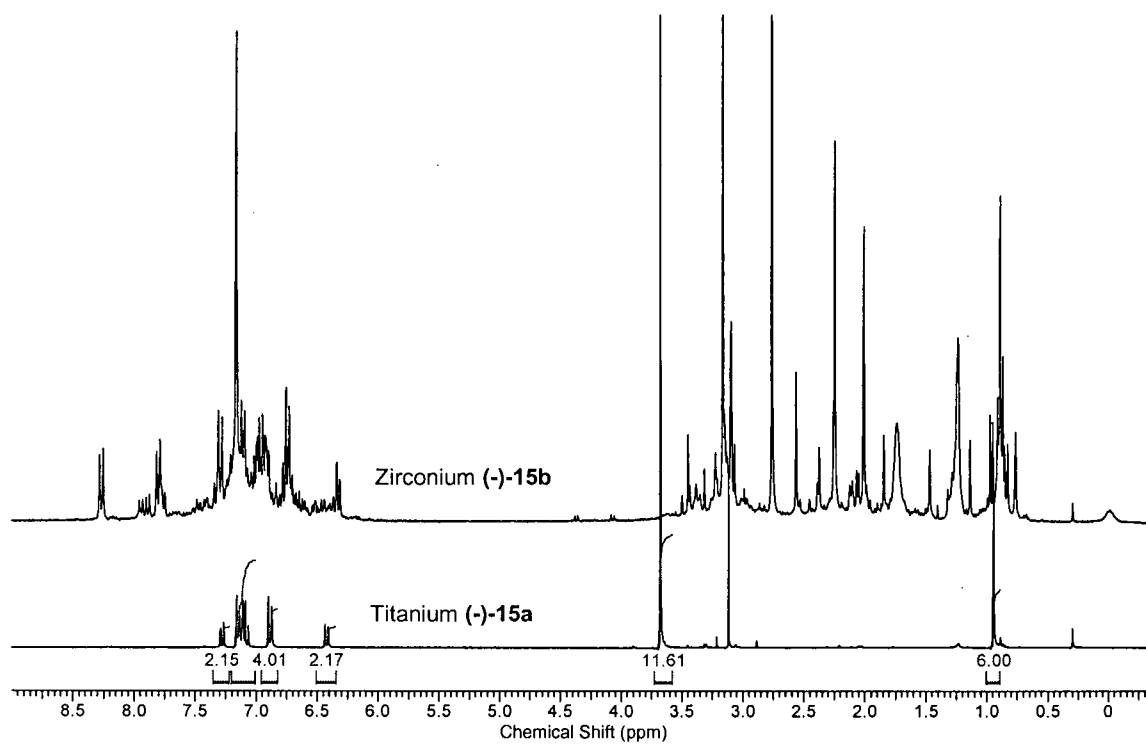


**Figure 2.7** Comparison of  $^1\text{H}$  NMR spectra for titanium (-)-15a and (+)-16a vs. the zirconium analogues (-)-15b and (+)-16b.



In addition, the zirconium analogues **(-)-15b** and **(+)-16b** were synthesized through an analogous method. Unfortunately, the characterization of these complexes was not as straightforward. Figure 2.6 shows the  $^1\text{H}$  NMR spectra for titanium complexes **(-)-15a** and **(+)-16a** as well as zirconium complexes **(-)-15b** and **(+)-16b** after isolation. For complexes **(-)-15b** and **(+)-16b**, EI mass spectrometry analysis did not contain a molecular ion peak for a monomeric complex, and the sensitivity of the instrument can not exceed 1400 mass units were made. Therefore, no structural conclusions were made based on the data collected. Complexes **(-)-15b** and **(+)-16b** were not fully characterized due to the complexity of the  $^1\text{H}$  NMR spectrum.

## 2.4 Summary and Conclusions

The increase in the ionic radius for Zr(IV) in comparison to Ti(IV) was quite significant when comparing the structural behaviour of complexes with identical amidate ligands. For example, the steric bulk of the methyl substituents at the 2,6-positions of ligand **10** were required to stabilize the  $C_2$  symmetric zirconium complexes **13b/13c**, while a simple  $C_2$  symmetric titanium analogue could not be obtained for complex (-)-**13a**. The methyl groups at the 2,6-position of the mesityl appear to be too sterically demanding for titanium. A structure of (-)-**13a** could not be proposed based on the characterization data collected, but the 2D-DOSY NMR experiment gave evidence that a monomer / dimer equilibrium is not occurring when higher temperature NMR experiments were conducted (see Appendix).

The opposite trend in complex stability was observed for (-)-**15b** and (+)-**16b**, which contained less sterically demanding, trifluoromethyl substituted, amidate ligands (-)-**11** and (+)-**12**. Simple complexes could not be obtained for zirconium ((-)-**15b** and (+)-**16b**) but the titanium analogues ((-)-**15a** and (+)-**16a**) were fully characterized. The *p*-trifluoromethylphenyl and 3,5-bis(trifluoromethyl)phenyl substituents did not provide a sufficient amount of steric bulk to stabilize discrete bis(amidate)bis(amido) zirconium complexes ((-)-**15b** and (+)-**16b**); however, the lack of steric bulk on these amidate ligands, did result in well behaved titanium complexes ((-)-**15a** and (+)-**16a**). Overall, the tethered bis(amidate)bis(amido) complexes of titanium gave simple solution phase structures for the less sterically demanding ligands (-)-**11** and (+)-**12**, while ligand (+)/(-)-**10** was an ideal fit for zirconium. In Chapter 3, the bis(amidate)bis(amido) titanium and zirconium complexes will be employed as aminoalkene hydroamination precatalysts.

## 2.5 Experimental

**General Procedures:** All chemicals and solvents were commercially available and used as received unless stated otherwise. Complexes **13** to **16** were prepared using Schlenk line and/or glove box (Mbraun LabMaster) techniques under a dry, oxygen free, nitrogen atmosphere.  $d_6$ -benzene,  $d_8$ -toluene and  $d_{10}$ -xylenes were degassed using a freeze-pump-thaw method and stored over 3 Å molecular sieves. Solvents used for the synthesis of complexes **13** to **16** were purified and dried as follows: Pentane, benzene and diethyl ether were sparged with nitrogen and dried using alumina and copper columns; THF, toluene and hexanes were sparged with nitrogen and dried using an alumina column.  $^1\text{H}$ ,  $^{13}\text{C}\{\text{H}\}$ , and  $^{19}\text{F}\{\text{H}\}$  NMR spectra were recorded on either a Bruker Avance 300 MHz or Avance 400 MHz spectrometer. Enantiopurity of the resolved bis[(*S*)-(+)- $\alpha$ -methoxy- $\alpha$ -(trifluoromethyl)phenylacetyl chloride] derivative of 2,2'-diamino-6,6'-dimethylbiphenyl was determined using an Agilent 6890N GC system with a 5973 mass selective detector. Mass spectrometry (ESI, EI) and elemental analyses were performed by analytical services in the Department of Chemistry at the University of British Columbia. Optical rotation was measured using a cylindrical glass cell (10mm I.D., 100mm path) on a Jasco P-1010 digital polarimeter at 589 nm. Single-crystal X-ray structure determinations were performed and processes by Dr. Brian O. Patrick at the University of British Columbia. Resolution of the 2,2'-diamino-6,6'-dimethylbiphenyl and proligand synthesis were completed under ambient atmosphere. 2,2'-diamino-6,6'-dimethylbiphenyl was prepared according to modified literature procedures.<sup>81,82</sup> All proligands were thoroughly milled with a mortar and pestle and dried under vacuum at 60 °C prior to reaction with  $\text{Ti}(\text{NMe}_2)_4$  and  $\text{Zr}(\text{NMe}_2)_4$ .  $\text{Zr}(\text{NMe}_2)_4$  was sublimed under high vacuum prior to reaction with ligands **9** to **12**.

### Proligand synthesis

**Resolution of (-)-(S)-2,2'-diamino-6,6'-dimethylbiphenyl ((-)-8).** To a solution of racemic 2,2'-diamino-6,6'-dimethylbiphenyl (24 g, 113 mmol) in absolute ethanol (120 mL) heated to 80 °C, was added a solution of L-(+)-tartaric acid (17 g, 113 mmol) in

absolute ethanol (80 mL). The solution was cooled to room temperature and then placed in a refrigerator to aid crystallization. After 2 h, the supernatant was decanted and the remaining crystalline solid was re-dissolved in absolute ethanol (100 mL) at 80 °C. The solution was cooled to room temperature for 2 h and the supernatant was again decanted. This recrystallization process was repeated two additional times, then the remaining solid was neutralized with 1 M NaOH (50 mL) and extracted with dichloromethane (3 x 100 mL). The combined dichloromethane extracts were dried on MgSO<sub>4</sub>, filtered and reduced under vacuum to give (-)-(S)-2,2'-diamino-6,6'-dimethylbiphenyl as a beige solid (5.19 g, 21 %). Characterization was consistent with literature values.<sup>81</sup> Specific rotation (10 % HCl)  $[\alpha]_D^{20} = -22^\circ$ . Literature value: (10 % HCl)  $[\alpha]_D = -34^\circ$ .<sup>81</sup> The enantiopurity was further improved by recrystallization of the neutral amine from dichloromethane and hexanes as two phases. This was achieved by dissolving 1 (5.19 g, 24.5 mmol) in dichloromethane (10 mL) and carefully layering this solution with hexanes (50 mL). The solution was left overnight at room temperature to produce large clear colorless prisms that form at the solvent interface (2.13 g, 18 % based on 50 % single enantiomer yield).  $[\alpha]_D^{20} = -35^\circ$ . (10 % HCl), percent ee > 98 % (determined by GC-MS analysis of the bis[(S)-(+)- $\alpha$ -methoxy- $\alpha$ -(trifluoromethyl)phenylacetyl chloride] derivative\*\*).

**Resolution of (+)-(R)-2,2'-diamino-6,6'-dimethylbiphenyl ((+)-8).** The combined supernatants from the resolution of (-)-(R)-2,2'-diamino-6,6'-dimethylbiphenyl were reduced under vacuum, dissolved in 1M NaOH (50 mL), and extracted with dichloromethane (3 x 100 mL). The combined extracts were reduced to a beige solid (12.5 g). The (+)-enriched 2,2'-diamino-6,6'-dimethylbiphenyl (12.5 g, 59 mmol) was dissolved in absolute ethanol (50 mL) at 80 °C and D-(+)-tartaric acid (9.2 g, 61 mmol) was added as a solution in absolute ethanol (25 mL). The solution was cooled to room temperature and the supernatant was decanted to yield a white colorless crystalline solid. The above procedure was repeated, and then the solid was neutralized with 1M NaOH (50 mL) and extracted with dichloromethane (3 x 100 mL). The combined extracts were dried on MgSO<sub>4</sub> and concentrated to a white solid. The solid was dissolved in dichloromethane (10 mL) and layered with hexanes (50 mL) and left at room temperature

overnight to produce large clear colorless prisms (3.81 g, 32 % yield based on 50 % single enantiomer yield). Characterization was consistent with literature values.<sup>81</sup>  $[\alpha]_D^{20} = +37^\circ$ . (10 % HCl), percent ee > 98 % (determined by GCMS analysis of the bis[(*S*)-(+)- $\alpha$ -methoxy- $\alpha$ -(trifluoromethyl)phenylacetyl chloride] derivative\*\*).

**\*\*Procedure for GC/MS analysis to determine the enantiopurity 2,2'-diamino-6,6'-dimethylbiphenyl (8) as the bis[(*S*)-(+)- $\alpha$ -methoxy- $\alpha$ -(trifluoromethyl)phenylacetyl chloride] derivative.** Resolved 2,2'-diamino-6,6'-dimethylbiphenyl (7.5 mg, 0.035 mmol) was placed in a scintillation vial and dissolved in  $\text{CHCl}_3$ .  $\text{NEt}_3$  (10.7 mg, 0.106 mmol) and *S*-(+)- $\alpha$ -methoxy- $\alpha$ -trifluoromethylphenylacetyl chloride (26.8 mg, 0.106 mmol) were individually dissolved in  $\text{CHCl}_3$  and added by pipette. The reaction vessel was heated to 50 °C and progress was monitored by thin-layer chromatography (TLC). Two additional equivalents of Mosher's acid chloride (17.9 mg, 0.071 mmol) was added to the mixture and the solution was heated overnight. The resulting solution was analyzed by GC-MS (Agilent HP-5ms GC column, split mode injection 1:10, 1 min at 150 °C, ramp to 290 °C at 20 °C/min, held for 15 min at 290 °C). Retention times: 14.3 min [*R*-(+)-enantiomer], 16.5 min [*S*-(-)-enantiomer]. MS (EI):  $m/z$  644 ( $\text{M}^+$ ), 455 ( $\text{M}^+ - \text{C}_9\text{H}_8\text{F}_3\text{O}$ ).

**Proligand (-)-9.** To a solution of (-)-8 (250 mg, 1.2mmol) and  $\text{Et}_3\text{N}$  (500ul, 350mg, 3.5 mmol) in chloroform was added dropwise trifluoroacetic anhydride (750mg, 3.5 mmol). Reaction was complete by TLC analysis immediately after the addition of TFAA. The solvent was removed through rotary evaporation to yield a brown residue that was purified by silica column chromatography (eluted with 4:1 hexanes/ethyl acetate. The product was isolated as a white solid (439 mg, 94 %).  $^1\text{H}$  NMR ( $\text{CDCl}_3$ , 300 MHz):  $\delta$  7.93 (2 H, d,  $^3J_{\text{HH}}=8.2$  Hz, Ar-*H*), 7.60 (2 H, br s, amide-NH), 7.44 (2 H, t,  $^3J_{\text{HH}}=7.9$  Hz, Ar-*H*), 7.26 (2 H, d,  $^3J_{\text{HH}}=7.6$  Hz, Ar-*H*), 1.96 (6 H, s, Ar- $\text{CH}_3$ );  $^{19}\text{F}$  NMR ( $\text{CDCl}_3$ , 282 MHz)  $\delta$  0.302 (s, -C(O)CF<sub>3</sub>); MS (ESI):  $m/z$  427.1 ( $\text{M}^+ + \text{Na}$ ).

**Proligands (+)-10 / (-)-10** To a solution of resolved (+)-(R)- or (-)-(S)-2,2'-diamino-6,6'-dimethylbiphenyl 8 (1.0 g, 4.67 mmol) and pyridine (2.0 g, 25 mmol) in toluene (20 mL) was added 2,4,6-trimethylbenzoyl chloride (2.55 g, 14.0 mmol) in one portion. The

reaction mixture was stirred at 90 °C overnight. The following day the reaction mixture was cooled to room temperature and the toluene was removed under high vacuum. The remaining residue was dissolved in dichloromethane and flushed through a silica plug (2.5 cm length, 3 cm width). The collected solution was concentrated to a beige solid that was recrystallized by dissolving the solid in dichloromethane (3-5 mL) and layering with hexanes (25 mL) in two phases. The product was isolated as colourless clear needles (1.51 g, 64 %).  $^1\text{H}$  NMR ( $\text{CDCl}_3$ , 300 MHz):  $\delta$  7.97 (2 H, d,  $^3J_{\text{HH}}=8.1$  Hz, Ar-*H*), 7.34 (2 H, t,  $^3J_{\text{HH}}=7.9$  Hz, Ar-*H*), 7.15-7.13 (4 H, m, Ar-*H*), 6.73 (4 H, s, Mesityl-*H*), 2.20 (6 H, s, - $\text{CH}_3$ ), 2.08 (12 H, s, - $\text{CH}_3$ ), 1.95 (6 H, s, - $\text{CH}_3$ );  $^{13}\text{C}$  NMR ( $\text{CDCl}_3$ , 75 MHz):  $\delta$  169.32, 138.58, 137.31, 135.50, 134.36, 134.06, 129.34, 129.01, 128.25, 127.50, 121.90, 20.97, 19.93, 18.82. MS (ESI):  $m/z$  528.2 ( $\text{M}^+ + \text{Na}$ );  $\text{C}_{34}\text{H}_{36}\text{N}_4\text{O}_2$ , Anal Calcd: C, 80.92; H, 7.19; N, 5.55. Found: C, 80.83; H, 7.33; N, 5.83;  $[\alpha]_{\text{D}}^{20} = +139^\circ$ . ((+)-**10**,  $\text{CH}_2\text{Cl}_2$ ).

**Proligand (-)-11.** To a solution of (-)-(S)-2,2'-diamino-6,6'-dimethylbiphenyl **8** (1.0 g, 4.67 mmol) and pyridine (4 mL, excess) dissolved in chloroform (40 mL) was added 4-trifluoromethylbenzoyl chloride (2.3 g, 12 mmol) dropwise. The solution was refluxed for 2 h, cooled to room temperature then washed with 1 M HCl (3 X 50 mL). The remaining chloroform layer was washed with 1M NaOH (25 mL) then dried on  $\text{MgSO}_4$ . The chloroform was removed under vacuum and the isolated solid was recrystallized from dichloromethane / hexanes (10 mL dichloromethane and 50 mL hexanes) where the solid was first dissolved in dichloromethane then carefully layered with hexanes to create two phases. The product was isolated as colourless clear needles (2.11 g, 81 %).  $^1\text{H}$  NMR ( $\text{CDCl}_3$ , 300MHz):  $\delta$  8.19 (2 H, d,  $^3J_{\text{HH}}=8.2$  Hz, Ar-*H*), 8.78 (2 H, br s, amide-NH), 7.60-7.50 (8 H, m, Ar-*H*), 7.45 (2 H, t,  $^3J_{\text{HH}}=8.0$  Hz, Ar-*H*), 7.24 (2 H, d,  $^3J_{\text{HH}}=7.4$  Hz, Ar-*H*), 2.02 (6 H, s, Ar- $\text{CH}_3$ );  $^{13}\text{C}$  NMR ( $d_6$ -benzene, 100 MHz):  $\delta$  165.76 (C=O), 137.69, 137.62, 135.58, 133.59 (q,  $^2J_{\text{C-F}} = 32.6$  Hz), 129.60, 128.53, 127.77, 127.41, 125.89 (q,  $^3J_{\text{C-F}} = 3.7$  Hz), 123.64 (q,  $^1J_{\text{C-F}} = 272.4$  Hz), 121.21, 19.86;  $^{19}\text{F}$  NMR ( $\text{CDCl}_3$ , 282 MHz):  $\delta$  63.14 (s, Ar- $\text{CF}_3$ ); MS (EI):  $m/z$  556 ( $\text{M}^+$ );  $\text{C}_{30}\text{H}_{22}\text{N}_2\text{O}_2$ , Anal Calcd for (-)-**11**: C, 64.75; H, 3.98; N, 5.03. Found: C, 65.00; H, 4.00; N, 8.20.

**Proligand (+)-12.** To a solution of (+)-8 (500 mg, 2.36 mmol) and pyridine (400 mg, 0.5 mL, 5.0 mmol) dissolved in chloroform (50 mL) was added 4-trifluoromethylbenzoyl chloride (1.4 g, 5.0 mmol) dropwise. The mixture was refluxed for 16 h, the cooled to room temperature. The mixture was filtered through a plug of silica gel and eluted with dichloromethane (100 mL). The yellow residue obtained was recrystallized by the same biphasic method described for proligands 10 and (-)-11 (3 mL dichloromethane / 20 mL hexanes). The proligands was isolated as colorless needles (1.2 g, 74 %). <sup>1</sup>H NMR (CDCl<sub>3</sub>, 300MHz):  $\delta$  8.19 (2 H, d, <sup>3</sup>J<sub>HH</sub> = 8.2 Hz, Ar-*H*), 7.92 (1 H, s, Ar-*H*), 7.88 (1 H, s, Ar-*H*), 7.83 (2 H, s, Ar-*H*), 7.47 (1 H, t, <sup>3</sup>J<sub>HH</sub> = 8.0 Hz, Ar-*H*), 7.29 (1 H, d, <sup>3</sup>J<sub>HH</sub> = 7.60 Hz, Ar-*H*), 2.07 (6 H, s, Ar-CH<sub>3</sub>); <sup>13</sup>C NMR (*d*<sub>6</sub>-benzene, 100 MHz):  $\delta$  162.87 (C=O), 137.99, 137.62, 136.31, 132.40 (q, <sup>2</sup>J<sub>C-F</sub> = 33.9 Hz), 129.82, 128.35, 128.01, 127.19, 125.36 (m, <sup>3</sup>J<sub>C-F</sub>), 122.71 (q, <sup>1</sup>J<sub>C-F</sub> = 272.7 Hz), 121.13, 19.75; <sup>19</sup>F NMR (CDCl<sub>3</sub>, 282 MHz):  $\delta$  63.49 (s, Ar-CF<sub>3</sub>); MS (ESI): *m/z* 715.3 (M + Na<sup>+</sup>); C<sub>32</sub>H<sub>20</sub>F<sub>12</sub>N<sub>2</sub>O<sub>2</sub>, Anal Calcd for (-)-12: C, 55.50; H, 2.91; N, 4.05. Found: C, 55.80; H, 3.25; N, 4.32.

## Precatalyst Synthesis

### General procedure for the preparation of complexes 13 - 16.

**Example: Complexes (-)-13b or (+)-13c.** In a nitrogen filled glove box, a solution of Zr(NMe<sub>2</sub>)<sub>4</sub> (106 mg, 0.397 mmol) in benzene (2 mL) was added to a suspension of proligand 10 (200 mg, 0.397 mmol) in benzene (2 mL). Upon addition of the Zr(NMe<sub>2</sub>)<sub>4</sub>, the solution turned pale yellow and the insoluble proligand 10 slowly dissolved upon reaction. The solution was stirred overnight at room temperature followed by concentration under vacuum to give a pale yellow solid (246 mg, 90 %). It is important to note that hydroamination reactions employing precatalysts 13 - 16 in were completed using non purified material (Chapter 3). Recrystallization of (+)-13c from pentane at -20 °C was achieved for solid state structural analysis by X-ray crystallography.

**Complex (-)-13a** <sup>1</sup>H NMR (*d*<sub>6</sub>-benzene, 400 MHz):  $\delta$  7.33-7.31 (2 H, m, Ar-*H*), 7.21 (1 H, d, <sup>3</sup>J<sub>HH</sub> = 7.6 Hz, Ar-*H*), 7.15 (1 H, t, <sup>3</sup>J<sub>HH</sub> = 7.6 Hz, Ar-*H*), 7.06 (1 H, d, <sup>3</sup>J<sub>HH</sub> = 7.6 Hz, Ar-*H*), 6.90-6.82 (6 H, m, Ar-*H*), 6.78 (1 H, s, mesityl-*H*), 6.63 (1 H, s, mesityl-*H*), 6.58

(1 H, s, mesityl-*H*), 6.49 (1 H, s, mesityl-*H*), 3.77 (6 H, s, -N(CH<sub>3</sub>)<sub>2</sub>), 3.25 (6 H, s, -N(CH<sub>3</sub>)<sub>2</sub>), 2.99 (6 H, s, -N(CH<sub>3</sub>)<sub>2</sub>), 2.44 (3 H, s, Ar-CH<sub>3</sub>); 2.41 (3 H, s, Ar-CH<sub>3</sub>), 2.25 (3 H, s, Ar-CH<sub>3</sub>), 2.17 (3 H, s, Ar-CH<sub>3</sub>), 2.11 (3 H, s, Ar-CH<sub>3</sub>), 2.09 (3 H, s, Ar-CH<sub>3</sub>), 2.07 (3 H, s, Ar-CH<sub>3</sub>), 2.01 (3 H, s, Ar-CH<sub>3</sub>), 1.76 (3 H, s, Ar-CH<sub>3</sub>), 1.43 (3 H, s, Ar-CH<sub>3</sub>); <sup>1</sup>H NMR at 408K (*d*<sub>10</sub>-xylene, 400MHz): δ 6.99 (2 H, s, Ar-*H*) 6.91-6.84 (4 H, m, Ar-*H*), 6.70 (4 H, s, mesityl-*H*), 3.20 (12 H, s, N(CH<sub>3</sub>)<sub>2</sub>), 2.20 (12 H, s, Ar-CH<sub>3</sub>), 2.14 (6 H, s, Ar-CH<sub>3</sub>), 2.20 (6 H, s, Ar-CH<sub>3</sub>). <sup>13</sup>C APT45 NMR at 300 K (*d*<sub>6</sub>-benzene, 100 MHz); δ 180.49 (C=O), 175.47 (C=O), 160.62, 150.21, 143.54, 142.30, 140.64, 139.36, 139.07, 128.66, 138.58, 137.42, 137.25, 136.43, 135.97, 135.75, 135.68, 135.35, 133.83, 133.58, 133.13, 131.68, 131.02, 129.04, 128.92, 128.81, 128.77, 128.72 (2 signals overlapping), 128.20, 127.84, 127.42, 127.20, 124.70, 123.85, 120.67, 120.04, 47.98 (N(CH<sub>3</sub>)<sub>2</sub>), 46.74, (N(CH<sub>3</sub>)<sub>2</sub>), 44.12(N(CH<sub>3</sub>)<sub>2</sub>), 22.42 (Ar-CH<sub>3</sub>), 21.53 (Ar-CH<sub>3</sub>), 21.47 (Ar-CH<sub>3</sub>), 21.32 (Ar-CH<sub>3</sub>), 21.29, (Ar-CH<sub>3</sub>), 20.96 (Ar-CH<sub>3</sub>), 20.90 (Ar-CH<sub>3</sub>), 20.49 (Ar-CH<sub>3</sub>), 20.38 (Ar-CH<sub>3</sub>), 20.31 (Ar-CH<sub>3</sub>) 22.42 (Ar-CH<sub>3</sub>), 19.83 (Ar-CH<sub>3</sub>); MS(EI): *m/z* 638 (M<sup>+</sup>), 594 (M<sup>+</sup>-NMe<sub>2</sub>), 550 (M<sup>+</sup>-2•NMe<sub>2</sub>); C<sub>38</sub>H<sub>46</sub>N<sub>4</sub>O<sub>2</sub>Ti, Anal. Calcd. for (-)-**13a**: C, 71.46; H, 7.26; N, 8.77. Found: C, 71.40; H, 7.32; N, 8.40; Variable temperature <sup>1</sup>H NMR is illustrated in Appendix I.

**Complexes (-)-13b or (+)-13c.** <sup>1</sup>H NMR (*d*<sub>6</sub>-benzene, 300 MHz): δ 6.88-6.75 (6 H, m, Ar-*H*), 6.70 (2 H, s, Mesityl-*H*), 6.49 (2 H, s, Mesityl-*H*), 3.30 (12 H, s, -N(CH<sub>3</sub>)<sub>2</sub>), 2.61 (6 H, s, -CH<sub>3</sub>), 2.00 (6 H, s, -CH<sub>3</sub>), 1.91 (6 H, s, -CH<sub>3</sub>), 1.81 (6 H, s, -CH<sub>3</sub>); <sup>13</sup>C NMR (*d*<sub>6</sub>-benzene, 400 MHz): δ 189.85, 143.12, 139.13, 138.68, 136.43, 134.65, 132.95, 132.07, 128.77, 128.53, 128.16, 126.15, 121.50, 42.19, 20.83 (2 signals overlap), 20.06, 19.51; MS(EI): *m/z* 680 (M<sup>+</sup>), 636 (M-NMe<sub>2</sub>), 593 (M-2•NMe<sub>2</sub>); C<sub>38</sub>H<sub>46</sub>N<sub>4</sub>O<sub>2</sub>Zr, Anal. Calcd. C, 66.92; H, 6.80; N, 8.21. Found: C, 67.30; H, 7.20; N, 8.00. [α]<sub>D</sub><sup>20</sup> = +422°. ((+)-**13c**), benzene). See Appendix II for <sup>1</sup>H and <sup>13</sup>C NMR spectra.

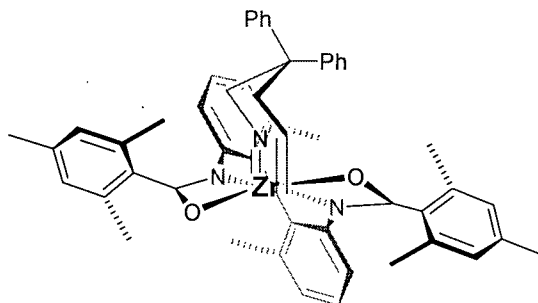
**Complex (-)-15a.** <sup>1</sup>H NMR (*d*<sub>6</sub>-benzene, 300 MHz): δ 7.28 (2 H, dd, <sup>3</sup>J<sub>HH</sub> = 7.2 Hz, 2J = 0.7 Hz, Ar-*H*), 7.13 (6 H, m, Ar-*H*), 6.89-6.87 (4 H, m, Ar-*H*), 6.42 (2 H, dd, <sup>3</sup>J<sub>HH</sub> = 7.6 Hz, <sup>2</sup>J = 0.6 Hz, Ar-*H*), 3.68 (12 H, s, -N(CH<sub>3</sub>)<sub>2</sub>), 0.95 (6 H, s, Ar-CH<sub>3</sub>).); <sup>13</sup>C NMR (*d*<sub>6</sub>-benzene, 100 MHz): δ 172.35 (C=O), 143.49, 140.34, 135.84, 132.1 (q, <sup>2</sup>J<sub>C-F</sub> = 32.3 Hz),



130.36, 128.55, 128.32, 128.10, 126.05, 124.49 (q,  $^3J_{C-F} = 3.8$  Hz), 125.51 (q,  $^1J_{C-F} = 268.5$  Hz), 122.84, 46.23 18.88;  $^{19}\text{F}$  NMR ( $d_6$ -benzene, 282.4 MHz):  $\delta$  63.34 (s, Ar- $\text{CF}_3$ ); MS(EI):  $m/z$  690 ( $\text{M}^+$ ), 646 ( $\text{M}^+ - \text{NMe}_2$ ), 602 ( $\text{M}^+ - 2 \cdot \text{NMe}_2$ );  $\text{C}_{34}\text{H}_{32}\text{N}_4\text{O}_2\text{Ti}$ , Anal. Calcd. for (-)-**15a**: C, 59.14; H, 4.67; N, 8.11. Found: C, 58.80; H, 4.97; N, 8.30.

**Complex (+)-16a:**  $^1\text{H}$  NMR ( $d_6$ -benzene, 300MHz):  $\delta$  7.54 (4 H, s, Ar- $H$ ), 7.52 (2 H, s, Ar- $H$ ), 7.18 (2 H, d,  $^3J_{\text{HH}} = 8.0$  Hz, Ar- $H$ ), 7.04 (2 H, t,  $^3J_{\text{HH}} = 8.0$  Hz, Ar- $H$ ), 6.41 (2 H, d,  $^3J_{\text{HH}} = 7.6$  Hz, Ar- $H$ ), 3.61 (12 H, s,  $-\text{N}(\text{CH}_3)_2$ ), 0.82 (6 H, s, Ar- $\text{CH}_3$ );  $^{13}\text{C}$  NMR ( $d_6$ -benzene, 100MHz):  $\delta$  171.50 (C=O), 143.45, 140.98, 135.66, 132.17 (q,  $^2J_{C-F} = 34.2$  Hz), 130.55, 129.76, 128.85, 127.58, 124.86 (m,  $^3J_{C-F}$ ), 124.00 (q,  $^1J_{C-F} = 272.7$  Hz), 123.73, 47.21, 19.64.  $^{19}\text{F}$  NMR ( $d_6$ -benzene, 282.4 MHz):  $\delta$  63.39 (s, Ar- $\text{CF}_3$ ); MS(EI):  $m/z$  826 ( $\text{M}^+$ ), 782 ( $\text{M}^+ - \text{NMe}_2$ ), 738 ( $\text{M}^+ - 2 \cdot \text{NMe}_2$ );  $\text{C}_{36}\text{H}_{30}\text{F}_{12}\text{N}_4\text{O}_2\text{Ti}$ , Anal Calcd for (-)-**16a**: C, 52.32; H, 3.66; N, 6.78. Found: C, 52.13; H, 3.86; N, 7.12.

## Chapter 3



### Asymmetric Aminoalkene Hydroamination Using Neutral Chiral Zirconium and Titanium Bis(amidate)Bis(amido) Precatalysts

---

#### 3.1 Introduction

Group 4 catalysts for alkene hydroamination have been limited to only a few known reports, and amongst these, only two papers address enantioselectivity.<sup>36,53-56,58-60,92</sup> The Schafer group has recently become focused on preparing chiral group 4 amidate complexes for asymmetric hydroamination. The axially chiral titanium and zirconium precatalysts described in Chapter 2 were designed to examine reactivity and enantioselectivity in aminoalkene hydroamination.

In this chapter, we will first develop a structure activity relationship based on the group 4 metal (titanium versus zirconium) and chiral amidate ligand employed. From the structure activity results, we will utilize the most active and enantioselective catalyst to complete an aminoalkene substrate scope analysis. The mechanism of this reaction will then be probed through the results of the aminoalkene substrate analysis, the X-ray solid state molecular structure of (+)-13b and kinetic investigations.

### 3.2 Precatalyst Reactivity

2,2-Diphenylpent-4-ene-1-amine (**17**) was chosen for initial hydroamination screening of precatalysts **13** - **16** (Figure 3.1). The results are summarized in Tables 3.1 and 3.2, where relative reactivity and enantioselectivity was examined at different catalyst loadings and temperatures.

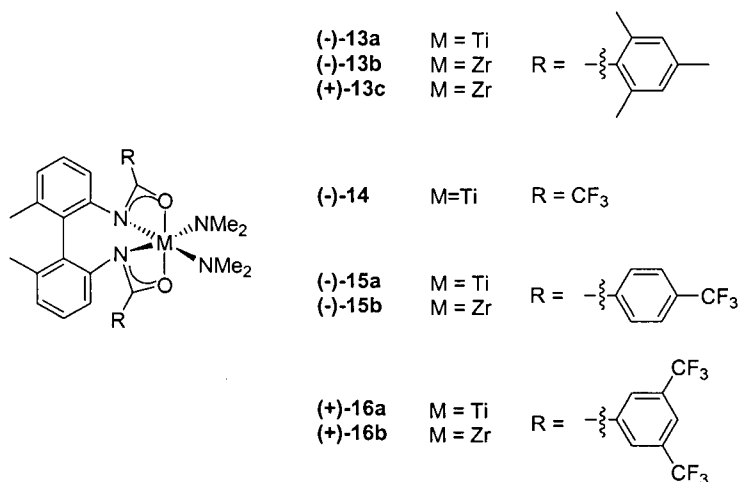
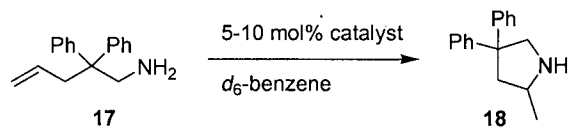


**Figure 3.1** Summary of the titanium and zirconium precatalysts screened for alkene hydroamination catalysis.

Hydroamination reactions in Table 1 were completed using 50 mg of substrate **17** in a Teflon sealed J. Young NMR tube with the specified catalyst and reaction conditions. Reactions were completed at 110 °C in a silicone oil bath with deuterated benzene or toluene as the solvent. Initial hydroamination screening of titanium complex (-)-**13a** showed poor reactivity where reaction times ranged from 24 hours to 5 days depending on the catalyst loading and temperature (Table 1, Entries 3 - 6). At 110 °C and 5 mol % loading, the hydroamination of **17** only proceeded to 24 % conversion after 5 days. Increasing catalyst loading to 10 % resulted in a conversion 86 % over 5 days at 110 °C. The best conditions for precatalyst (-)-**13a** showed 81 % conversion after 24 h with temperatures elevated to 130 °C and 10 mol % catalyst.

**Table 3.1:** Investigation of reactivity for alkene hydroamination using precatalysts **13** - **16** and 2,2-diphenylpent-4-ene-1-amine (**17**) as the aminoalkene test substrate.



Entry	Catalyst	Metal	Mol %	Temp [°C] <sup>a</sup>	Time	% conv. <sup>b</sup>
1	Ti(NMe <sub>2</sub> ) <sub>4</sub>	Ti	10	110	1 h	> 98
2	Zr(NMe <sub>2</sub> ) <sub>4</sub>	Zr	10	110	1 h	> 98
3	(-)-13a	Ti	5	110	5d	24
4	(-)-13a	Ti	10	110	5d	86
5	(-)-13a	Ti	10	130 <sup>c</sup>	24h	81
6	(-)-13a	Ti	10	95	5d	41
7	(+)-13c	Zr	10	110	1h 15 min	>98
8	(+)-13c	Zr	5	110	2.5 h	>98
9	(-)-13b	Zr	10	110	1h 15 min	>98
10	(-)-13b	Zr	10	90	8h	>98
11	(-)-13b	Zr	10	70	48h	>98
12	(-)-14	Ti	5	110	5d	<5
13	(-)-14	Ti	10	110	5d	(stalled) 13
14	(-)-15a	Ti	10	110	6d	(stalled) 33
15	(-)-15b	Zr	10	110	45 min	>98
16	(+)-16a	Ti	10	110	7d	13
17	(+)-16b	Zr	10	110	40 min	>98

[a] Solvent: *d*<sub>6</sub>-benzene [b] based on relative integration of the <sup>1</sup>H NMR for aminoalkene substrate vs. 1,3,5-trimethoxybenzene internal standard. [c] Solvent: *d*<sub>8</sub>-toluene.

To address the poor reactivity observed with titanium catalyst (-)-13a, complexes (-)-14, (-)-15a and (+)-16a were prepared. Our group has shown that installing non-coordinating electron withdrawing substituents into our amidate ligands increases the electrophilicity of the metal center. This has proven to have a positive effect on the rate of reaction for alkyne hydroamination.<sup>65</sup> To investigate this effect on alkene hydroamination, trifluoromethyl substituents were installed at different positions on the

axially chiral amidate ligands (Figure 3.1). Of the ligands analyzed, Complex (-)-**14** contains a trifluoromethyl substituent directly attached to the amide carbonyl (trifluoroacetamide), while (-)-**15a** and (+)-**16a** have trifluoromethylphenyl substituents at the amide carbonyl.

Precatalyst (-)-**14** displayed catalytic reactivity, but the reaction was extremely slow compared to (-)-**13a** and stalled with less than 5 % conversion after 5 days at 110 °C with 5 mol % catalyst loading (Table 3.1, Entry 12 and 13). Increasing the catalyst loading to 10 mol % showed further conversion to 13 %, however, the reaction stalled once again after 5 days. Closer analysis of the <sup>1</sup>H NMR spectrum showed catalyst decomposition. In order to understand the decomposition pathway, a stoichiometric reaction was completed using a hydrogenated analogue of substrate **17** (**17b**, Figure 3.2). Substrate **17b** was chosen so that only *N*-substituted byproducts would form, and no pyrrolidine product would be produced. The reaction was left heating overnight at 110 °C in a sealed NMR tube, then diluted with dichloromethane, filtered through celite and analyzed by <sup>1</sup>H NMR spectroscopy and GC-MS analysis. The GC-MS chromatogram in Figure 3.2 shows the catalyst decomposition products for the reaction of **17b** with precatalyst (-)-**14**. Compounds B and D are transamidation byproducts, A is proligand and C, E and F were not identified.

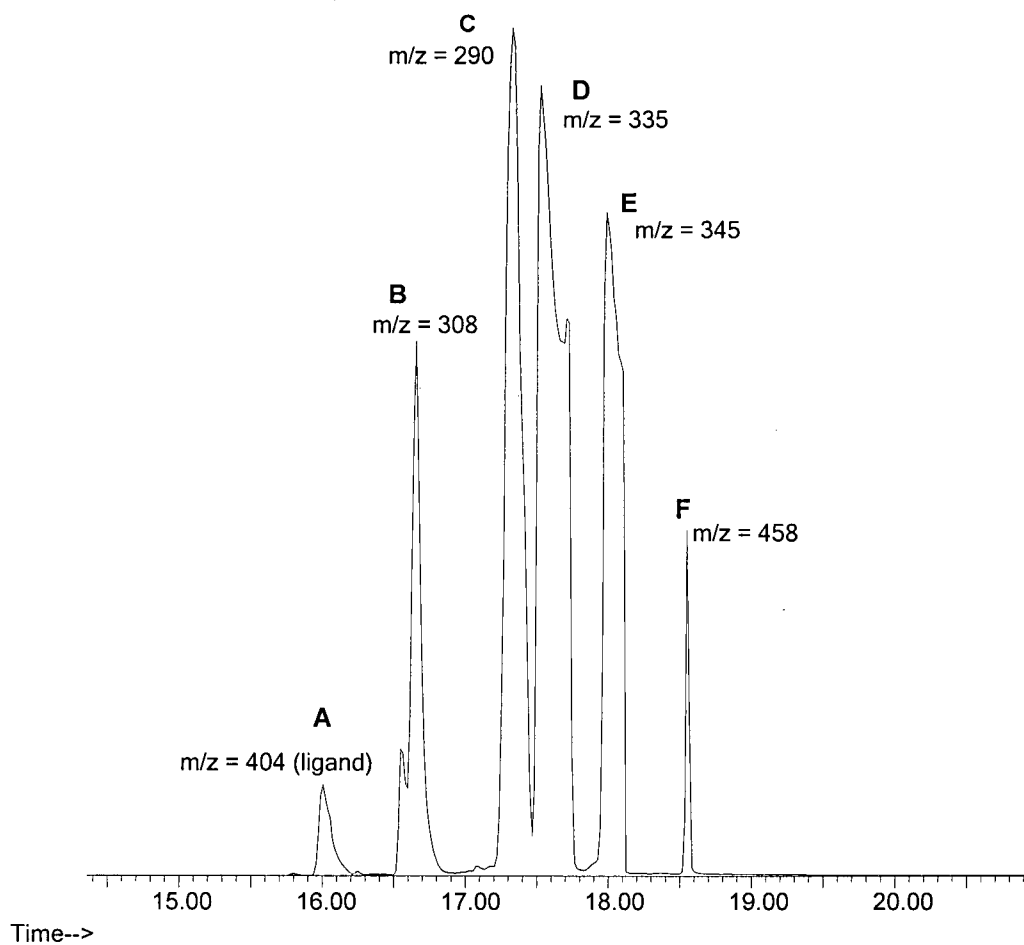
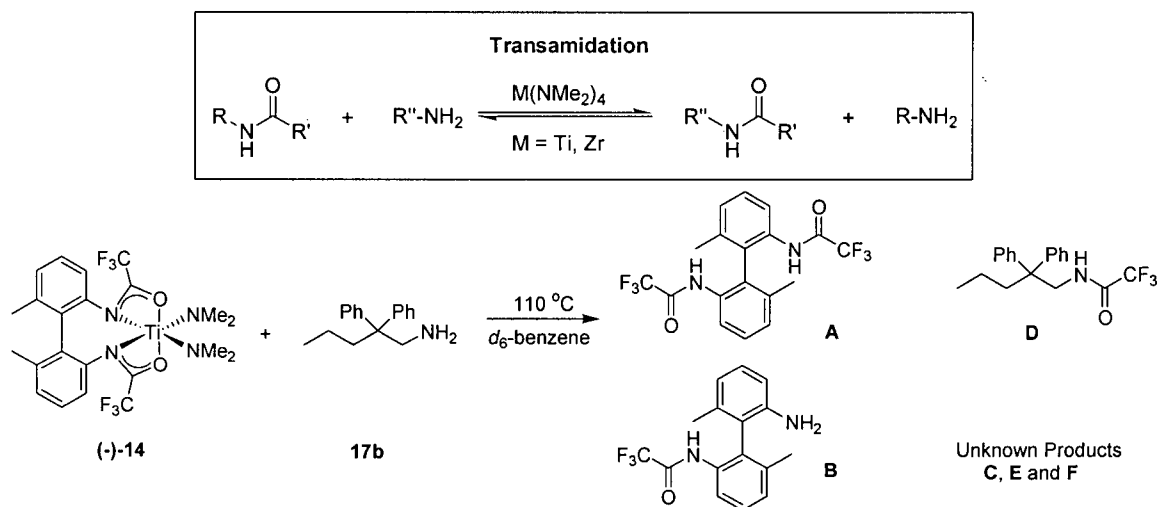


**Figure 3.2** GC-MS analysis of products obtained from the stoichiometric reaction of **17b** with precatalyst **(-)-14**. [**A**] = proligand **(-)-9**, [**B**] = monosubstituted ligand, and [**D**] = transamidation product. [**C**], [**E**] and [**F**] are unidentified byproducts.

Transamidation has been identified by Stahl and coworkers who showed that Ti(IV) has the ability to activate carboxamides.<sup>93</sup> It is an efficient way to interconvert the N-substituent of an amide with another primary amine under moderate conditions. For Stahl and coworkers, transamidation showed the most promising results with catalytic amounts of Ti(NMe<sub>2</sub>)<sub>4</sub> at 90 °C (toluene, 16 h). For this catalysis, it is likely that amidate complexes are formed as intermediates during this reaction, and it is possible that our complexes could show similar reactivity. Since the catalytic hydroamination reactions with precatalyst (-)-**14** (Table 3.1, entries 12 and 13) were completed with excess amine at 110 °C, transamidation is a feasible decomposition pathway. Although results were poor for hydroamination using catalyst (-)-**14**, we discovered that our system requires more steric bulk and less reactive amides in order to avoid such undesired reactive pathways. Transamidation has not been observed for any other bis(amidate)bis(amido) group 4 complexes prepared by our group, therefore, bulky aryl and alkyl amidate ligands are considered.

To increase the steric bulk of the electron withdrawing substituent on the amidate ligand, *p*-trifluoromethylphenyl and 3,5-bis(trifluoromethyl)phenyl were employed in complexes (-)-**15a** and (+)-**16a**. Hydroamination of substrate **17**, using precatalysts (-)-**15a** and (+)-**16a**, also displayed poor reactivity similar to precatalyst (-)-**13a**, however, no decomposition was observed (Table 3.1, entries 14 & 16). Cyclization of **17** with precatalyst (-)-**15a** went to 33 % conversion after 6 days at 110 °C, while with catalyst (+)-**16a**, the reaction only went to 13 % conversion after 7 days. The low reactivity of titanium precatalysts (-)-**13a**, (-)-**15a** and (+)-**16a** may well be attributed to a congested coordination environment around titanium. Results by Bergman and coworkers showed similar trends when they employed bis(dimethylamido) titanium and zirconium catalysts as aminoalkene hydroamination.<sup>58</sup> They employed the same ligand on both zirconium and titanium, and the titanium analogue showed lower reactivity. They also showed that the most sterically demanding ligands on titanium gave poor reactivity (<5 % conversion, 20 mol % catalyst, 24 h at 135 °C) while the zirconium analogues showed excellent conversion under identical reaction conditions (90 % conversion, 20 mol % catalyst, 24 h at 135 °C). Additionally, we have showed that Zr(NMe<sub>2</sub>)<sub>4</sub> and Ti(NMe<sub>2</sub>)<sub>4</sub> have similar reactivity for hydroamination of aminoalkene **17** (Table 3.1,

Entries 1 and 2). Therefore, the steric influence for  $\text{Zr}(\text{NMe}_2)_4$  versus  $\text{Ti}(\text{NMe}_2)_4$  is not significantly different and this suggests that the steric bulk imposed by a ligand is what affects reactivity and not the metal itself. Overall, increasing the size of the metal decreases the amount of steric congestion imposed by the amidate ligands, and therefore an improvement in reactivity is observed.

Investigations by the Schafer group have also shown that bis(amidate)bis(amido) zirconium precatalysts are more reactive toward aminoalkene hydroamination than their titanium counterpart.<sup>53</sup> To determine if this same trend could be observed with the axially chiral tetradentate amidate ligands employed, the zirconium analogs were also prepared. Zirconium complexes **(-)-13b** and **(+)-13c**, which are enantiomers, cyclized substrate **17** in 75 min at 110 °C with 10 mol % catalyst loading (Table 3.1, Entries 7 and 9). When the catalyst loading of **(+)-13c** was decreased from 10 mol % to 5 mol %, the reaction time doubles. The zirconium complexes showed significantly higher reactivity in comparison to the titanium analogue **(-)-13a**. This result is in correspondence with the literature for aminoalkene hydroamination employing group 4 catalysts.<sup>53,58</sup> The enhancement in reactivity was also observed for the *p*-trifluoromethylphenyl and 3,5-bis(trifluoromethyl)phenyl substituted bis(amidate) zirconium complexes **(-)-15b** and **(+)-16b**. Hydroamination of **17** was complete in 45 minutes for complex **(-)-15b**, and 40 minutes with complex **(+)-16b**. As anticipated, the trifluoromethyl substituted catalysts were more reactive than the mesityl complexes **(-)-13b** and **(+)-13c**.

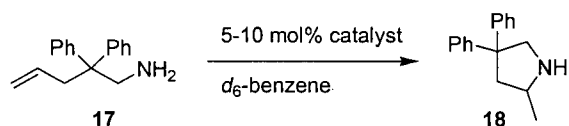
The ultimate achievement would be a general group 4 catalyst capable of alkene hydroamination at room temperature. Though hydroamination with **(-)-13b** and **(+)-13c** does not proceed at room temperature, it does proceed at temperatures as low as 70 °C, though at a much slower rate (48 h). When the temperature was raised to 90 °C, the reaction was complete in 8 h which was more practical than a 48 h reaction time (Entry 10, Table 3.1). Overall we have shown that the zirconium complexes **(-)-13b**, **(+)-13c**, **(-)-15b** and **(+)-16b** are much more reactive than the titanium complexes **(-)-13a**, **(-)-15a** and **(+)-16a**. The addition trifluoromethyl substituents also showed an increased reactivity, with the exception of complex **(-)-14** which showed decomposition by transamidation.



### 3.3 Asymmetric Hydroamination

The aminoalkene hydroamination reactions discussed in Section 3.2 were also examined for enantioselectivity. Once again, 2,2-diphenylpent-4-ene-1-amine **17** was used as a test substrate (Table 3.2).

**Table 3.2:** Investigation of enantioselectivity for alkene hydroamination using precatalysts **13** - **16** and 2,2-diphenylpent-4-ene-1-amine as the aminoalkene test substrate.



Entry	Catalyst	Metal	Mol %	Temp [°C] <sup>a</sup>	Time	% conv. <sup>b</sup>	% ee <sup>c</sup>
1	(-)-13a	Ti	5	110	5d	24	69
2	(-)-13a	Ti	10	110	5d	86	70
3	(-)-13a	Ti	10	130 <sup>d</sup>	24h	81	64
4	(-)-13a	Ti	10	95	5d	41	69
5	(+)-13c	Zr	10	110	1h 15min	>98	74(R) <sup>e</sup>
6	(+)-13c	Zr	5	110	2.5 h	>98	71
7	(-)-13b	Zr	10	110	1h 15min	>98	72(S) <sup>e</sup>
8	(-)-13b	Zr	10	90	8h	>98	70
9	(-)-13b	Zr	10	70	48h	>98	70
10	(-)-15a	Ti	10	110	6d	33	55 %
11	(-)-15b	Zr	10	110	45 min	>98	18 %
12	(+)-16a	Ti	10	110	7d	13	-
13	(+)-16b	Zr	10	110	40 min	>98	11 %

[a] Solvent: *d*<sub>6</sub>-benzene [b] based on relative integration of the <sup>1</sup>H NMR for aminoalkene substrate vs. 1,3,5-trimethoxybenzene internal standard [c] determined by <sup>1</sup>H NMR of the (*S*)-(+)- $\alpha$ -methoxy- $\alpha$ -(trifluoromethyl)phenylacetyl chloride derivative [d] Solvent: *d*<sub>8</sub>-toluene [e] absolute stereochemistry based on <sup>19</sup>F NMR of (*S*)-(+)- $\alpha$ -methoxy- $\alpha$ -(trifluoromethyl)phenylacetyl chloride derivative matched to literature values.<sup>32</sup>

Enantiomeric excess in Table 3.2 was determined by <sup>1</sup>H NMR analysis after derivatization with (*S*)-(+)- $\alpha$ -methoxy- $\alpha$ -(trifluoromethyl)phenylacetyl chloride (Mosher's amide derivative). The resulting amide products are a mixture of diastereomers that are inequivalent by NMR spectroscopic analysis. The  $\alpha$ -methyl

hydrogens of the (R)- and (S)-pyrrolidine products (**18**) are in different chemical environments, and as a result, display two different doublets separated by 0.2 ppm in the  $^1\text{H}$  NMR spectrum. The pyrrolidine  $\alpha$ -methyl region of the  $^1\text{H}$  NMR spectrum of **18** is illustrated in Figure 3.3 for the Mosher amide diastereomer products. Figure 3.3A shows the derivatized product obtained when (-)-**13b** is used as the precatalyst and the (S)-enantiomer is the major product (Entry 7). Figure 3.3B shows the derivatized product obtained from precatalyst (+)-**13c** where the (R)-enantiomer is the major product (Entry 5).  $^{19}\text{F}$  NMR spectroscopy was not used to determine enantioselectivities because the  $^{19}\text{F}$  resonances are very broad signals at room temperature.  $^1\text{H}$  NMR was a sufficient method to determine the ee's of **18**, and no broadening was observed.

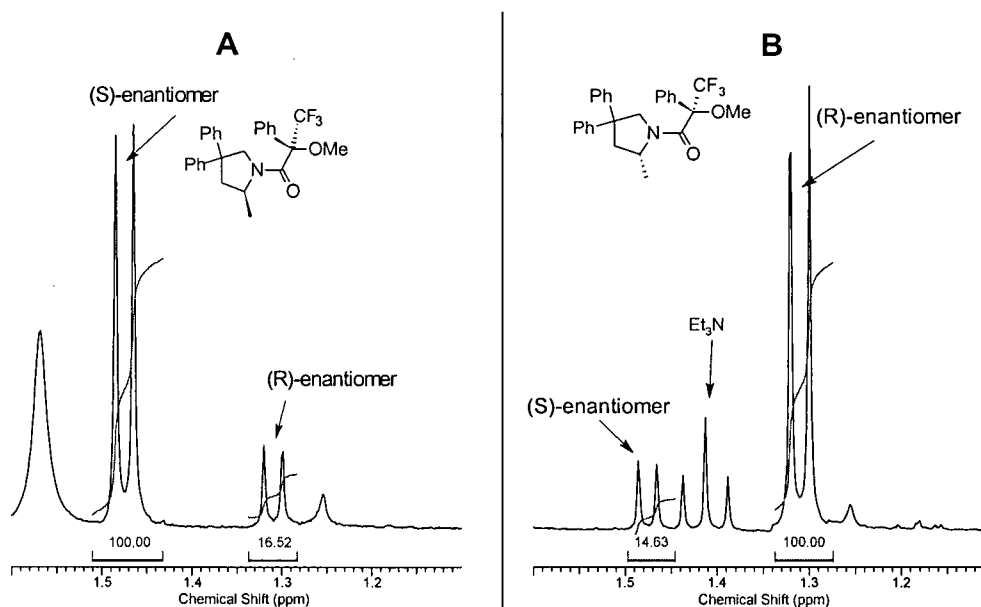


**Figure 3.3**  $^1\text{H}$  NMR spectrum for Mosher amide derivatives of the (S)- and (R)-pyrrolidine products (**18**) obtained using precatalyst (-)-**13b** [A] and (+)-**13c** [B].

The ee obtained for pyrrolidine **18**, employing the less reactive titanium complex (-)-**13a**, was 69 % at 5 mol % catalyst loading (Entry 1). Increasing the catalyst loading (10 mol %, Entry 2) or varying the temperature (130 °C, Entry 3 / 95 °C, Entry 4) did not dramatically alter the enantioselectivity. On the other hand, the more reactive zirconium complexes (-)-**13b** and (+)-**13c** produced similar ee's of 72 % and 74 % respectively. When the catalyst loading was decreased to 5 mol %, no loss in enantioselectivity was observed, however, reaction time doubled (Table 1, Entry 8). Fortunately, no change in ee was observed when the temperature of the reaction was varied using precatalyst (-)-

**13b** (90 °C, Entry 8 / 70 °C, Entry 9). Complexes **(-)-13b** and **(+)-13c** also produced slightly improved enantioselectivities over their titanium counterpart **13a** (Table 1, Entries 8-11). Most importantly, reversed selectivity was also observed where precatalyst **(-)-13b** produces the (S)-pyrrolidine product (Entry 7), while precatalyst **(+)-13a** produces the (R)-pyrrolidine (Entry 5).

The increase in reactivity for the *p*-trifluoromethylphenyl and 3,5-bis(trifluoromethyl)phenyl substituted catalysts **15** and **16** was not reflected in the observed enantioselectivity (Entries 10 - 13). For the titanium complex **(-)-15a** the observed enantioselectivity was 55 %, however the ee was not determined for complex **(+)-16a** due to low the conversion of **17** (13 %). For the zirconium analogues **(-)-15b** and **(+)-16b**, the ee's were 18 % and 11 % respectively. Overall, the low ee's obtained for the trifluoromethyl substituted precatalysts **15** and **16** were unattractive, so further investigations were not completed on these precatalysts. Nevertheless, the higher reactivity observed for **(-)-15b** and **(+)-16b** are a step in the right direction towards a more reactive alkene hydroamination catalyst.

Based on the trends in Table 3.2, the steric bulk imposed by the mesityl group was much more significant compared to *p*-trifluoromethylphenyl and 3,5-bis(trifluoromethyl)phenyl. Our group has also investigated adamantyl and naphthyl substituted biphenylamidate zirconium analogs of these precatalysts and lower ee's of 39% and 31% were also observed.<sup>57</sup> The mesityl substituted complexes **13** have produced the most excellent enantioselectivities, and the steric bulk imposed by the mesityl substituent appears to be very important for this transformation. The rationale behind this trend will be examined in further detail in Chapter 3.4.

Precatalysts **(-)-13b** and **(+)-13c** were identified as the most reactive and selective catalysts for hydroamination of 2,2-diphenyl-pent-4-enylamine. Substrate scope investigations were performed to probe the effects that different *gem*-substituents have on enantioselectivity and reactivity (Table 3.3). Since the enantioselectivity was shown not to be affected by temperature, catalytic reactions were completed at 110 °C to minimize reaction time. Focusing on the entries in Table 3.3, we first examined *gem*-diphenyl (Entry 1-3) and *gem*-dimethyl (Entries 4 - 7) substituted aminoalkenes. Hydroamination of **17** at 5 mol% was complete in 2.5 h at 110 °C producing pyrrolidine **18** with an ee of

74% and an isolated yield of 93 %. Precatalyst (+)-**13c** showed similar reactivity to  $\text{Zr}(\text{NMe}_2)_4$  for the cyclization of compound **17**. Precatalyst (+)-**13c** cyclized **17** in 2.5 hours and  $\text{Zr}(\text{NMe}_2)_4$  cyclized **17** in 2 hours (Table 2, Entry 2). 2,2-diphenyl-hex-5-enylamine **19** was converted to piperidine **19b** in 3h at 110 °C. The product was isolated with a yield of 91 % and an ee of 29 %. This lower ee has also been observed in the literature when the aminoalkene chain length is increased by one carbon.<sup>58</sup> This is likely associated with the higher degree of freedom in an eight-membered metallocycle versus the seven-membered metallocycle in pyrrolidine formation (*vide infra*).

**Table 3.3** Aminoalkene substrate scope investigations with precatalysts (-)-**13b** and (+)-**13c** in  $d_6$ -benzene at 110 °C.

Entry	Catalyst loading [mol %]	Aminoalkene substrate	Product	Time [h]	Yield [%]	ee [%]
1	5 (+)- <b>13c</b>			2.5 h	93 <sup>a</sup>	74 (R) <sup>d,f</sup>
2	5 mol% $\text{Zr}(\text{NMe}_2)_4$	<b>17</b>	<b>18</b>	2 h	>98 <sup>b</sup>	-
3	10 (+)- <b>13c</b>			3	91 <sup>a</sup>	29 <sup>d</sup>
4	10 (+)- <b>13c</b>			7	80 <sup>c</sup>	93 <sup>d</sup> (92) <sup>i</sup>
5	10 mol% $\text{Zr}(\text{NMe}_2)_4$	<b>20</b>	<b>20b</b>	20	>98 <sup>b</sup>	-
6	10 mol% (+)- <b>13c</b>			18 <sup>g</sup>	92 <sup>a</sup>	20 <sup>i</sup>
7	10 mol% $\text{Zr}(\text{NMe}_2)_4$	<b>21</b>	<b>21b</b>	18 <sup>g</sup>	>98 <sup>b</sup>	-
8	10 (+)- <b>13c</b>			4.5	82 <sup>a</sup>	74 <sup>d</sup> (76) <sup>i</sup>

[a] isolated yield [b] NMR yield [c] isolated yield following derivatization with benzoyl chloride. [d] enantiomeric excess based on  $^1\text{H}$  NMR of the product (+)-(S)-a-methoxy-a-trifluoromethylphenylacetyl chloride derivative. [e] enantiomeric excess based on  $^{19}\text{F}$  NMR of the product (+)-(S)-a-methoxy-a-trifluoromethylphenylacetyl chloride derivative. [f] absolute stereochemistry assigned based on  $^{19}\text{F}$  NMR of the (+)-(S)-a-methoxy-a-trifluoromethylphenylacetyl chloride derivative. [g] reaction time not monitored [h] diastereomeric ratios determined by  $^1\text{H}$  NMR. [i] ee determined by GM-MS analysis of (+)-(S)-a-methoxy-a-trifluoromethylphenylacetyl chloride derivative.

When *gem*-diphenyl substituents are replaced with *gem*-dimethyl, the reaction rate decreases, however selectivity was greatly improved. Hydroamination of 2,2-dimethyl-pent-4-enylamine **20** was achieved in 7 h at 110 °C to produce **20b** with an ee of 93 % (92 % by GC-MS) and isolated yield of 80 % as the benzoyl amide derivative (Table 3.3, Entry 4). This is the highest enantiomeric excess ever reported for a neutral group 4 hydroamination catalyst, and the highest ever observed for this common test substrate. The hydroamination of 2,2-dimethyl-hex-5-enylamine **21** produced **21b** with an ee of 20 %, which was lower than the diphenyl analogue 2,2-diphenyl-hex-5-enylamine **19**. Hydroamination of **22**, which contains two *gem* diallyl substituents, was complete in 4.5 h with an isolated yield of 82 % and an ee of 74 % (Table 3.3, Entry 8).

Complex (-)-**13b** and (+)-**13c** displayed the highest enantioselectivities among the catalysts prepared. Enantioselectivities were reproducible, and opposite enantiomers could be obtained when either (-)-**13b** and (+)-**13c** were employed. Enantioselectivities for the formation of pyrrolidine products ranged from 74 to 93 % percent, while piperidine products showed lower ee's of 20 to 29 %. Most reactions displayed high conversions (>98 %) and isolated yields ranging from 80 to 93 %. From here in, the mechanistic aspects behind the observed enantioselectivity will be discussed, and additional substrate scope analysis will be completed to further justify the mechanistic hypotheses.

### 3.4 Mechanistic Rationale

One of the key focuses of our group has been understanding which of the proposed hydroamination mechanisms in the literature is an accurate model for our bis(amidate)bis(amido) group 4 complexes. For group 4 hydroamination catalysts, we can predict that the mechanism is either going through a metal imido complex followed by a [2+2] cycloaddition with a C-C multiple bond, or metal amido complex followed by sigma-bond insertion of a C-C multiple bond. Having an understanding of mechanism should help us determine how and why we observe enantioselectivity as well as what can be done to improve it. Section 3.4 will describe the experiments conducted that support an imido mechanism, and will also explain the rationale behind the observed enantioselectivity for aminoalkene hydroamination using precatalyst **13**.

Depending upon the catalyst, the mechanism for hydroamination can either involve the activation of the carbon-carbon multiple bond, or the N-H amine bond.<sup>6</sup> Reaction at the C-C multiple bond typically occurs in late transition metal complexes. With the early transition metals and lanthanides, N-H activation is the primary mechanism where either an imido-cycloaddition or an amido-sigma bond insertion reaction can occur.

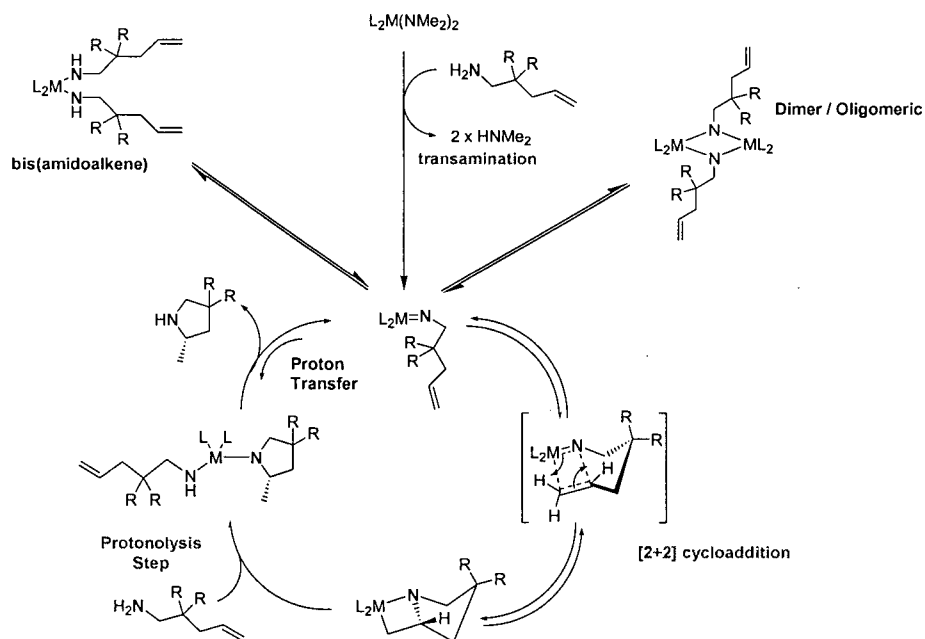


**Figure 3.4:** Proposed catalytic cycle for bis(amidate)bis(amido) group 4 metal catalyzed hydroamination of *gem*-disubstituted aminoalkenes.

As described in the Introduction, the proposed mechanism for group 4 alkyne hydroamination catalysts is well established in the literature.<sup>2,47,50-52</sup> We have strong evidence that our bis(amidate) catalytic systems follow a similar mechanism.<sup>53,57,65,66,73,74,92</sup> The reaction, as understood, proceeds through an metal-imido species which subsequently undergoes a [2+2] cycloaddition with the C-C multiple bond (Figure 3.4). The resulting metallocycle then undergoes a second protonolysis with another equivalent of substrate followed by a subsequent proton transfer to give the product and regenerate the imido complex. From this catalytic cycle, it is also apparent that the enantioselectivity is introduced during the cycloaddition step.

It appears that the catalytic cycle is straightforward, but there are a number of unproductive pathways that may reduce the efficacy of the precatalyst. For instance, from the catalytically active imido species, there are several unproductive equilibria that could take place. Two examples of these competitive pathways are displayed in Figure 3.4. The imido can self condense to form dimeric or oligomeric compounds, or react with another equivalent of the aminoalkene substrate to make a bis(amidoalkene). If these unproductive pathways are more stabilized than the imido, the catalyst could be less efficient. In order to avoid these, bulky substituents are built into the ligand backbone.

While Figure 3.4 represents a common mechanism in the literature, it has also been suggested that Lewis acidic metals are prone to the generation of a proton *in-situ*.<sup>61</sup> In order to rule this out, complex (+)-13c was also tested for catalytic activity in the presence of a bulky non-coordinating base 2,6-di-*tert*-butyl-4-methylpyridine. The reaction remained unaffected thus opposing the likelihood that a proton catalyzed process is taking place. For example, other claims of group 4 catalyzed hydroamination, such as the TiCl<sub>4</sub> hydroamination reported by Ackermann,<sup>59,60</sup> have been shown to proceed through a proton catalyzed route rather than metal mediated.<sup>61</sup>

Preliminary kinetic investigations with complex (+)-13c for the hydroamination of 2,2-diphenylpent-4-ene-1-amine 17 show the reaction is first order in substrate (Figure 3.5). The reaction shows first order kinetics for 5 %, 7.5 %, 10 % and 12.5 % catalyst loading until approximately 60 % consumption of the aminoalkene substrate. First order kinetics for consumption of substrate is consistent with a protonolysis reaction being a rate limiting step.<sup>53</sup> It is recognized that group 3 and lanthanoid complexes proceed

through an insertion mechanism, and typically display zero-order dependence on substrate and first order dependence on catalyst.<sup>6</sup> Zero order dependence on substrate is consistent with the olefin insertion step being the rate limiting. Other group 4 catalysts developed for hydroamination show an induction period which is proposed to be due to the formation of the imido-intermediate.<sup>47</sup> Since we do not detect an induction period, this imido formation must be very fast, and as a result the imido formation must not be the rate limiting step. This implies that the rate limiting step is the second protonolysis event in Figure 3.4.

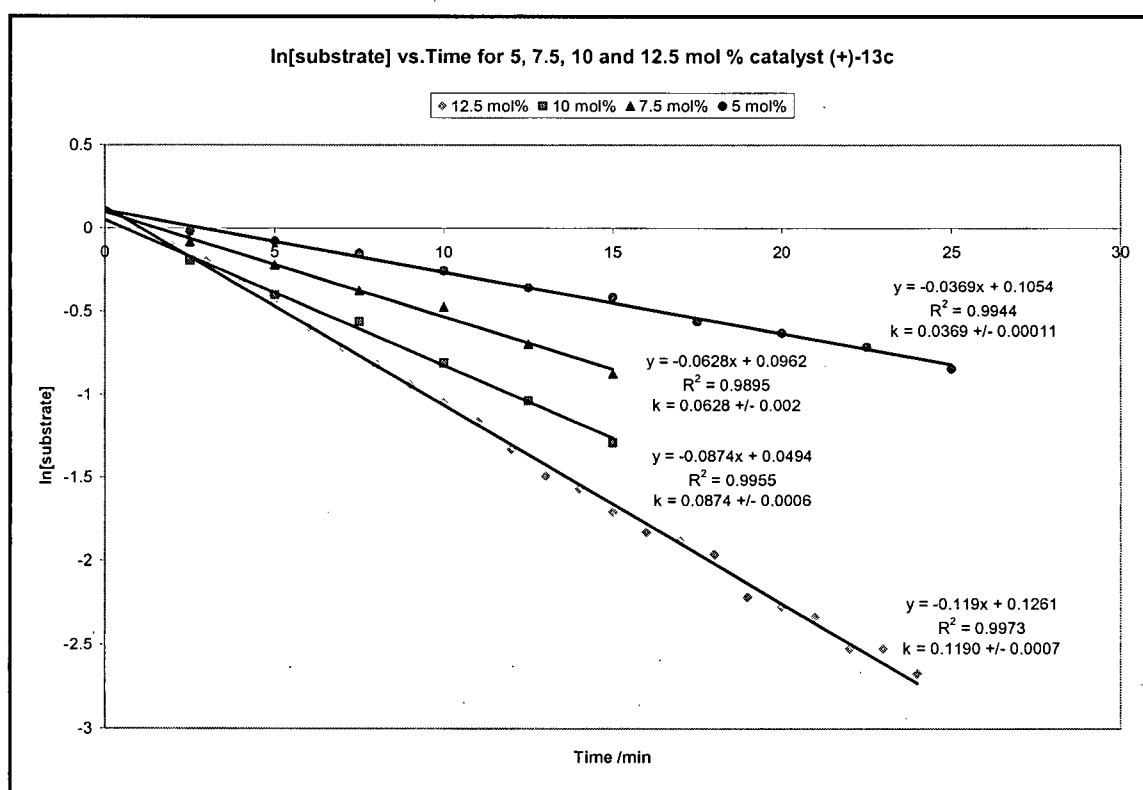


**Figure 3.5** Plot of ln[substrate 17] vs time for hydroamination of 17 at 140 °C in  $d_8$ -toluene using precatalyst (+)-13c. First order in substrate consumption up to ~60% conversion.



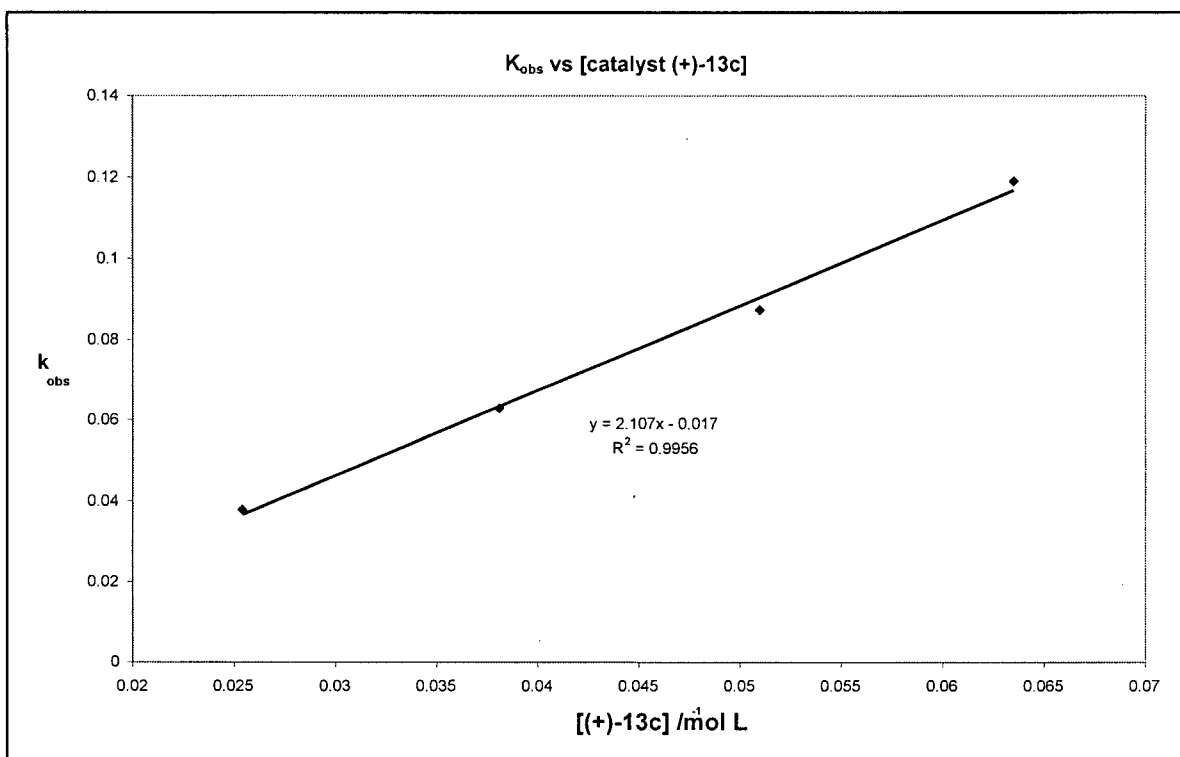


**Figure 3.6** Plot of  $k_{obs}$  vs  $[(+)\text{-}13\text{c}]$  for hydroamination of **17** at 110 °C in  $D_8$ -toluene at 5, 7.5, 10 and 12.5 mol % precatalyst  $(+)\text{-}13\text{c}$  at constant substrate concentration.

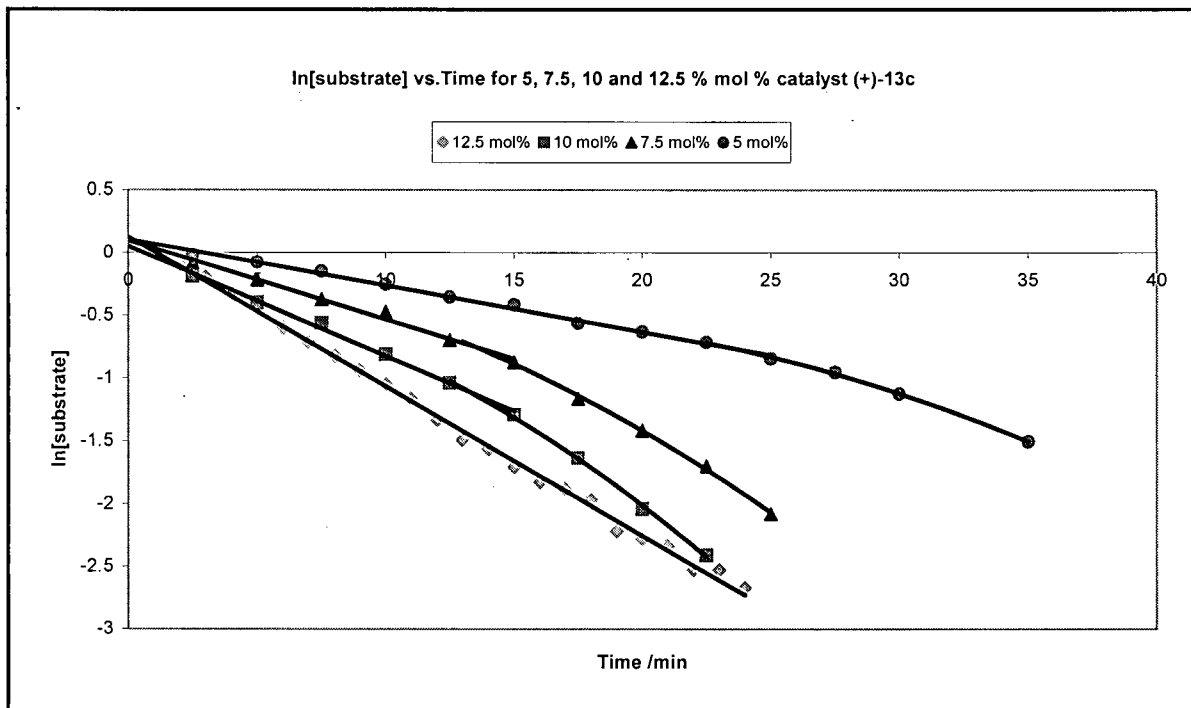


**Figure 3.7** Plot of ln[substrate **17**] vs time for hydroamination of **17** at 110 °C in  $d_8$ -toluene using precatalyst  $(+)\text{-}13\text{c}$ . Shows extended plot where product inhibition of the catalyst is observed in the latter part of the reaction.

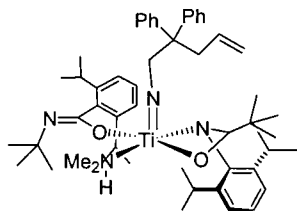
A plot of the observed rate constant  $k_{\text{obs}}$  vs the concentration of catalyst (+)-**13c** yields a linear curve which shows first order kinetics in catalyst and is indicative of a monomeric catalytically active species (Figure 3.6). Therefore, there is rate dependence on the concentration of catalyst (+)-**13c**. After approximately 60 % conversion, the mechanism changes and first order kinetics are no longer observed. Figure 3.7 shows the extended plot for the reactions where linearity is no longer observed for the remaining reaction time. The deviations in the late stages of this reaction suggest that first order kinetics no longer apply. Similar deviations have also been reported in the literature for product inhibition,<sup>26,94</sup> however, the increasing rate (slope) at later stages of these reactions suggests substrate inhibition could be occurring (Figure 3.7).

In further support of an imido mechanism, it has been observed that our bis(amidate) group 4 catalysts show no reactivity toward secondary aminoalkene substrates.<sup>53,55</sup> Secondary aminoalkene **28** (Table 3.5, Entry 4) displayed no reactivity with the zirconium precatalyst (+)-**13c**, even with extended reaction times (days) and elevated temperatures (140 °C). If hydroamination of the secondary aminoalkene substrate **28** had proceeded with precatalyst (+)-**13c**, it would be indicative of sigma-bond insertion rather than an imido cycloaddition mechanism.

Based on X-ray solid state structures of bis(amidate)imido zirconium complexes and experimental data described by our group,<sup>53</sup> we suggest that the catalysis occurs through an imido mechanism and not a sigma-bond insertion mechanism. A six coordinate triphenylphosphine oxide stabilized bis(amidate) zirconium imido complex (Chapter 1, complex **2**) has been prepared and fully characterized by our group.<sup>53</sup> In this complex, the amidate and triphenylphosphine oxide (TPPO) ligand are in the equatorial plane and the 2,6-dimethylphenyl imido ligand is in the axial position generating a distorted pentagonal pyramidal geometry. The amidate and TPPO ligands orient themselves in the equatorial plane while the M=N overlap is maximized along the z-axis. The short bond length of 1.853 Å, and nearly linear bonding mode, suggests that triple bond character exists in the metal imido bond. This metal imido complex illustrates that the imido ligand occupies the axial position perpendicular to the amidate ligands. Other non-cyclopentadienyl based group 4 imido complexes, such as the bis(guanidinate)

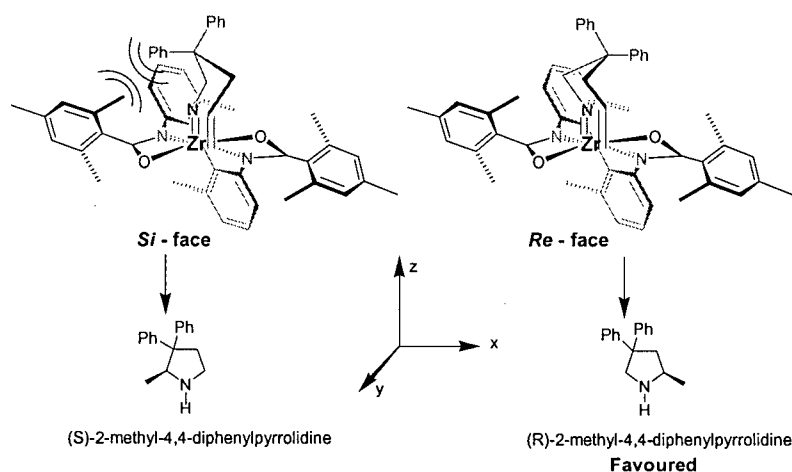
complex reported by Richeson and coworkers, also supports an axial imido coordination mode.<sup>67</sup>

Closer examination of the solid state structure of complex (+)-**13c** (Chapter 2, Figure 2.4), shows that one 4e<sup>-</sup> dimethylamido ligand as well as an 8e<sup>-</sup> tethered bis(amidate) ligand occupy the equatorial plane. The axial positions are occupied by a 4e<sup>-</sup> dimethylamido and a 2e<sup>-</sup> neutral dimethylamine donor resulting in an 18e<sup>-</sup> complex. It can be predicted, based on the bis(amidate) imido complexes reported by our group and others,<sup>67</sup> that a 6e<sup>-</sup> imido ligand will likely be in the axial position (z-axis), while the tethered tetradentate amidate ligand would occupy the equatorial plane. The rigid biphenyl pulls the amidates back so the two oxygens of the amidates are at a 167° angle. This opens up the fifth coordination site in the xy-plane which can be occupied by another donor such as, for example, the alkene from the substrate prior to cycloaddition. The open reactive site of complex **13** may explain why the cyclization of aminoalkene **17** is faster than zirconium complex **4** (Figure 1.4, Chapter 1) which contains two bidentate amidate ligands rather than a tetradentate amidate ligand.<sup>53</sup>



**Figure 3.8** Illustration that is representative of the X-ray solid state structure for an imido complex recently prepared by our group.

Recent unpublished results by our group include the isolation of a bis(amidate)titanium imido complex seen in Figure 3.8.<sup>95</sup> The solid state structural of this complex contains substrate **17** bound as an imido with the one amidate ligand bound  $\kappa_2$ , and the other monodentate ( $\kappa_1$ ) through the amidate oxygen. A neutral dimethylamine is bound occupying the free coordination site rather than the alkene from the substrate or the nitrogen from the monodentate ligand. The amidate and dimethylamine ligands are pseudo-square planar with the imido ligand occupying the axial position producing a pseudo-square pyramidal geometry. This isolated imido-alkene titanium complex further supports invoking an imido intermediate in our proposed mechanism in Figure 3.7. The amidate ligand hemi-lability may also rationalize the poor enantioselectivity observed with titanium complex (-)-**13a**.



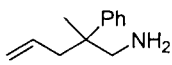
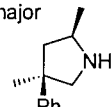
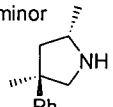
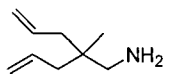
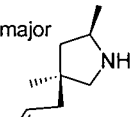
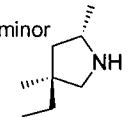
**Figure 3.9:** Proposed mechanism for enantioselectivity of aminoalkene **17** using precatalyst **(+)-13c**. The approach of the alkene is preferential from the *Re*-face rather than the *Si*-face resulting in enantiomeric excess favoring the (R)-pyrrolidine product **18**.

Figure 3.9 illustrates a working model to rationalized observed enantioselectivity induced by complex **(+)-13c** for the hydroamination of substrate **17**. This mechanism is based on a combination of solid state structural data (Chapter 2, Figure 2.4), the proposed catalytic cycle (Figure 3.4), and the axial metal-imido coordination mode described earlier. Based on the NMR data collected for precatalyst **(+)-13c**, the complex is  $C_2$  symmetric in solution with no evidence of a neutral dimethylamine ligand. When the zirconium imido is produced as the active intermediate, it is equivalent in either the positive or negative z-axis based on symmetry. As illustrated, the imido in Figure 3.9 is a  $14e^-$  square pyramidal complex, but clearly during a hydroamination reaction there is no shortage of donor ligands available to fill the vacant coordination sites. The terminal alkene from the aminoalkene imido intermediate approaches the Zr-N bond from the front face opposite the biphenyl backbone. During the cycloaddition, a ‘chair-like’ transition state is produced where the alkene can approach from either the *Si*- or the *Re*-face. If the olefin approaches from the *Si*-face, the diphenyl substituents in the geminal position are interacting unfavorably with the mesityl groups on the ligand forcing the chair to ring-flip. The ring-flip minimizes the steric interaction favoring (R)-2-methyl-4,4-diphenylpyrrolidine **(R)-18**. The absolute stereochemistry in **18** was determined by comparison of  $^{19}\text{F}$  NMR of the **(+)-(S)- $\alpha$ -methoxy- $\alpha$ -trifluoromethylphenylacetyl chloride** derivative with results by Hultzs and coworkers.<sup>32</sup>

### 3.5 Substrate Scope Investigations

When the *gem*-disubstituents are inequivalent, diastereomeric products are formed along with their enantiomers. Hydroamination of 2-methyl-2-phenylpent-4-enylamine **23** produces four products **23b**, **23c** and their associated enantiomers (Table 3.4, Entry 1). Previous results by our group for hydroamination of substrate **23** with  $\text{Ti}(\text{NEt}_2)_4$  produced a racemic mixture with a diastereomeric ratio of 1.4 : 1 as measured by GC-MS analysis, favoring compound **23b**.<sup>55</sup> This reaction was repeated with  $\text{Zr}(\text{NMe}_2)_4$  and a diastereomeric ratio of **23b** to **23c** was found to be 2.1 : 1 by  $^1\text{H}$  NMR spectroscopy. When (+)-**13c** and (-)-**13b** were employed, the diastereomeric ratios of **23b** to **23c** were 1.9 : 1 and 2.2 : 1 respectively. Hydroamination of **23** with precatalyst (+)-**13c** gave an ee of 62 % for **23b** and 86 % for **23c** (Table 3.4, entry 1). A reversal in enantioselectivity was observed for precatalyst (-)-**13c** where the ee's were 88 % for **23b**, and 56 % for **23c** (Table 3.4, entry 2). Hydroamination of **23** was complete in 12 h with an isolated yield of 87 %. The diastereoselectivity was essentially unaffected when employing either the (+) or (-) chiral amidate ligand; however the enantioselectivity's were reversed.

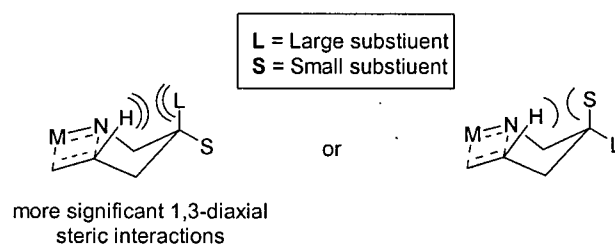
**Table 3.4** Aminoalkene substrate scope investigations with precatalysts (-)-**13b** and (+)-**13c** in  $d_6$ -benzene at 110 °C.

Entry	Catalyst loading [mol %]	Aminoalkene substrate	Product	Time [h]	Yield [%]	ee [%]
1	10 (+)- <b>13c</b>		<div> <div>major </div> <div>minor </div> </div> <div> <b>23b</b>      <b>23c</b> </div>	12	87 <sup>a</sup>	dr (b) : (c) <sup>h</sup> 1.9 : 1  ee (b): 62 <sup>c</sup> ee (c): 86 <sup>c</sup>
2	10 (-)- <b>13b</b>	<b>23</b>		12	>98 <sup>b</sup>	dr (b) : (c) <sup>h</sup> 2.3 : 1  ee (b): 56 <sup>c</sup> ee (c): 88 <sup>c</sup>
3	10 (+)- <b>13c</b>		<div> <div>major </div> <div>minor </div> </div> <div> <b>24b</b>      <b>24c</b> </div>	2	94 <sup>a</sup>	dr (b) : (c) <sup>h</sup> 2.2 : 1  ee (b): 92 <sup>d</sup> ee (c): 88 <sup>d</sup>

[a] isolated yield [b] NMR yield. [c] enantiomeric excess based on  $^1\text{H}$  NMR of the product (+)-(S)-a-methoxy-a-trifluoromethylphenylacetyl chloride derivative. [d] enantiomeric excess based on  $^{19}\text{F}$  NMR of the product (+)-(S)-a-methoxy-a-trifluoromethylphenylacetyl chloride derivative.

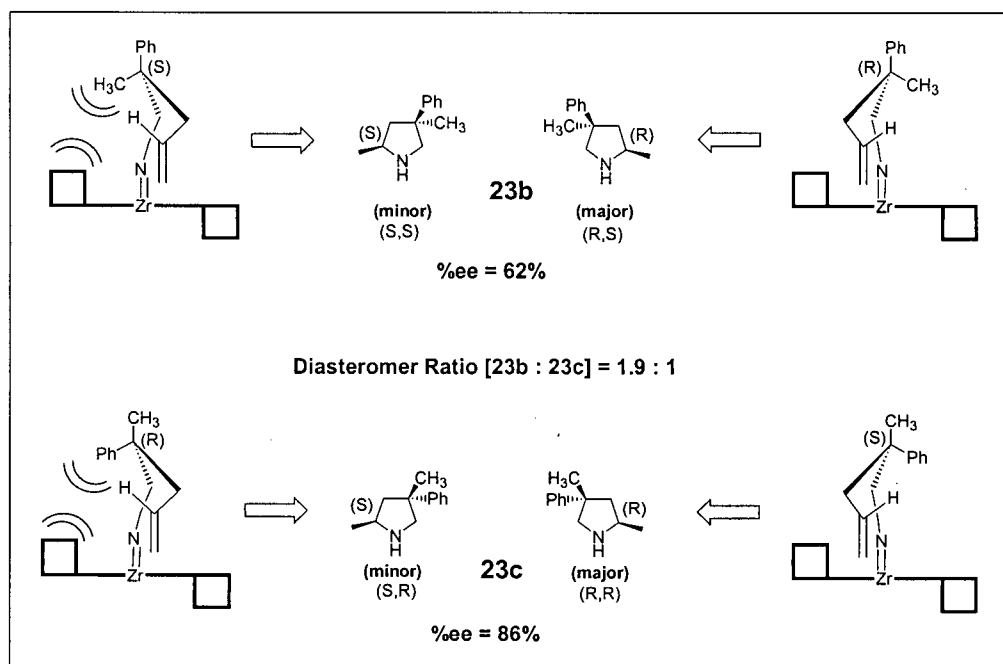
Similarly, substrate **24** was also subjected to hydroamination using precatalyst (+)-**13c**. The reaction was complete in 2 h at 110 °C, and was isolated in 94 % yield (Table 3.4, Entry 3). The diastereomeric ratio of **24b** to **24c** was 2.2 : 1 with ee's of 92 % and 88 % respectively. Despite the fact that the diastereomeric ratios were essentially the same, the enantioselectivities were high for both diastereomeric products **24b** and **24c**.

The same arguments used to propose a mechanism for the enantioselectivity in substrate **17** (Figure 3.9) was also used for substrates **23** and **24** (Figures 3.10 and 3.11). These substrates produce diastereomeric products and corresponding enantiomers to give four possible stereoisomers. The intermediates in Figures 3.10 and 3.11 illustrate the steric interactions between the mesityl substituents on the amidate ligands, and the inequivalent *gem*-disubstituents on the aminoalkene chain. Complexes (-)-**13b** and (+)-**13c** are depicted as a  $C_2$  symmetric complexes, where the square boxes represent the steric influence of the mesityl group. Substrate **23** is used here as an example to demonstrate how the product ratio for **23b** and **23c** (Table 3.4, Entry 1 and 2) can be rationalized based on the same model used for substrate **17** in Figure 3.8. When precatalyst (+)-**13c** is employed (Figure 3.10), the diastereomer ratio is 1.9 : 1 in favor of pyrrolidine **23b** where the methyl groups are in the *anti*-orientation. The diastereomeric ratio was not influenced by the chiral ligand and the ratio was not affected when (-)-**13b**, (+)-**13c** or  $Zr(NMe_2)_4$  were used for catalysis. This diastereoselectivity can be described by looking at the 1,3-diaxial interactions that occur in the chair-like transition state.

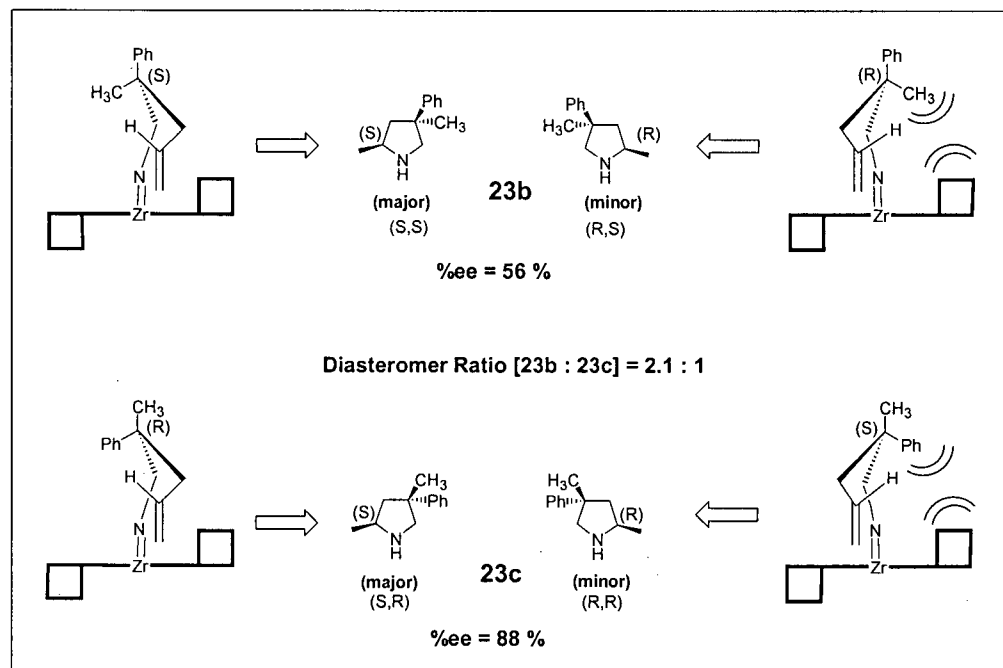


The 1,3-diaxial interaction between the alkene hydrogen and the *gem* substituents is more significant when the larger group (ie: phenyl in substrate **23**) is in the axial position. When the smaller substituent is axial, the steric interaction is minimized leading to the major product which has the large group *syn* to the  $\alpha$ -methyl on the pyrrolidine. The enantiomeric excess for **23b** was determined experimentally to be 62 % (Figure 3.10). The chair-like transition state leading to the (S)-enantiomer is less favored due to the

steric interaction of the methyl on the substrate and the mesityl groups on the ligand. When the chair is flipped, the interaction is minimized leading to the major enantiomer.



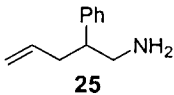
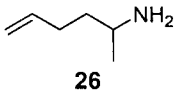
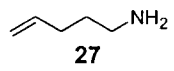
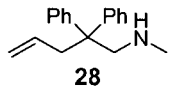
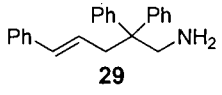
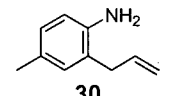
**Figure 3.10** Proposed mechanism for enantioselectivity of aminoalkene **23** using precatalyst **(+)-13c**.



**Figure 3.11** Proposed mechanism for enantioselectivity of aminoalkene **23** using precatalyst **(-)-13b**.

For the *syn*-diastereomer **23c**, the steric interaction between the phenyl substituent on the substrate and the mesityls is more significant leading to higher enantioselectivity. In this circumstance, the (*R*)-enantiomer is favored leading to the higher observed ee of 86%. Alternatively, when complex (-)-**13b** is employed for the hydroamination of **23**, the same *anti* / *syn* ratio of 2.2 : 1 is observed, but the enantioselectivity is reversed. The same rationale that was used to describe the enantioselectivity observed for (+)-**13c** was also consistent for precatalyst (-)-**13b** and is described in Figure 3.11.

**Table 3.5:** Substrates that are Unreactive toward hydroamination using precatalyst (-)-**13b** and (+)-**13c** when employed at 110 °C

Entry	Catalyst loading [mol %]	Aminoalkene substrate	Product	Time [h]
1	10 (+)- <b>13b</b>		No Reaction	96
2	10 (-)- <b>13c</b>		No Reaction	24
3	10 (-)- <b>13c</b>		No Reaction	120
4	10 (-)- <b>13c</b>		No Reaction	48
5	10 (+)- <b>13b</b>		No Reaction	24
6	10 (-)- <b>13c</b>		No Reaction	24

Hydroamination of the substrates listed in Table 3.5 did not show any reactivity when precatalysts (-)-**13b** and (+)-**13c** were employed. The lack of reactivity for the  $\beta$ -



phenyl aminoalkene **25**,  $\alpha$ -methyl aminoalkene **26** and unsubstituted aminoalkene **27** can be attributed to the lack of the *gem*-disubstituent effect. The *gem*-disubstituent effect, otherwise known as the *gem*-dialkyl effect, was first recognized in 1915 and has been used to increase rates of cyclization reactions, and promote intramolecular cyclization, that otherwise would not have been possible.<sup>96</sup> The *gem*-dialkyl effect was first realized by Thorpe, Ingold and Beesley when they proposed the steric repulsion effects of *gem*-dimethyl substituents on the angle  $\theta$  seen in Figure 3.12. The unsubstituted example **A** shows the largest angle  $\theta$  followed by mono-substituted **B** and finally the smallest angle in disubstituted compound **C**. Incorporating *gem*-disubstituents forces the two reactive bi-functionalized branches of the reactant to be closer and therefore increases the likelihood of intramolecular ring closure.

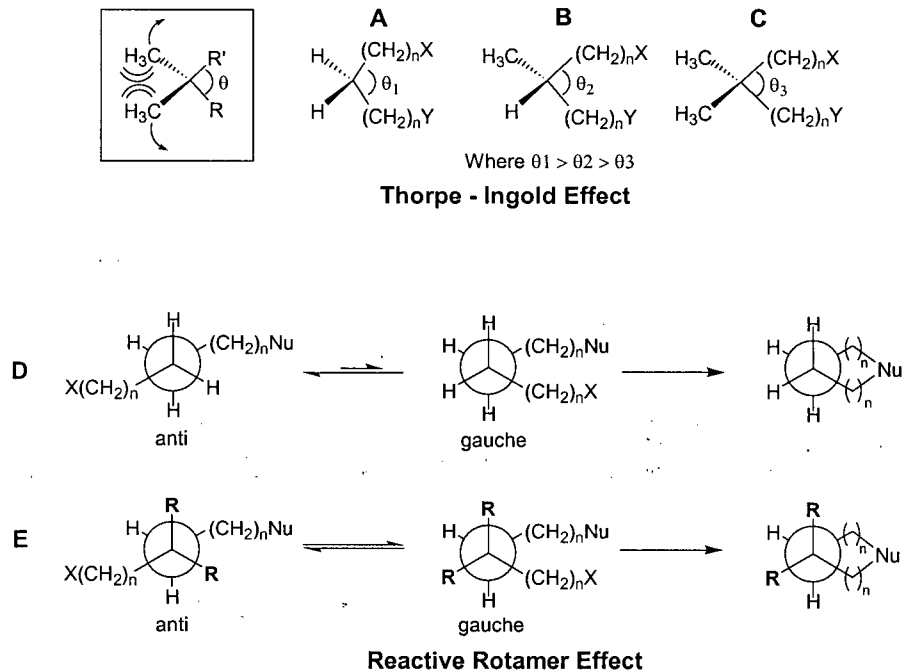


**Figure 3.12** *Gem*-disubstituent effect: A description that incorporates the Thorpe-Ingold and reactive rotamer effects as explanations that rationalize why there is no observed reactivity for the hydroamination of substrates **25** - **27** using precatalyst **13**.

Another theorem that is included in the *gem*-disubstituent effect is known as the reactive rotamer effect. The reactive rotamer effect considers gauche interactions between the reactive bi-functionalized branches of the reactant and the *gem*-disubstituents. For instance, the Newman projections in Figure 3.12**D** show an unsubstituted reactant

cyclizing. The conformation on the right hand side of the equilibrium is not favored due to gauche interactions. The equilibrium therefore lies primarily on the left hand side, and cyclization is consequently less favored. When a substrate contains *gem*-disubstituents (Figure 3.12, E), the number of gauche interactions are the same on both sides of the equilibrium. The probability of either rotamer is equally favorable and therefore the likelihood of cyclization is amplified. Although this theorem does not specify the effects of different size substituents, one would expect larger R-groups would force the equilibrium more to the right side in order to minimize the most significant gauche interactions.

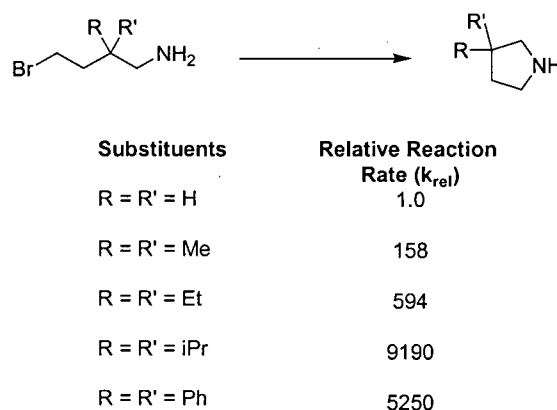


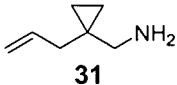
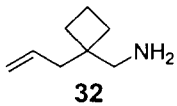
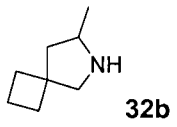
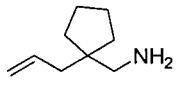
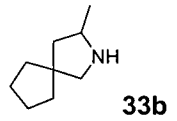
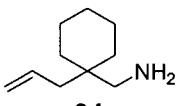
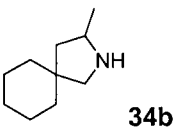
**Figure 3.13** Example of the relative reaction rates for *gem*-disubstituted 4-bromoalkylamines versus unsubstituted 4-bromoalkylamine.<sup>97</sup>

The example in Figure 3.13 show the relative reaction rates for *gem*-disubstituted 4-bromoalkylamines versus unsubstituted 4-bromoalkylamine.<sup>97</sup> The trends observed are very similar to those for the intramolecular hydroamination reactions described in Tables 3.1 through 3.6. It appears that increasing the size of the *gem*-disubstituents has a positive effect on the rate of cyclization where  $iPr > Ph > Et > Me > H$ . The aminoalkene cyclizations performed with precatalyst **13** showed a general trend where  $Ph > Me$  and no reaction was observed for the mono- and unsubstituted substrates. This demonstrates the significance of the *gem*-disubstituent effect and how important it is for intramolecular hydroamination.

The substrates in Table 3.6 were selected to probe the *gem*-dialkyl effects with tethered disubstituents including cyclopropyl, cyclobutyl, cyclopentyl and cyclohexyl. The cyclohexyl substituted aminoalkene **34** showed the highest reactivity which was

complete in 3 h with an ee of 82 % (79 % by GC-MS). The cyclopentyl derivative **33**, which was slightly slower, was complete in 5h with an ee of 88 % (90 % by GC-MS). The cyclobutyl (**32**) was complete in 12h with an ee of 77 %, while no reaction was observed at all for the cyclopropyl aminoalkene (**31**).

**Table 3.6** Effects of tethered *gem*-dialkyl substituents on reactivity and enantioselectivity

Entry	Catalyst loading [mol %]	Aminoalkene substrate	Product	Time [h]	Yield [%]	ee [%]
1	10 (+)- <b>13c</b>	 <b>31</b>	No Reaction	48	-	-
2	10 (+)- <b>13c</b>	 <b>32</b>	 <b>32b</b>	12	92 <sup>a</sup>	77 <sup>d</sup>
3	10 (+)- <b>13c</b>	 <b>33</b>	 <b>33b</b>	5	91 <sup>a</sup>	88 <sup>b</sup> (90) <sup>d</sup>
4	10 (+)- <b>13c</b>	 <b>34</b>	 <b>34b</b>	3	88 <sup>a</sup>	82 <sup>c</sup> (79) <sup>d</sup>

[a] isolated yield [b] enantiomeric excess based on <sup>1</sup>H NMR of the product (+)-(S)-α-methoxy-α-trifluoromethylphenylacetyl chloride derivative. [c] enantiomeric excess based on <sup>19</sup>F NMR of the product (+)-(S)-α-methoxy-α-trifluoromethylphenylacetyl chloride derivative. [d] ee determined by GC-MS analysis of (+)-(S)-α-methoxy-α-trifluoromethylphenylacetyl chloride derivative.

Substrate **31** did not react which was not surprising considering the *gem*-dialkyl effects described before. The strained cyclopropyl ring has an internal sp<sup>2</sup> angle of 60° that pulls the amine and alkene branches away from one another. These cyclo *gem*-dialkyl substituents probe the importance of the Thorpe-Ingold effect more than the reactive rotamer because the substituents are tethered. For the reactive rotamer, the steric interaction of the tethered group in the *anti*-conformation would likely impose an effect on the equilibrium favoring the right hand side in all cases (Figure 3.14).

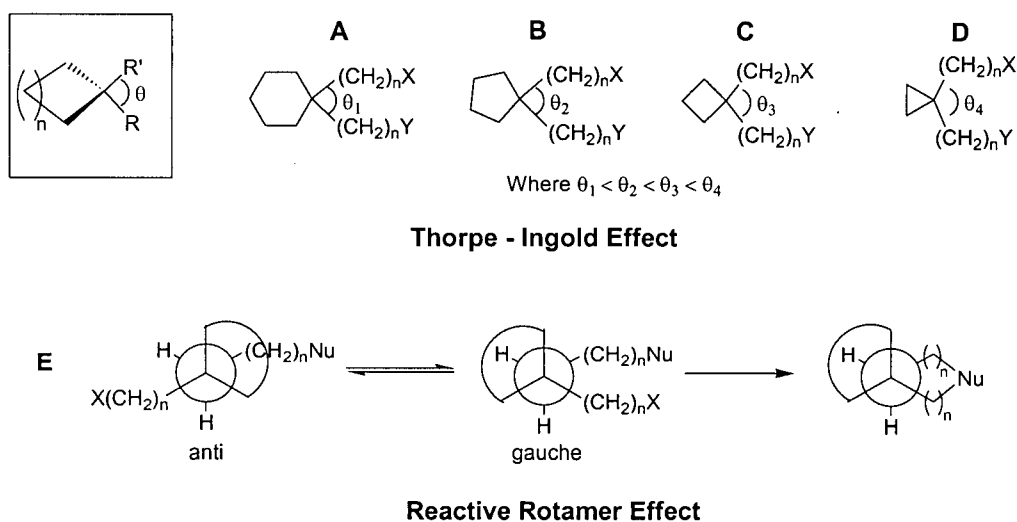


**Figure 3.14** The effect different size tethered *gem*-dialkyl ring systems have on the rate of aminoalkene hydroamination.

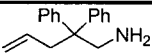
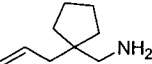
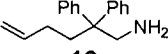
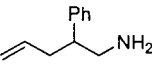
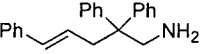
Throughout this chapter we have only discussed intramolecular hydroamination of aminoalkenes that contain terminal alkenes. Hydroamination of aminoalkenes that contain internal olefins were also considered (Table 3.5, Entry 5). However, catalyst (+)-**13c** displayed no reactivity for the internal alkene substrate **29**. This may be attributed to the amount of steric bulk imposed in the transition state when an internal alkene contains a bulky terminal substituent. Substrate **30** also showed no reactivity. This can be attributed to the additional strain the rigid phenyl group induces on the seven-membered metallocycle.

Intermolecular hydroamination was also considered, but was met with little success. Hydroamination of styrene and *t*-butylamine (4 equiv.) was attempted using (-)-**13b**, but proved unsuccessful under the same reaction conditions used for intramolecular hydroamination (110 °C, 10 mol % cat.). The catalyst activity is not high enough to overcome the high reaction barrier for this transformation. This was not surprising considering the high temperatures required for cyclization, and limited reactivity toward only *gem*-disubstituted aminoalkene substrates. The only group 4 intermolecular hydroamination catalysts are  $\text{TiCl}_4$ . Hydroamination of styrene<sup>60</sup> and norbornene<sup>59</sup> using  $\text{TiCl}_4$  have been recently predicted to go through a proton catalyzed route rather than an imido cycloaddition or amido insertion mechanism.

### 3.6 *In-situ* Hydroamination Reactions

As a means of complementing the work completed by Bergman and coworkers<sup>58</sup> we developed preliminary investigations for *in-situ* aminoalkene hydroamination reactions. Preparing the catalysts *in-situ* is a much more attractive means of catalysis for research groups that do not have access to a nitrogen filled glove box. The reactions could potentially be completed using syringe techniques with the  $\text{Zr}(\text{NMe}_2)_4$  starting material prepared as a standard solutions in the reaction solvent (ie: benzene). The preliminary investigations to demonstrate this technique are displayed in Table 3.7 for a small selection of aminoalkene substrates.

**Table 3.7:** *In-situ* hydroamination reactions at 110 °C in  $d_6$ -benzene at [0.5M] with 10 mol %  $\text{Zr}(\text{NMe}_2)_4$  and 11 mol % proligand **10**, **11** or **12**.

Substrate	Proligand	Conversion [%] <sup>a</sup>	Reaction time [h]	ee [%] <sup>b</sup>
 <b>17</b>	(+)- <b>10</b>	> 98	1.25	68
	(-)- <b>11</b>	> 98	1	9 %
	(+)- <b>12</b>	> 98	1	<5 %
 <b>33</b>	(+)- <b>12</b>	> 98	16	85
 <b>19</b>	(+)- <b>10</b>	> 98	16	24
	(-)- <b>11</b>	43		0
	(+)- <b>12</b>	75		0
 <b>25</b>	(+)- <b>10</b>	NR	16	-
	(-)- <b>11</b>	NR		-
	(+)- <b>12</b>	NR		-
 <b>29</b>	(+)- <b>10</b>	NR	16	-
	(-)- <b>11</b>	NR		-
	(+)- <b>12</b>	NR		-

[a] conversion based on relative integration of substrate consumption vs 1,3,5-trimethoxybenzene internal standard (0.33 mol%). [b] determined by <sup>1</sup>H NMR of the (S)-(+)-α-methoxy-α-(trifluoromethyl)phenyl acetyl chloride derivative.

Reactions were completed with 10 mol%  $\text{Zr}(\text{NMe}_2)_4$  and 11 mol% of proligand (**10**, **11** or **12**, see Chapter 2). Based on earlier results for hydroamination using  $\text{Zr}(\text{NMe}_2)_4$  (Table 3.1 and 3.2), it is likely that residual  $\text{Zr}(\text{NMe}_2)_4$  would cyclize the product faster than the amidate complex itself. As a result, lower reaction times and enantioselectivities would be observed. To avoid such problems, excess proligand (1.1 equiv.) was used. This would ensure that no residual  $\text{Zr}(\text{NMe}_2)_4$  could compete with the bis(amidate)bis(amido) precatalyst for hydroamination reactivity. Hydroamination reactions were left at 110 °C overnight (16 h) in a J. Young Teflon sealed NMR tube. Upon derivatization with Mosher's acid chloride, enantioselectivities for *in-situ* preparation of precatalyst (+)-**13c** (proligand (+)-**10**) were consistent with previous results in Tables 3.1 and 3.2 (Substrates **17**, **19** and **33**). Substrates **25** and **29** did not show any reactivity also consistent with previous results for the isolated precatalyst (+)-**13**.

When trifluoromethyl substituted proligands (-)-**11** and (+)-**12** were employed, poor enantioselectivity was achieved for substrates **17** and **19**, and no reactivity was observed for substrates **25** and **29**. Reaction mixtures employing ligands (-)-**11** and (+)-**12** turned an intense emerald green color during catalysis; indicating decomposition may be an issue. If such decomposition is occurring, this could explain the lower enantioselectivities observed. Overall, *in-situ* catalyst preparation produces comparable reactivity and enantioselectivity to the isolated precatalysts. Optimization is still in progress to improve the enantioselectivity employing proligands (-)-**11** and (+)-**12**.

### 3.7 Summary and Conclusions

This chapter has focused on employing axially chiral bis(amidate)bis(amido) group 4 catalysts for asymmetric aminoalkene hydroamination. We developed a structure-reactivity relationship for a series of titanium and zirconium catalysts containing different axially chiral bis(amidate) ligands. From this structure reactivity relationship, we completed an aminoalkene substrate scope analysis for the most selective zirconium complex (-)-**13b** and (+)-**13c**. We provided further evidence of a metal imido / cycloaddition mechanism and have developed a mechanistic rationale for enantioselectivity based on the X-ray solid state molecular structure of (+)-**13c**. Most importantly, we have described the first fully characterized, axially chiral bis(amidate)bis(amido) neutral titanium and zirconium complexes for asymmetric alkene hydroamination, and have achieved enantioselectivities of up to 93 % ee.<sup>57</sup>

### 3.8 Experimental

**General Procedures:** All chemicals and solvents were commercially available and used as received unless stated otherwise. Catalytic reactions were completed using Schlenk line and/or glove box (Mbraun LabMaster) techniques under a dry, oxygen free, nitrogen atmosphere.  $d_6$ -benzene,  $d_8$ -toluene and  $d_{10}$ -xylenes were degassed using a freeze-pump-thaw method and stored over 3 Å molecular sieves.  $^1\text{H}$ ,  $^{13}\text{C}\{\text{H}\}$ , and  $^{19}\text{F}\{\text{H}\}$  NMR spectra were recorded on either a Bruker Avance 300 MHz or Avance 400 MHz spectrometer. GC-MS analysis was determined using an Agilent 6890N GC system with a 5973 mass selective detector. Mass spectrometry (ESI, EI) and elemental analyses were performed by analytical services in the Department of Chemistry at the University of British Columbia. 2,2-diphenyl-4-pentenylamine<sup>55</sup>, 2,2-diphenyl-hex-5-enylamine<sup>55</sup>, 2,2-dimethyl-pent-4-enylamine<sup>55</sup>, 2,2-dimethyl-hex-5-enylamine<sup>32</sup>, 2,2-diallyl-pent-4-enylamine<sup>57</sup>, 2-methyl-2-phenyl-pent-4-enylamine<sup>55</sup>, 2-allyl-2-methyl-pent-4-enylamine<sup>37</sup>, 2-Phenyl-pent-4-enylamine<sup>55</sup>, 1-methyl-pent-4-enylamine<sup>32</sup>, pent-4-enylamine<sup>55</sup>, (2,2-diphenyl-pent-4-enyl)-*N*-methyl-amine<sup>55</sup>, 2,2,5-triphenyl-pent-4-enylamine<sup>55</sup>, 2-allyl-4-methyl-phenylamine<sup>98</sup>, C-(1-allyl-cyclopentyl)-methylamine,<sup>28</sup> C-(1-allyl-cyclohexyl)-methylamine<sup>32</sup> were prepared according to modified literature preparations using commercially available starting materials.  $^1\text{H}$  NMR spectroscopy and mass spectrometry of aminoalkene substrates were in agreement with literature values. Before use in hydroamination reactions, substrates were distilled from  $\text{CaH}_2$  and stored over 3 or 4 Å molecular sieves unless stated otherwise. Heterocyclic products: 2-methyl-4,4-diphenylpyrrolidine,<sup>55</sup> 2-methyl-5,5-diphenylpiperidine,<sup>55</sup> 2,4,4-trimethylpyrrolidine,<sup>55</sup> 2,5,5-trimethylpiperidine,<sup>42</sup> 2,4-dimethyl-4-phenylpyrrolidine,<sup>55</sup> 4-allyl-2,4-dimethylpyrrolidine,<sup>41</sup> 3-Methyl-2-aza-spiro[4.4]nonane<sup>28</sup> and 3-methyl-2-aza-spiro[4.5]decane<sup>28</sup> are known compounds.  $^1\text{H}$  NMR spectroscopy and mass spectrometry of pyrrolidine products were in agreement with literature values. Enantiopurity of these products were determined using either  $^1\text{H}$ ,  $^{19}\text{F}$  NMR (60 °C) and/or GC-MS analysis of the (+)-(S)- $\alpha$ -methoxy- $\alpha$ -trifluoromethylphenylacetyl amide derivative.



**C-(1-allyl-cyclopropyl)-methylamine (31).** To a solution of diisopropylamine (8.3 g, 11.5 mL, 82 mmol) in anhydrous diethyl ether (150 mL) cooled to -78 °C under a nitrogen atmosphere was added *n*-BuLi (50mL, 1.6 M in hexanes, 82 mmol) slowly by syringe. The solution was stirred at -78 °C for 30 minutes then cyclopropylcyanide (5 g, 75 mmol) was added dropwise over 5 minutes. The solution was stirred for an additional 1 hour then allyl bromide (9.84 g, 82 mmol) was added and the solution was stirred overnight at room temperature. To the reaction mixture was washed with 1M HCl (3 x 50 mL) and 1M NaOH (1 x 50 mL). The ether layer was dried on MgSO<sub>4</sub> and filtered into a 500 mL round bottom flask. The solution was cooled to 0 °C on an ice/water bath then lithium aluminum hydride (4.2 g, 113 mmol) was added in 500 mg aliquots. The solution was stirred overnight at room temperature then quenched carefully with 2 mL of distilled water and 2 mL of 1M NaOH until a slurry of white aluminum oxide solid was formed. The solution was filtered through a micro-porous frit, and the solvent was removed by rotary evaporation to yield a pale yellow oil. The oil stirred overnight on CaH<sub>2</sub> then purified by short path distillation and isolated as a clear colorless oil (2.1 g, 25%). The product was dried over sieves before use in catalysis and stored in a nitrogen glove box at -20 °C in a Teflon sealed vial. <sup>1</sup>H NMR (CDCl<sub>3</sub>, 300MHz): δ 5.77 (1 H, m, -CH=CH<sub>2</sub>), 5.07-4.95 (2 H, m, -CH=CH<sub>2</sub>), 2.48 (2 H, s, -CH<sub>2</sub>NH<sub>2</sub>), 2.07 (2H, d, <sup>3</sup>J<sub>HH</sub> = 7.04 Hz, CH<sub>2</sub>CH=CH<sub>2</sub>), 1.34 (2 H, s, -NH<sub>2</sub>), 0.30 (4 H, m, cyclopropyl-H). <sup>13</sup>C NMR APT (CDCl<sub>3</sub>, 75 MHz): δ 136.41 (-CH=CH<sub>2</sub>), 116.33 (-CH=CH<sub>2</sub>), 48.61 (-CH<sub>2</sub>NH<sub>2</sub>), 38.87 (-CH<sub>2</sub>CH=CH<sub>2</sub>), 22.35 (Cyclopropyl-C(CH<sub>2</sub>)<sub>4</sub>), 9.98 (Cyclopropyl-CH<sub>2</sub>). HRMS (ESI), *m/z* calc'd for C<sub>7</sub>H<sub>14</sub>N (M<sup>+</sup> + H): 112.1126, found: 112.1125. 94 % purity by GC-MS.

**Synthesis of 2,2-bis(2-propenyl)-4-pentenylamine, (22):** Diisopropylamine (8.33 g, 11.54 mL, 82.3 mmol) was dissolved in THF (50 mL). The solution was cooled to -78 °C prior to the slow addition of *n*-BuLi (1.6 M in hexanes, 50 mL, 80 mmol). The cold bath was replaced with an ice bath and the reaction was warmed to 0 °C and stirred for 45 minutes. During this time, a separate flask was charged with acetonitrile (1.15 g, 1.47 mL, 28.1 mmol) and THF (50 mL). This solution was cooled to -78 °C. A third of the LDA solution (34 mL) was added slowly to the acetonitrile solution. After 15 minutes of

stirring at -78 °C, allyl bromide (3.57 g, 2.50 mL, 29.5 mmol) was added. The reaction was warmed to room temperature with stirring for 30 minutes before being cooled to -78 °C again. Another equivalent of LDA solution (34 mL) was added, followed by 15 minutes of stirring, followed by the addition of another equivalent of allyl bromide (3.57 g, 2.50 mL, 29.5 mmol). The reaction was again warmed to room temperature with stirring for 30 minutes before being cooled to -78 °C. The remaining LDA solution was added, followed by 15 minutes of stirring, followed by the addition of a third equivalent of allyl bromide (3.57 g, 2.50 mL, 29.5 mmol). The reaction was allowed to warm to room temperature with stirring overnight. Workup of a small aliquot of the reaction mixture revealed incomplete alkylation by  $^1\text{H}$  NMR spectroscopy. A fresh batch of LDA (2.84 g, 3.94 mL, 28.1 mmol of diisopropylamine, 17.5 mL, 28 mmol of *n*-BuLi) was prepared as described above. The nitrile solution was cooled to -78 °C, followed by the slow addition of LDA. After 15 minutes of stirring, a fourth equivalent of allyl bromide (3.40 g, 2.40 mL, 28.1 mmol) was added. The reaction was warmed to room temperature with stirring for one hour. The reaction was then quenched by the addition of water (5 mL). The volatiles were removed under reduced pressure and the residue dissolved in 100 mL of diethyl ether. The organic phase was washed with 2 x 100 mL water, 1 x 100 mL brine, and dried over  $\text{MgSO}_4$ . The solvent was removed under reduced pressure to give the crude product, which was used in the next step without further purification.

**LAH Reduction:** A flask was charged with lithium aluminum hydride (1.60 g, 42.2 mmol) and anhydrous diethyl ether (50 mL) and cooled to 0 °C. 2,2-Bis(2-propenyl)-4-pentenitrile (4.52 g, 28.1 mmol) dissolved in anhydrous diethyl ether (50 mL) was added dropwise to the LAH suspension over a period of 10 minutes. The reaction was warmed to room temperature and stirred overnight. The reaction was again cooled to 0 °C prior to the addition of water (4 mL) and 1 M NaOH (5 mL). The reaction was stirred at room temperature until no grey colour remained in the suspension. The solution was filtered through Celite, and washed with diethyl ether (3 x 50 mL). The solvent was removed under reduced pressure to give the crude amine, which was determined to be pure by  $^1\text{H}$  NMR spectroscopy. Calcium hydride was added to the oil which was stirred under nitrogen overnight. The product was degassed by several freeze-pump-thaw cycles before being filtered through a plug of Celite to remove any calcium hydride and calcium

hydroxide. A GC-MS trace determined that the product was 93 % pure; therefore, no further purification was undertaken. The impurity was found to have negligible effect on catalytic efficiency. Yield: 3.48 g, 75 %.  $^1\text{H}$  NMR ( $\text{CDCl}_3$ , 300 MHz):  $\delta$  5.73 (3 H, m,  $\text{H}_2\text{C}=\text{CH}-$ ), 4.98 (6 H, m,  $\text{H}_2\text{C}=\text{CH}-$ ), 2.42 (2 H, s,  $-\text{CH}_2\text{NH}_2$ ), 1.94 (6 H, d,  $^3J_{\text{HH}}=7.5$  Hz,  $\text{H}_2\text{C}=\text{CHCH}_2-$ ), 0.98 (2 H, br s,  $-\text{NH}_2$ ).  $^{13}\text{C}$  NMR ( $\text{CDCl}_3$ , 300 MHz):  $\delta$  39.28, 40.75, 47.52, 117.71, 134.63. HR-MS (ESI),  $m/z$  calc'd for  $\text{C}_{11}\text{H}_{20}\text{N}$  ( $\text{M}^+ + \text{H}$ ): 166.1596, found: 166.1597.

**General procedure for NMR-scale intramolecular aminoalkene hydroamination**

(Tables 3.1 and 3.6): All catalytic runs were conducted using the same general procedure, where only the catalyst employed, the catalyst loading (5 or 10 mol %) and the substrate utilized were changed. All NMR scale hydroamination reactions were prepared in a nitrogen filled glove box. To a J. Young Teflon sealed NMR tube was added the appropriate amino alkene substrate (0.2 mmol), the appropriate precatalyst (5 or 10 mol %) and  $d_6$ -benzene or  $d_8$ -toluene (500 mg). The NMR tube was then placed in an oil bath at the temperature and duration listed in Tables 3.1 - 3.6. Reactions were monitored by  $^1\text{H}$  NMR spectroscopy frequently to accurately obtain the reaction times for complete conversion. Yields were determined by either  $^1\text{H}$  NMR (integration of product resonances relative to a 1,3,5-trimethoxybenzene internal standard.) or an isolated yield.

**Isolated Yield:** pyrrolidine and piperidine products were purified by flash silica chromatography (length: 3cm, diameter: 2.5 cm) eluted first with 1:1 hexanes/ethyl acetate (100 mL) to remove prolignand, followed by 89:10:1 dichloromethane/methanol/isopropylamine (200 mL) or 90:5:5 dichloromethane/methanol/ ammonium hydroxide to isolate the product. 2,4,4-trimethylpyrrolidine was purified as the benzoyl amide derivative according to a literature method.<sup>55</sup> The enantioselectivity was determined using (+)-(S)- $\alpha$ -methoxy- $\alpha$ -trifluoromethylphenylacetyl amide derivatives (see procedure below\*\*)

**General procedure for *in-situ* NMR-scale intramolecular aminoalkene hydroamination (Table 3.7):** All *in-situ* catalytic runs were conducted using the same general procedure, where only the ligand employed and substrate utilized were changed.

All *in-situ* NMR scale hydroamination reactions were prepared in a nitrogen filled glove box. To a 5 mL scintillation vial was added the appropriate ligand (0.11 equiv.),  $\text{Zr}(\text{NMe}_2)_4$  (0.10 equiv.) and  $\text{d}_6$ -benzene (so the [substrate] = 0.5 M). The ligand /  $\text{Zr}(\text{NMe}_2)_4$  mixture was left to react for 15 min prior to the addition of the appropriate amino alkene substrate (1 equiv). The reaction mixture was added to a J. Young Teflon sealed NMR tube and placed in an oil bath at  $100^\circ\text{C}$  for the duration listed in Table 3.7. The mixture was diluted with dichloromethane and the enantioselectivity was determined using (+)-(S)- $\alpha$ -methoxy- $\alpha$ -trifluoromethylphenylacetyl amide derivatives (see procedure below\*\*)

**2-Methyl-4,4-bis(2-propenyl)pyrrolidine (22b)** Purity: 92% by GC-MS.  $^1\text{H}$  NMR ( $\text{CDCl}_3$ , 300 MHz): 5.73 (2 H, m,  $\text{H}_2\text{C}=\text{CH}-$ ), 4.99 (4 H, m,  $\text{H}_2\text{C}=\text{CH}-$ ), 3.12 (1 H, m), 2.75 (1 H, d,  $J = 11.3$  Hz), 2.62 (1 H, d,  $^3J_{\text{HH}} = 11.3$  Hz), 2.07 (4 H, m,  $\text{H}_2\text{C}=\text{CHCH}_2-$ ), 1.71 (1 H, dd,  $^3J_{\text{HH}} = 12.8$  Hz,  $^4J_{\text{HH}} = 6.7$  Hz), 1.10 (3 H, d,  $^3J_{\text{HH}} = 6.3$  Hz,  $-\text{CH}_3$ )  $\delta$  1.07 (dd, 1H, obscured by methyl signal; coupling constants not determined).  $^{13}\text{C}$  NMR ( $\text{CDCl}_3$ , 300 MHz):  $\delta$  135.42, 135.32, 117.60, 117.54, 57.31, 54.60, 46.46, 45.59, 43.86, 42.84, 21.35. HR-MS (ESI),  $m/z$  calcd for  $\text{C}_{11}\text{H}_{20}\text{N}$  ( $\text{M}^+ + \text{H}$ ): 166.1596, found: 166.1595.

**7-Methyl-6-aza-spiro[3.4]octane (32b)** Purity: 89 % by GC-MS.  $^1\text{H}$  NMR ( $\text{CDCl}_3$ , 300 MHz):  $\delta$  3.32 (1 H, m,  $\text{CH}$ ), 2.94 (1 H, d,  $J = 10.8$  Hz,  $\text{CH}$ ), 2.78 (1 H, d,  $J = 10.8$  Hz,  $\text{CH}$ ), 1.97 - 1.64 (10 H, m), 1.27 (1 H, dd,  $J = 12.4$  Hz,  $J = 10.4$  Hz,  $\text{CH}$ ), 1.08 (3 H, d,  $^3J = 6.3$  Hz,  $\text{CH}_3$ );  $^{13}\text{C}$  NMR ( $\text{CDCl}_3$ , 400 MHz):  $\delta$  59.75, 53.78, 48.43, 46.99, 33.97, 33.51, 22.85, 16.56.

**\*\*General procedure for the NMR scale preparation of Mosher amides for enantiopurity investigations of pyrrolidine and piperidine products.** To a solution of the hydroamination pyrrolidine / piperidine product (5.0 mg, 0.021 mmol) and triethylamine (10 mg, 0.10 mmol) in dichloromethane (~1 mL) was added (S)-(+)- $\alpha$ -methoxy- $\alpha$ -(trifluoromethyl)phenylacetyl chloride (6.0 mg, 0.023 mmol) as a solution dichloromethane (~1 mL). The solution was filtered through a silica gel plug (pipette

column, eluent: dichloromethane, 5mL) and concentrated under vacuum to give a clear colorless residue. The % ee was determined by  $^1\text{H}$  NMR at room temperature,  $^{19}\text{F}$  NMR at 60°C referenced to literature<sup>32</sup> or GC-MS analysis of the (+)-(S)- $\alpha$ -methoxy- $\alpha$ -trifluoromethylphenylacetyl amide derivative (see Table 3.8 for NMR spectroscopic data).

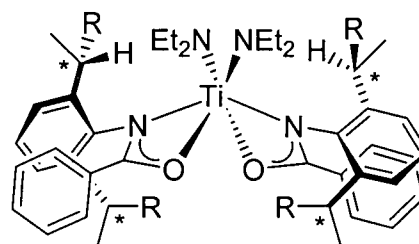
**Table 3.8**  $^1\text{H}$  and  $^{19}\text{F}$  NMR resonances for Mosher amide derivatives of pyrrolidine and piperidine products utilized for ee determination

Compound	Table, Entry	$^1\text{H}^a$ or $^{19}\text{F}^b$ NMR	Enantiomer A ppm (integration)	Enantiomer B ppm (integration)	ee %
18	3.2, entry 5	$^1\text{H}$	1.48 doublet (0.146)	1.31 doublet (1.00)	74 (R)
18	3.2, entry 7	$^1\text{H}$	1.48 doublet (1.00)	1.31 doublet (0.165)	72 (S)
19b	3.3, entry 3	$^1\text{H}$	1.25 doublet (3.00)	0.34 doublet (1.64)	29
20b	3.3, entry 4	$^1\text{H}$	0.95 singlet (0.111)	0.32 singlet (2.846)	93
21b	3.3, entry 6	-	GC-MS analysis only		20
22b	3.3, entry 8	$^{19}\text{F}$	-70.0 singlet (0.1485)	-70.9 singlet (1.000)	74
23b	3.4, entry 1	$^1\text{H}$	1.27 singlet (39.692)	0.63 singlet (9.178)	62
23c	3.4, entry 1	$^1\text{H}$	1.24 singlet (1.92)	1.20 singlet (24.58)	86
24b	3.4, entry 3	$^{19}\text{F}$	-70.12 singlet (0.123)	-71.07 singlet (2.844)	92
24c	3.4, entry 3	$^{19}\text{F}$	-70.02 singlet (0.063)	-70.82 singlet (1.000)	88
32b	3.6, entry 2	-	GC-MS analysis only		77
33b	3.6, entry 3	$^1\text{H}$	3.29 doublet (1.00)	2.90 doublet (0.060)	88
34b	3.6, entry 4	$^{19}\text{F}$	-70.08 singlet (0.102)	-70.94 singlet (1.000)	82

[a]  $\text{CDCl}_3$ , 25°C, 300 MHz [b]  $\text{CDCl}_3$ , 60°C, 300 MHz

**General procedure for kinetic investigations employing precatalyst (+)-13c.** Kinetic studies were all performed for the conversion of 2,2-diphenyl-pent-4-enylamine (**17**) to 2-methyl-4,4-diphenylpyrrolidine **18**. Kinetic NMR experiments were repeated to ensure consistency of data within  $\pm 1$  % error (Figures 3.5, 3.6 and 3.7). **Example: (10 mol % catalyst loading)** 2,2-diphenyl-pent-4-enylamine (**17**) (100 mg, 0.42 mmol), 1,3,5-trimethoxybenzene (23.6 mg, 0.14 mmol), precatalyst (+)-**13c** (28.6 mg, 0.042 mmol) and *d*<sub>8</sub>-toluene (1.0 g) were combined in a Teflon sealed J. Young NMR tube. The NMR tube was placed in a preheated 400 MHz NMR spectrometer (110 °C). <sup>1</sup>H NMR spectra were collected in 2.5 min intervals until >80 % conversion was observed. First order consumption of substrate was only observed up to approximately 60 % conversion. Comparison of the integration of aminoalkene substrate peaks with internal standard peaks was used to determine the concentration of substrate and product at any given time. This procedure was repeated for 5, 7.5 and 12.5 mol % catalyst loading.

## Chapter 4



### Summary and Future Directions

---

#### 4.1 Future Directions

##### 4.1.1 Proposed Modification to Precatalysts **(-)-13b** and **(+)-13c** to enhance enantioselectivity and reactivity

While the results for precatalyst **(-)-13b** and **(+)-13c** were ground breaking for the field of group 4 hydroamination, there is still an abundance of research that is necessary before a general alkene hydroamination catalyst is discovered. The problematic limitation of precatalyst **13** to *gem*-disubstituted aminoalkenes must be addressed. To fully recognize what is required in a more reactive catalyst, our group is looking at what alterations can be made to complex **13** without significantly altering the enantioselectivity. With an abundance of commercially available amine and acid chloride starting materials, modifications to amidate ligands can be easily accomplished to influence the catalyst both electronically and sterically (Figure 4.1).

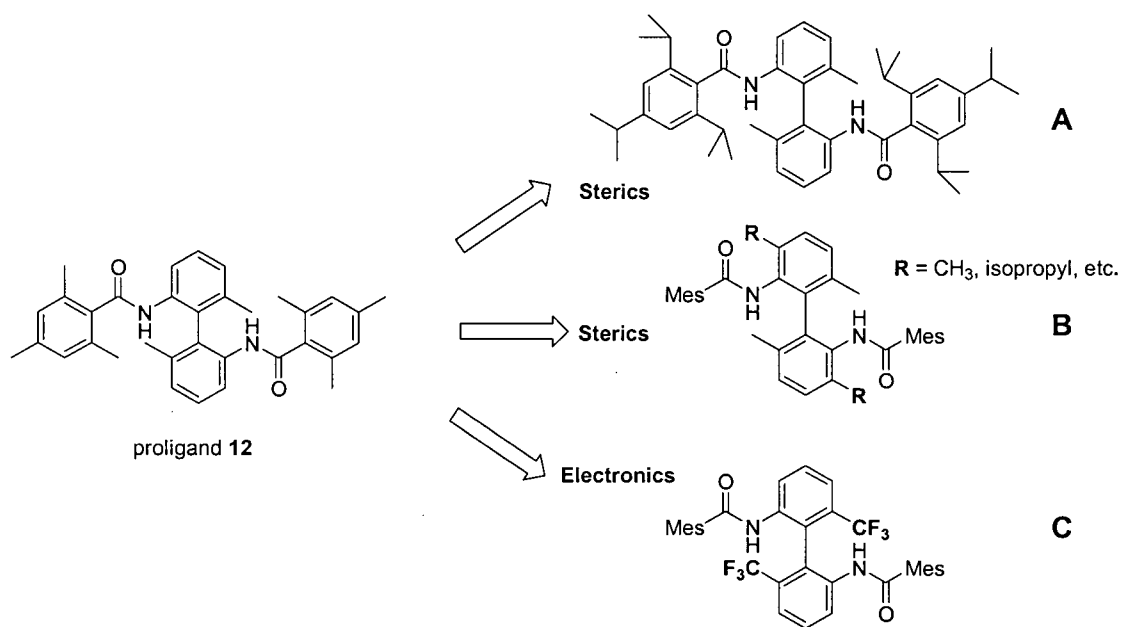


**Figure 4.1** Suggested modifications to proligand **12** to enhance reactivity and/or enantioselectivity

Figure 3.9 in Chapter 3 illustrated a proposed mechanism for the enantioselectivity during cyclohydroamination with precatalyst (+)-**13c**. Our preliminary hypothesis is that the 2,6-dimethyl substituents on the mesityl group are essential for producing high enantioselectivity. As proposed, the steric interaction between these 2,6-dimethyl substituents and the geminal disubstituents on the substrate are what influences the enantioselectivity. Therefore, increasing the size of these 2,6-dimethyl substituents should positively influence the enantioselectivity if this proposed mechanism holds true. To test this hypothesis, we could potentially replace the methyl substituents with bulkier isopropyl substituents. 2,4,6-Triisopropyl benzoyl chloride is commercially available and the synthesis of the bis(amide) should be analogous to the synthesis of proligand **10** in Chapter 2 (Figure 4.2). The synthesis of this proligand is under current investigation in our group.



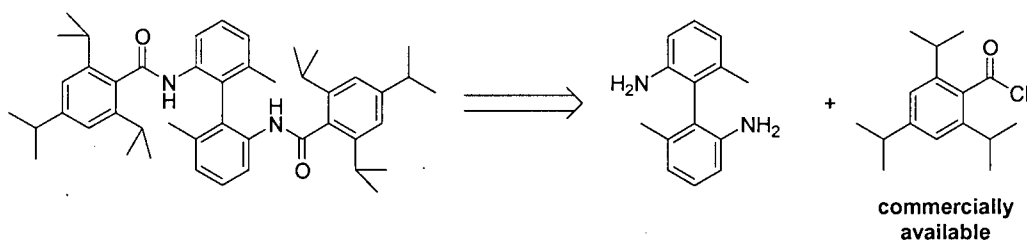


**Figure 4.2** Retrosynthetic approach to the synthesis of the 2,4,6-triisopropylphenyl analog of prolignand **12**.

The second method to change the steric influence of the mesityls in precatalyst **13** could be the addition of 3,3'-substituents ortho to the amide nitrogens on the prolignand (structure B, Figure 4.1). It appears from the X-ray solid state molecular structure (Chapter 2, Figure 2.4) that ortho 3,3'-substituents on the biphenyl backbone could interact with the mesityl substituents to potentially force the mesityl to be rigidly oriented with the methyl groups directed at zirconium. If the coordination geometry of the complex is not altered significantly, this could be an interesting way to indirectly influence the steric contributions from the mesityl substituents without further congesting the reactive metal center.

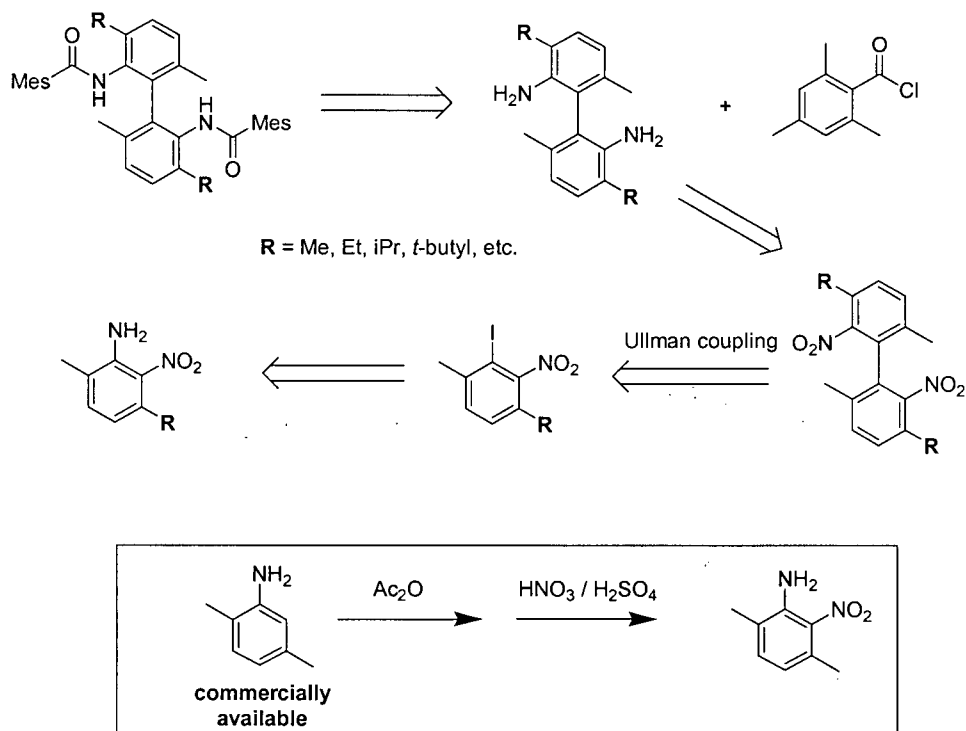


**Figure 4.3** Proposed synthesis of an ortho substituted biphenyl diamine prolignand precursor.



There are many modifications that can be envisioned to change reactivity of these axially chiral biphenyl bis(amide) proligands. The suggestions described herein are just a few examples of the many modifications that could be achieved. Some of this work is currently under investigation in the Schafer research group.

#### 4.1.2 Synthesis of a Chiral Aniline. Progress Towards a Chiral Bidentate Amidate Ligand for Asymmetric Hydroamination

With research not dedicated primarily to an axially chiral tethered ligand, a second approach to a group 4 asymmetric hydroamination catalyst is also in progress. This ongoing side project stemmed from earlier hydroamination precatalysts prepared by our research group. As discussed previously, titanium and zirconium complexes **3** and **4** were found to be effective precatalysts for the hydroamination of aminoalkenes.<sup>53</sup> In addition, hydroamination precatalyst **13** showed comparable reactivity and gave ee's up to 93 %. The results for complexes **3**, **4** and **13** motivated us to prepare a precatalyst that contained a chiral non-tethered  $\kappa_2$  amidate ligand rather than the tetradentate  $\kappa_4$  ligand in **13**. We were interested to see if we could maintain high enantioselectivity using a non-tethered chiral amidate ligand. The solid state structure of **3** in Figure 4.5 reveals that the diisopropyl substituents are closest to the catalytically active site. Theoretically, the isopropyl groups in **3** could be replaced with bulky chiral substituents. Furthermore, if no ligand rearrangement occurs during hydroamination, the chirality in this substituent may be close enough to the catalytically active imido intermediate to transfer chirality into the pyrrolidine or piperidine products.

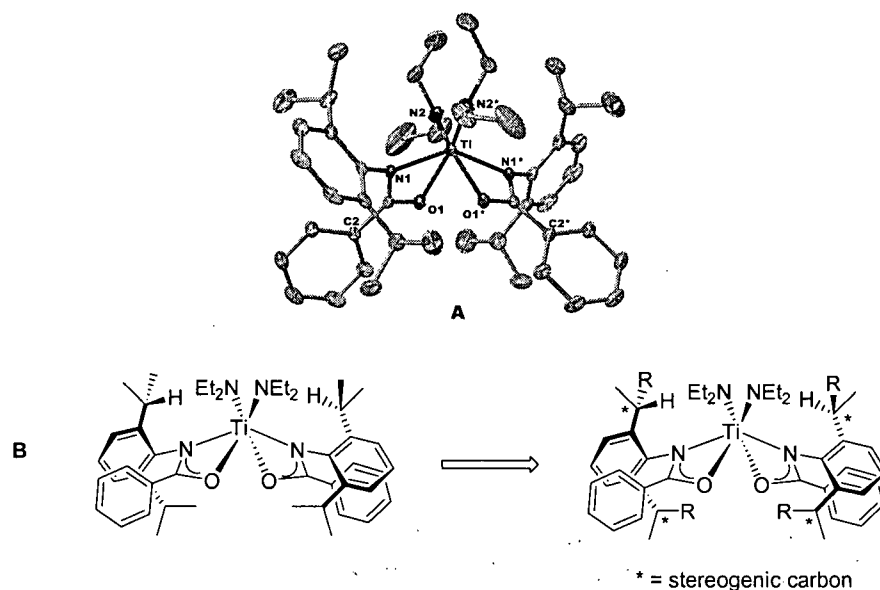


**Figure 4.5** A) Side view of precatalyst **3**<sup>73</sup>, and B) Proposed incorporation of the 2,6-substituted chiral aniline in precatalyst **3**.

When precatalyst **3** was employed as an alkyne hydroamination precatalyst, the diisopropyl substituents on the amidate ligands play a central role in the anti-Markovnikov regioselectivity observed.<sup>73</sup> The isopropyl groups are also important in the stabilization of monomeric complexes. To introduce chirality into the bis(amidate) ligands, we proposed to replace the 2,6-diisopropylphenyl substituent with a 2,6-chiral analog. At the outset of this research project there had been no reported synthesis of 2,6-chiral anilines in the literature. A 2,6-chiral aniline was reported two years earlier when Coates and coworkers incorporated this aniline into an  $\alpha$ -diimine nickel catalyst for isoselective 2-butene polymerization (Figure 4.6).<sup>100</sup> However, the synthesis of the chiral aniline employed was not included in that preliminary communication. Since many other catalysts in the literature also incorporate 2,6-diisopropylanilines into their ligands, we anticipated that a 2,6-substituted chiral aniline may not only be interesting for our precatalysts, but for many other catalysts as well.

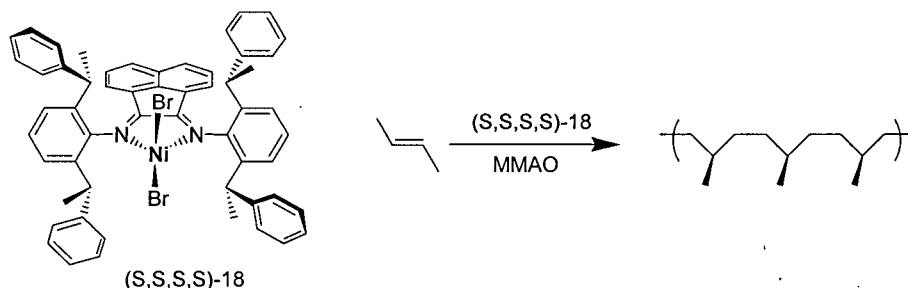
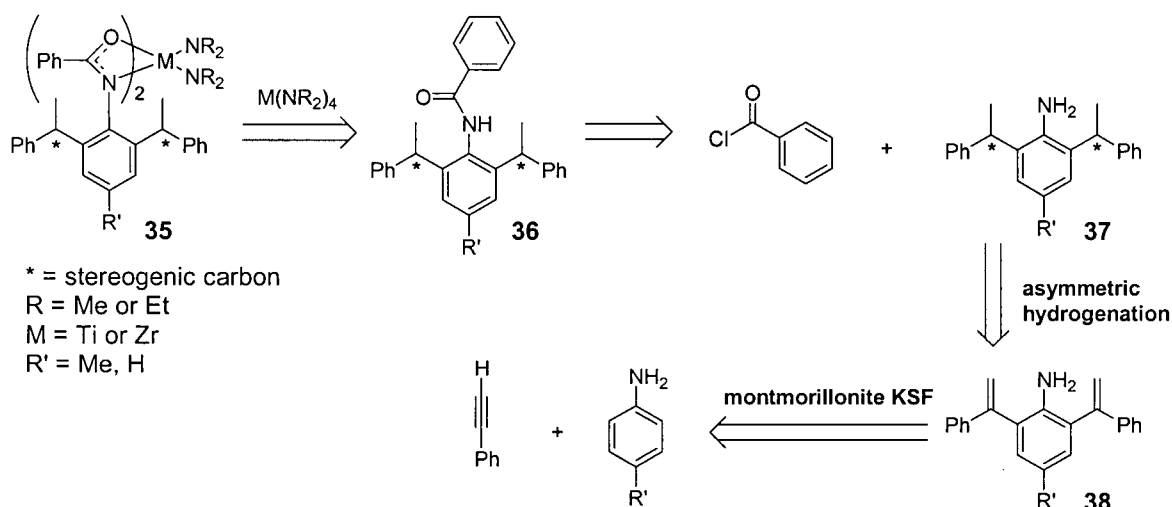


**Figure 4.6** Application of chiral aniline **37** incorporated into a  $\alpha$ -diimine nickel catalyst for isoselective 2-butene polymerization.

The most challenging part in the preparation of chiral precatalyst **35** is the synthesis of the chiral amidate proligand **36** (Scheme 4.1). A literature search of 2,6-disubstituted anilines resulted in a straightforward synthesis of 4-methyl-2,6-bis-(1-phenyl-vinyl)-phenylamine **38** reported by Sartori and coworkers.<sup>101</sup> Hydrogenation of the *gem*-dienes would produce two new stereogenic carbons at the 2,6-benzylic positions of aniline **37**. If non-asymmetric hydrogenation conditions are employed, a ratio of 2:1:1 would be obtained for the meso-isomer, and the R,R and S,S stereoisomers. The meso-isomer, however, is undesirable for asymmetric catalysis, so minimizing the formation of this compound would be ideal.



**Scheme 4.1** Proposed synthesis of a chiral amide proligand and bis(amidate)bis(amido) precatalyst

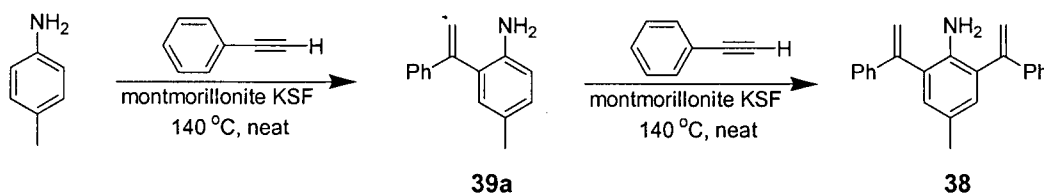
The synthesis of **38** was initially attempted using aniline to see if this reaction would proceed with ortho regioselectivity. However, when four equivalents of phenylacetylene were reacted with one equivalent of aniline and montmorillonite KSF as a catalyst, poor regioselectivity was observed. GC-MS analysis showed monosubstituted aniline **39a** (73.4 %) as well as two other products that are proposed to be the desired product **38** along with the 2,4-substituted product **40** (10.8% and 15.8%, Figure 4.7).

	Compound <b>39</b> (%)	Compound <b>38</b> or <b>39b</b> (%)	
Reaction time and Temperature			
5 h, 140°C	73.4	10.8	15.8
10 h, 140°C	63.3	18.6	18.1
24 h, 140°C	44.3	26.2	29.5

**Figure 4.7** GC-MS analysis of the reaction mixture for the synthesis of compound **38**

Although these are the likely byproducts that could form during this reaction, we can not dismiss the fact that anti-Markovnikov products (1,2-diaryl alkenes) are also possible. However, Sartori and coworkers reported high Markovnikov regioselectivity. Heating was continued at 140 °C for 5 hours to see if the prepared desired product **38** could be improved in yield. Unfortunately, GC-MS analysis showed further conversion of the mono-substituted product (63.3%) to the desired product **38** as well as the 2,4-disubstituted product (18.6% and 18.1%). Another 2 equivalents of phenylacetylene were added, and the reaction was heated for an additional 24 hours. GC-MS analysis of this reaction mixture showed additional conversion of the mono-substituted product (44.3%), however the quantity of the desired product **38** and the 2,4-disubstituted product also increased (26.2% **39a** and 29.5% **39b**). Overall, the reaction with aniline proved to have poor *ortho*-selectivity.

In order to reduce the undesired 2,4-disubstituted product, *p*-toluidine was used to block the para position from substitution. Identical reaction conditions were applied to *p*-toluidine, but a number of unidentified by-products were also produced. To minimize byproduct formation, compound **39a** was isolated and purified rather than preparing **38** through a one pot synthesis (Scheme 4.2). When one equivalent of phenylacetylene and *p*-toluidine are heated to 140 °C for 6 h, the major product is monosubstituted aniline **39a**. Compound **39a** was in a 90 % crude yield, and <sup>1</sup>H NMR, <sup>13</sup>C NMR spectroscopy and MS(EI) were in correspondence with literature values.<sup>101</sup>

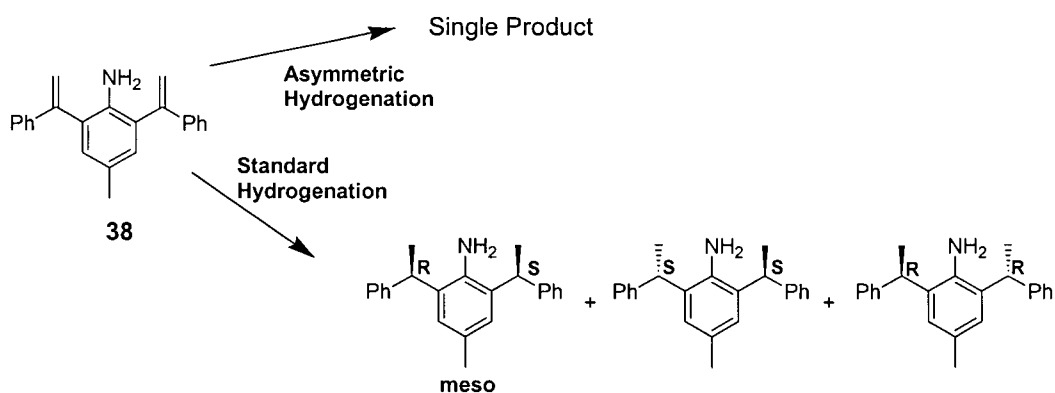


Scheme 4.2

Further reaction of the isolated monosubstituted aniline **39a** with phenylacetylene and montmorillonite KSF produced the disubstituted product **38** after 9 h at 140 °C (Scheme 4.2). Compound **38** was obtained in an 82 % yield from *p*-toluidine after purification by flash chromatography. <sup>1</sup>H NMR, <sup>13</sup>C NMR spectroscopy and mass spectrometry of compound **38** were also in correspondence with literature values.<sup>101</sup> The geminal alkene

protons had coupling constants of 1.5 Hz, indicative of Markovnikov addition of the phenylacetylene. Mass spectrometry and  $^1\text{H}$  NMR spectroscopy support disubstitution of the phenylacetylene.

With a straightforward synthesis of aniline **38** developed, we required a method that could convert this diene to the desired chiral aniline **37**, and resolve the compound into a single enantiomer. The methods proposed include asymmetric hydrogenation of **38**, or chiral salt resolution of the racemic mixture obtained through palladium catalyzed hydrogenation of **38** (Scheme 4.3). There are two approaches to asymmetric hydrogenation. These include the utilization of a chiral auxiliary followed by homogeneous palladium on carbon catalyzed hydrogenation, or homogeneous asymmetric hydrogenation catalysis.



**Scheme 4.3**

Derivatization at the amine on the 2,6-bis(1-phenylvinyl)-4-methylaniline can be accomplished with a bulky chiral auxiliary such as camphor sulphonyl chloride. The incorporated chiral functionality may control the stereochemical outcome upon hydrogenation. With a chiral auxiliary, a major diastereomeric product could be obtained upon hydrogenation. The mixture of diastereomers produced could then be separated by chromatography or recrystallization to give a single diastereomer. At this point, the chiral auxiliary would be cleaved and a single enantiomer obtained.



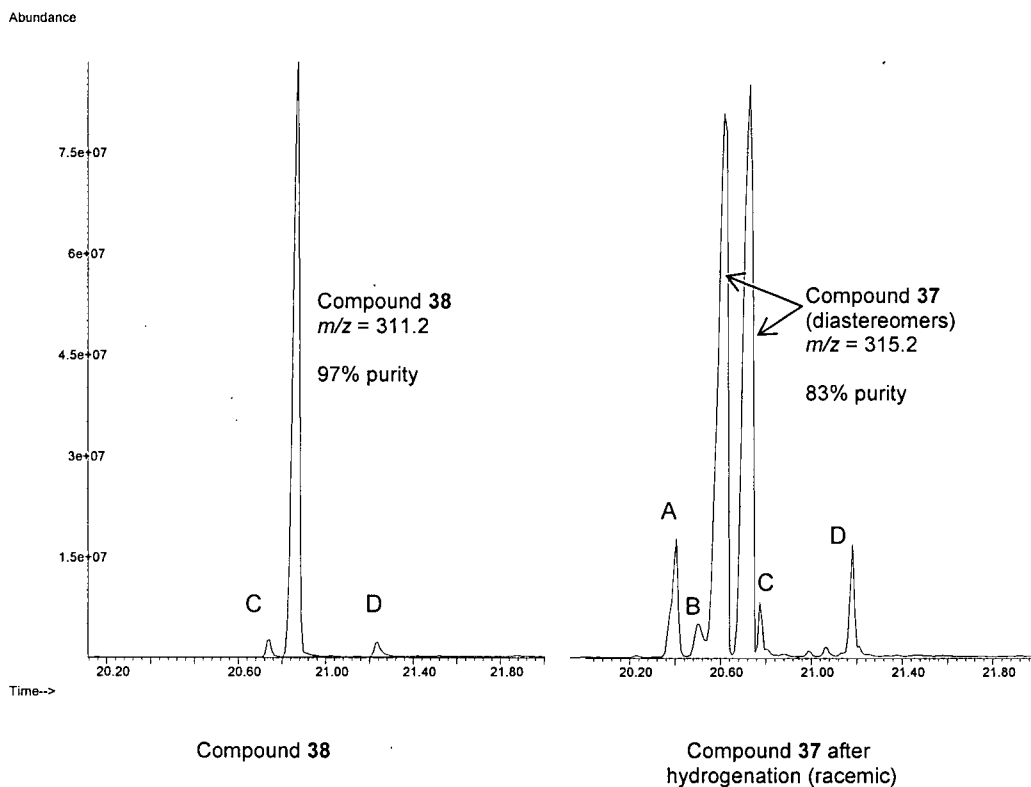
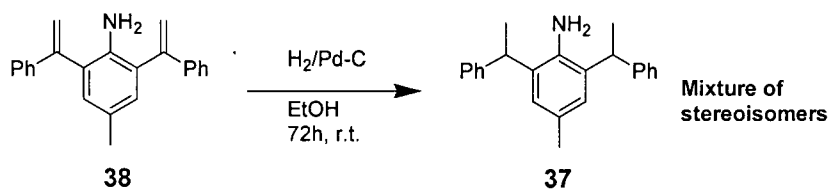
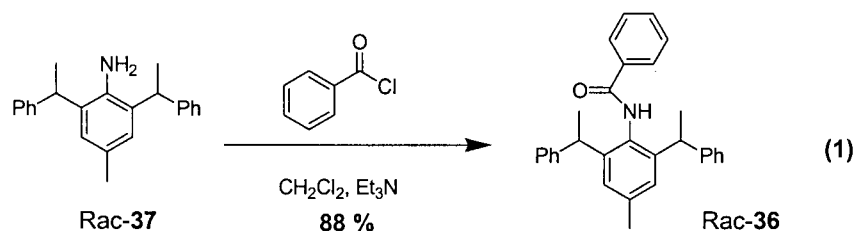
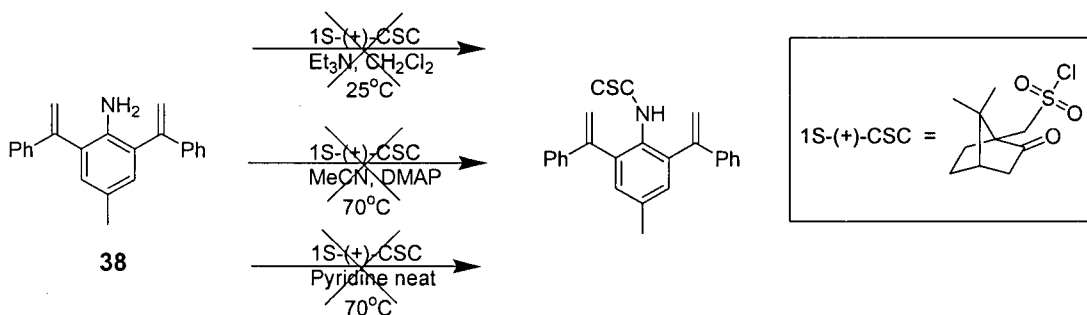


**Figure 4.8** GC-MS chromatograph for compound **38** before hydrogenation (left), and after hydrogenation (right, compound **37**).

To ensure that the synthesis of proligand **36** was achievable, we first prepared this compound as a racemate before efforts were directed towards the resolution of **37**. Hydrogenation of **38**, with 10 % palladium on carbon, produced a 1:1 racemic mixture of diastereomers by GC-MS analysis (Figure 4.8). The scale of this hydrogenation was increased to 1 g, but unknown impurities were also produced as 35 % of the total mixture (Figure 4.8, A through D). The impurities could not be separated by chromatography, so the crude mixture was reacted with benzoyl chloride to give racemic proligand (**rac-36**, Equation 1). Purification of the racemic proligand **36** was achieved by chromatography with an isolated yield of 88 %.

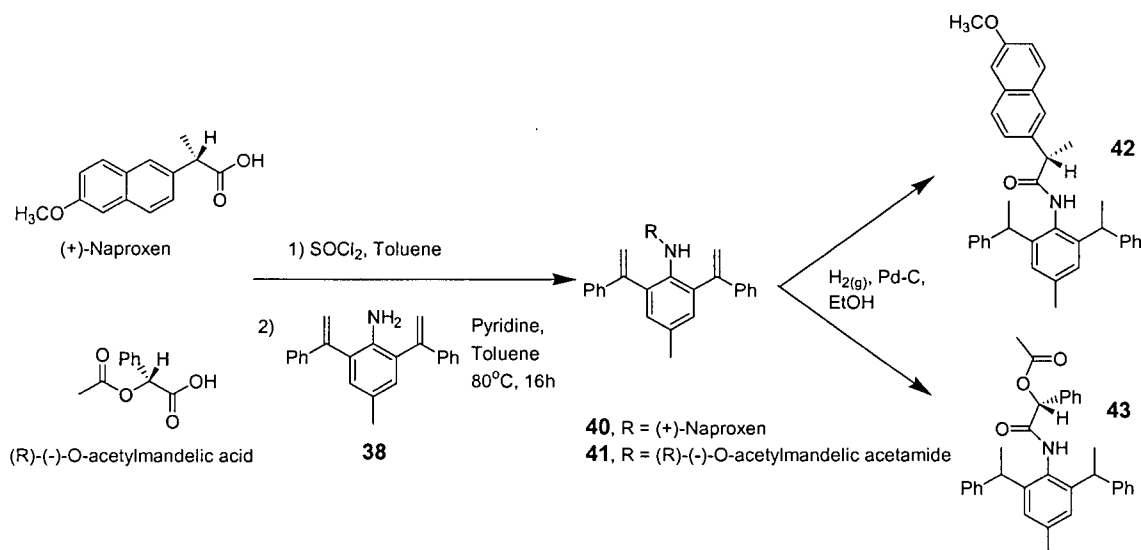


With the synthesis of proligand **36** achievable, we proceeded with the hydrogenation employing a chiral auxiliary directing substituent. The first chiral auxiliary used was (1S)-(+)-10-Camphorsulfonyl chloride (1S-(+)-CSC). Many efforts to prepare the (1S)-(+)-10-Camphorsulfonyl substituted aniline were problematic. Different reaction conditions employed for this transformation proved unsuccessful (Scheme 4.4). The camphorsulfonyl substituent appears to be too bulky to react with the 2,6-bis(1-phenylvinyl) substituted aniline under the conditions employed.



**Scheme 4.4** Unsuccessful reaction conditions employed for the preparation of the 1S-(+)-camphor sulfonamide derivative of aniline **38**.

As an alternative, commercially available carboxylic acids (+)-Naproxen and (R)-(-)-O-acetylmandelic acid were used as chiral auxiliaries. (+)-Naproxen and (R)-(-)-O-acetylmandelic acid were converted to the acid chlorides in quantitative yields by refluxing with excess thionyl chloride with toluene as the solvent. The acid chlorides were reacted with **38** to produce chiral amides **40** and **41** (Scheme 4.5).



**Scheme 4.5** Preparation of compounds **42** and **43** using chiral auxiliaries (+)-Naproxen and (R)-(-)-O-acetylmandelic acid.

The chiral amides produced (**40** and **41**) were first purified by column chromatography then subjected to hydrogenation with 10% palladium on carbon as the catalyst. After hydrogenation, the resulting products were analyzed by GC-MS and <sup>1</sup>H NMR spectroscopy. The <sup>1</sup>H NMR spectra of **42** and **43** contained no alkene protons confirming that the hydrogenation was complete, however, the complexity of the spectrum indicated that poor stereoselectivity was obtained in the hydrogenation step. GC-MS analysis of **42** was unsuccessful even at elevated temperatures and extended run times. In contrast, GC-MS analysis of compound **43** was successful; unfortunately a complex mixture containing 5 products was obtained (Figure 4.9).

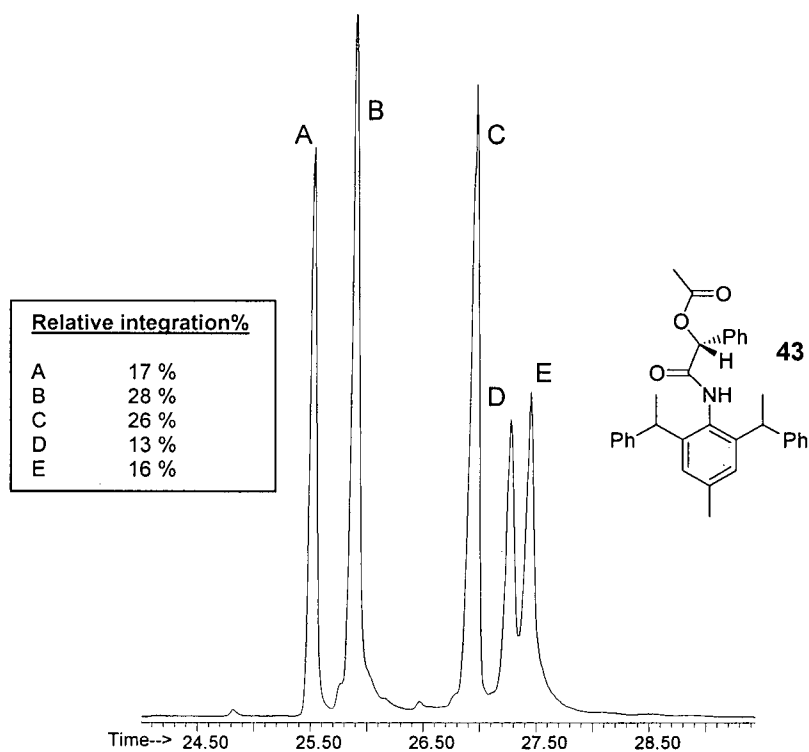


**Figure 4.9:** GC-MS chromatograph for the hydrogenation products of compound **43**.

The mass spectrum associated with compounds A-E (Figure 4.9) all contain the same mass and fragment pattern. This suggests that each peak represents a different stereoisomer of compound **43**. Although four diastereomeric products are possible from hydrogenation of **41**, the GC-MS chromatograph contains one more signal than expected. At present, there is no explanation for the fifth GC-MS signal. However, it is possible that fragmentation occurred in the GC-MS giving rise to an extra signal as an instrumental anomaly. The only conclusion from this chromatogram is that a complex mixture of stereoisomers was obtained, and the (R)-(-)-O-acetylmandelic substituent is not an effective chiral auxiliary for asymmetric hydrogenation.

While this project was in progress, a report by Coates and coworkers was published discussing a similar strategy towards chiral anilines **37**.<sup>102</sup> This strategy involved ortho-alkylation of *p*-toluidine using styrene in the presence of a catalytic

amount of triflic acid. This alternative method produced **37** in one pot using 10 equivalents of styrene and 20 mol % of triflic acid. The product was obtained in a 77 % yield, and the (R,R), (S,S) and Meso products were separated by flash chromatography followed by semi-preparative chiral HPLC. This reaction yielded 2.89 g of racemic product, but no yields were specified after chromatography or semi-preparative HPLC separations.

This method described by Coates to resolve chiral anilines (**(R,R)**-**37** and (**(S,S)**-**37**) may still be valuable for investigations into asymmetric alkene hydroamination using bidentate amidate ligands. However, future work could uncover a more efficient and economical method to prepare the chiral aniline **37**, that avoids semi-preparative chiral HPLC. At this stage in the research project, this project was abandoned to favor the development of the axially chiral complexes discussed in Chapters 2 and 3.

Future work to uncover a more efficient method to prepare the chiral aniline **37**, other than the chiral auxiliary/hydrogenation method described earlier, is homogeneous catalyzed asymmetric alkene hydrogenation. Research towards catalytic asymmetric hydrogenation has been ongoing for more than three decades, but asymmetric hydrogenation of unfunctionalized alkenes has been achieved with only limited success.<sup>103</sup> Pfaltz and Buchwald have developed catalysts that are reasonably efficient for asymmetric hydrogenation of unfunctionalized alkenes. Buchwald and coworkers have designed a chiral titanocene catalyst that is capable of asymmetric hydrogenation of unfunctionalized substituted styrene.<sup>104</sup> High yield, and ee's up to >99 % were obtained for these transformations. Catalysts developed by Pfaltz and coworkers have also shown high efficiency in asymmetric hydrogenation of substituted styrene substrates. Among the catalysts developed, the chiral phosphino-imidazole iridium complexes have shown enantioselectivities greater than 98 %.<sup>105,106</sup> Overall, the employment of asymmetric hydrogenation catalysts should be considered if efforts in this area are resumed.

Although the results presented in this chapter did not lead to the synthesis of a chiral aniline, the preliminary ground work sets the stage for future work in this area. Ultimately, once synthesized in an enantiopure form, this chiral aniline can be incorporated into bis(amidate)bis(amido) group 4 hydroamination precatalysts. Synthesis of a bidentate amidate precatalyst **35** would be an interesting compliment to the work

done in Chapters 2 and 3. Comparing the reactivity and enantioselectivity of complex **35** to the biphenyl tethered complex **13** described in Chapter 3, should provide a stronger understanding of how important a rigid ligand system is for asymmetric hydroamination. However, the lack of predictability with respect to geometry for octahedral complexes employing bidentate ligands may be a factor in the resulting enantioselectivity.

## 4.2 Summary and Conclusions

Four bis(amide) proligands that contain axially chiral biphenyl tethers were synthesized in a facile, modular manner. The effectiveness of these bis(amidates) as ligands for titanium and/or zirconium complexation was demonstrated, and the relative reactivities and enantioselectivities of these complexes were probed using the cyclohydroamination of 2,2-diphenylpent-4-ene-1-amine **17**. The modularity of the amidate ligands employed, allowed for the study of both electronic and steric effects on aminoalkene hydroamination. The initial screening of titanium and zirconium bis(amidate)bis(amide) complexes confirmed that zirconium precatalysts (-)-**13b** and (+)-**13c** display moderate reactivity and the highest enantioselectivities. Substrate scope and mechanistic analyses were performed using precatalyst (-)-**13b** and (+)-**13c**.

The reactivity of bis(amidate)bis(amido) titanium complexes **13a**, **15a** and **16a** for alkene hydroamination was initially investigated. Overall, the reactivity of the titanium complexes **13a**, **15a** and **16a** were very poor, displaying reaction times of up to 7 days with low conversions. Previous reports by our group have shown higher reactivity for bis(amidate)bis(amido) zirconium precatalysts compared to their titanium analogs.<sup>53</sup> To confirm that this same trend applied for these tethered ligand systems, zirconium analogs (-)-**13b**, (+)-**13c**, (-)-**15b** and (+)-**16b** were also prepared. Cyclohydroamination of aminoalkene **17** was approximately 2 orders of magnitude faster for the zirconium precatalysts, in comparison to their titanium analogs (Table 3.1). In addition, incorporating trifluoromethyl substituents in zirconium complexes (-)-**15b** and (+)-**16b**, displayed increased reactivity in comparison to non-fluorinated zirconium complexes (-)-**13b** and (+)-**13c**. Overall, the trifluoromethyl substituted zirconium complexes (-)-**15b**

and (+)-**16b** gave the highest reactivity amongst the titanium and zirconium complexes prepared.

Enantioselectivities for the hydroamination of 2,2-diphenylpent-4-ene-1-amine **17** were also determined for complexes **13** through **16**. Although the reactivity of titanium complex (-)-**13a** was poor in comparison to zirconium complexes (-)-**13c** and (+)-**13b**, enantioselectivities were comparable ranging from 64 % to 74 % under a variety of different reaction conditions (Table 3.2). On the other hand, the high enantioselectivity observed with precatalysts (-)-**13b** and (+)-**13c** was not reproducible with *p*-trifluoromethylphenyl and 3,5-bis(trifluoromethyl)phenyl substituted precatalysts (-)-**15b** and (+)-**16b**. The lack of steric bulk at the 2,6-positions in *p*-trifluoromethylphenyl and 3,5-bis(trifluoromethyl)phenyl decreased the enantioselectivity significantly. Based on these observations, the steric bulk imposed by the 2,6-dimethyl substituents of the mesityls groups in **13** appears to be significant for enantioselectivity. Overall, incorporating trifluoromethyl substituents into zirconium complexes (-)-**15b** and (+)-**16b** produced higher reactivity, but once again, the mesityl substituents in complexes (-)-**13b** and (+)-**13c** were essential for high enantioselectivities.

Previous investigations by our group,<sup>53</sup> in addition to the lack in reactivity of N-methyl-2,2-diphenylpent-4-ene-1-amine **28** with precatalyst (+)-**13c**, suggest that hydroamination proceeds through an titanium or zirconium imido intermediate followed by a [2+2] alkene cycloaddition. A  $\sigma$ -bond insertion mechanism cannot be ruled out, however, we have provided strong evidence in substrate scope experiments and kinetic investigations that suggests this is not the mechanism observed for our catalysts. Kinetic investigations for precatalyst (+)-**13c** show first order consumption in aminoalkene substrate **17**, and first order catalyst dependence which is indicative of a metal imido based mechanism. This is in stark contrast to zero order substrate dependence for lanthanide based systems, which are known to proceed in a  $\sigma$ -bond insertion mechanism.<sup>107</sup> Based on this imido intermediate and the observed solid state molecular structure of (+)-**13c** (Chapter 2, Figure 2.4), we have proposed a mechanism to explain observed enantioselectivity. This mechanism rationalized both diastereoselectivity and enantioselectivity in the hydroamination of aminoalkene substrates **17**, **23** and **24**.

Aminoalkene substrate scope analysis was performed on the most reactive and selective zirconium complexes (-)-**13b** and (+)-**13c** (Chapter 3, Tables 2, 3 and 4). Pyrrolidine products were obtained in high yields and enantioselectivities up to 93% could be achieved for the hydroamination of gem-disubstituted aminoalkenes. To our knowledge, 93% is highest enantioselectivity reported for a neutral group 4 catalyst, and is the highest selectivity reported for this particular test substrate (1-amino-3,3-dimethyl-4-pentene). Enantioselectivities were significantly reduced for the formation of  $\alpha$ -chiral piperidines (eg. **19b**, ee = 29 %), and unfortunately, both unsubstituted and monosubstituted aminoalkene substrates displayed no reactivity. This implies that the gem-disubstituent effect plays a vital role in the cyclohydroamination of aminoalkenes using complexes (-)-**13b** and (+)-**13c** under the conditions employed.

Herein the complex synthesis and challenging nature of controlling reactivity and enantioselectivity for aminoalkene hydroamination has been demonstrated. Alterations to the precatalyst, such as changing the metal and/or altering the electronics and sterics of the ligands can have a significant effect on reactivity and selectivity. As a major contribution to this area of research, we have synthesized the first fully characterized neutral group 4 catalyst capable of enantioselective alkene hydroamination.<sup>57</sup> We have demonstrated that this catalyst is capable of producing ee's up to 93 % for the hydroamination of *gem*-disubstituted aminoalkenes. Although this is an important result toward the overall advancement of asymmetric alkene hydroamination, research is ongoing in our group, and a considerable amount of work must be carried out to develop a general alkene hydroamination catalyst. The investigations and proposals described here provide the foundation for our ongoing research program.



### 4.3 Experimental

**General Procedures:** All chemicals and solvents were commercially available and used as received unless stated otherwise.  $^1\text{H}$  NMR, and  $^{13}\text{C}$  NMR spectra were recorded on either a Bruker Avance 300 MHz or Avance 400 MHz spectrometer. GC-MS analysis was completed using an Agilent 6890N GC system with a 5973 mass selective detector. Mass spectrometry (ESI, EI) and elemental analyses were performed by analytical services in the Department of Chemistry at the University of British Columbia. 1-phenyl-1-(2-amino-5-methylphenyl)ethylene and 4-Methyl-2,6-bis-(1-phenyl-vinyl)-phenylamine were prepared according to a modified literature procedure.<sup>101</sup>

**1-phenyl-1-(2-amino-5-methylphenyl)ethylene (39):** To a 50 mL sealed reaction vessel was added p-toluidine (1.01 g, 9.4 mmol), phenylacetylene (Aldrich, 1.0 mL, 0.97 g, 9.5 mmol), and montmorillonite KSF (Aldrich, 1.02 g). The neat mixture was heated to 140 °C until the reaction was complete by GC-MS (6 h). The brown residue obtained was dissolved in ethyl acetate (50 mL) and filtered through Celite. The ethyl acetate solution was dried on  $\text{MgSO}_4$ , and reduced under vacuum to yield a yellow oil (1.81 g, 90 %).  $^1\text{H}$  NMR (300 MHz,  $\text{CDCl}_3$ )  $\delta$  7.41 – 7.30 (5 H, m, Ar-H), 6.97-6.95 (2 H, m, Ar-H), 6.62 (1 H, d,  $^3J_{\text{HH}} = 8.0$  Hz, Ar-H), 5.79 (1 H, d,  $^2J_{\text{HH}} = 1.5$  Hz,  $\text{C}=\text{CH}_2$ ), 5.35 (1 H, d,  $^2J_{\text{HH}} = 1.5$  Hz,  $\text{C}=\text{CH}_2$ ), 3.44 (2 H, br s,  $\text{NH}_2$ ), 2.27 (3 H, s,  $\text{CH}_3$ );  $^{13}\text{C}$  NMR (75 MHz,  $\text{CDCl}_3$ ):  $\delta$  147.3, 141.3, 139.7, 131.2, 129.3, 128.5, 128.0, 127.5, 126.6, 126.5, 115.9, 115.8, 20.4; MS (EI):  $m/z$  208 ( $\text{M}^+$ ).

**4-Methyl-2,6-bis-(1-phenyl-vinyl)-phenylamine (38):** To a 50 mL sealed Kontes reaction vessel was added **39** (1.79 g, 8.6 mmol), phenylacetylene (Aldrich, 1.0 mL, 0.97 g, 9.5 mmol) and montmorillonite KSF (Aldrich, 1.01 g). The neat mixture was heated to 140 °C until the reaction was complete by GC-MS (7h). The residue was cooled to room temperature, dissolved in ethyl acetate and dried on  $\text{MgSO}_4$ . Purification by silica chromatography (9:1 Hexane/EtOAc) gave the desired product as a yellow oil that solidified upon standing (2.39 g, 79.6 %). Purity by GC-MS analysis was 98 %.  $^1\text{H}$  NMR (300 MHz,  $\text{CDCl}_3$ ):  $\delta$  7.41-7.25 (10 H, m, Ar-H), 6.95 (2 H, s, Ar-H), 5.78 (2 H, d,  $^2J_{\text{HH}} =$

1.4 Hz, C=CH<sub>2</sub>), 5.36 (2H, d, <sup>2</sup>J<sub>HH</sub> = 1.4 Hz, C=CH<sub>2</sub>), 3.39 (2 H, br s, NH<sub>2</sub>), 2.28 (3 H, s, CH<sub>3</sub>); <sup>13</sup>C NMR (75 MHz, CDCl<sub>3</sub>): δ 148.9, 141.2, 140.6, 132.3, 130.0, 129.5, 129.2, 128.8, 128.2, 128.1, 117.6, 20.4; MS (EI): *m/z* 311 (M<sup>+</sup>).

**4-Methyl-2,6-bis-(1-phenyl-ethyl)-phenylamine (rac-37):** A solution of **39** (1.0 g, 3.2 mmol) and Pd-C (10 % wt/wt, 200 mg, 20 % by weight) in EtOH (50 mL) was stirred vigorously under an 1 atm of hydrogen overnight. The solution was filtered through Celite and the solvent was removed by rotary evaporation to give a light yellow clear oil (1.0 g, quantitative). Purity by GC-MS analysis was 84 %. Characterization data was in agreement with literature values.<sup>102</sup>

**N-[4-Methyl-2,6-bis-(1-phenyl-ethyl)-phenyl]-benzamide (rac-36).** To a solution of **rac-37** (1.0 g, 3.3 mmol) in dichloromethane (35 mL) and Et<sub>3</sub>N (365 mg, 0.5 mL, 3.6 mmol) was added benzoyl chloride (475 mg, 0.4 mL, 3.3 mmol) dropwise at 0°C. The solution was stirred overnight at room temperature; followed by removal of solvent through rotary evaporation. To the residue was added 1M HCl (20 mL), and the mixture was extracted with EtOAc (3 x 25 mL). The combined extracts were dried on MgSO<sub>4</sub>, filtered and reduced to give a beige solid. Purification by chromatography (flash chromatography grade silica) with 4:1 Hexanes/EtOAc gave the product as a white solid (1.21 g, 88 %). Purity by GC-MS analysis was >98%. <sup>1</sup>H NMR (300 MHz, CDCl<sub>3</sub>): δ 7.54 - 7.36 (5 H, m, Ar-*H*), 7.25 - 7.10 (10 H, m, Ar-*H*), 6.97 (2 H, s, Ar-*H*), 4.30 - 4.19 (2 H, m, CH), 2.45 (1.5 H, s, Ar-CH<sub>3</sub>, diastereomer A), 2.36 (1.5 H, s, Ar-CH<sub>3</sub>, diastereomer B), 1.59 (3 H, d, <sup>3</sup>J<sub>HH</sub> = 7.2 Hz, diastereomer A), 1.53 (3 H, d, <sup>3</sup>J<sub>HH</sub> = 7.2 Hz, diastereomer B); MS (EI): *m/z* 419 (M<sup>+</sup>).

**(S)-2-(6-Methoxy-naphthalen-2-yl)-N-[4-methyl-2,6-bis-(1-phenyl-vinyl)-phenyl]-propionamide (40):** To a solution of (+)-Naproxen (500 mg, 2.1 mmol) in toluene (4 mL) was added SOCl<sub>2</sub> (0.4 mL, excess). The solution was heated for 16 h at 80 °C then the solvent and excess SOCl<sub>2</sub> were removed under high vacuum to produce a yellow residue. To this residue was added **39** (500 mg, 1.6 mmol), pyridine (0.5 mL), and toluene (5 mL). The solution was heated overnight at 90 °C. The toluene and pyridine were removed

under high vacuum to give a yellow residue that was purified by chromatography (flash chromatography grade silica) with 4:1 Hexanes/EtOAc gave the product as a white solid (425 mg, 51 %).  $^1\text{H}$  NMR (300 MHz,  $\text{CDCl}_3$ ):  $\delta$  7.50 (1 H, d,  $^3J_{\text{HH}} = 8.4$  Hz, Ar-*H*), 7.39 (1 H, d,  $^3J_{\text{HH}} = 8.4$  Hz, Ar-*H*), 7.17 - 7.06 (14 H, m, Ar-*H*), 7.00 (1 H, s, Ar-*H*), 6.66 (1 H, dd,  $^3J_{\text{HH}} = 8.4$  Hz,  $^4J_{\text{HH}} = 1.8$  Hz, Ar-*H*), 5.95 (1 H, br s, NH), 5.51 (2 H, d,  $^2J_{\text{HH}} = 1.0$  Hz, C=CH<sub>2</sub>), 5.22 (2 H, d,  $^2J_{\text{HH}} = 1.0$  Hz, C=CH<sub>2</sub>), 3.92 (3 H, s, CH<sub>3</sub>), 3.02 (1H, q,  $^3J_{\text{HH}} = 7.2$  Hz, CH) 2.36 (3 H, s, CH<sub>3</sub>), 1.16 (3 H, d,  $^3J_{\text{HH}} = 7.2$  Hz).

**Acetic acid [4-methyl-2,6-bis-(1-phenyl-vinyl)-phenylcarbamoyl]-phenyl-methyl ester (41):** To a solution of (R)-(-)-O-acetylmandelic acid (350 mg, 1.8 mmol) in toluene was added  $\text{SOCl}_2$  (0.4 mL, excess). The solution was heated for 6 h at 85 °C, and then the solvent and excess  $\text{SOCl}_2$  were removed under high vacuum to produce a clear colorless oil. To this residue was added **39** (470 mg, 1.5 mmol), pyridine (0.5 mL), DMAP (5 mg, catalyst) and toluene (10 mL). The solution was heated overnight at 90 °C. The toluene and pyridine were removed under high vacuum to give an oily residue which was dissolved in EtOAc (50 mL) and washed with saturated  $\text{NH}_4\text{Cl}$  solution (25 mL). The saturated  $\text{NH}_4\text{Cl}$  layer was further washed with EtOAc (2 x 50 mL) and dried on  $\text{MgSO}_4$ . The remaining solution was filtered, reduced to a white solid, then purified by flash chromatography (flash chromatography grade silica gel) with 4:1 Hexanes/EtOAc. The product was isolated as a white solid (575 mg, 73 %).  $^1\text{H}$  NMR (300 MHz,  $\text{CDCl}_3$ ):  $\delta$  7.27 - 7.15 (15 H, m, Ar-*H*), 7.02 (2 H, dd,  $^3J_{\text{HH}} = 7.7$  Hz,  $^4J_{\text{HH}} = 1.8$  Hz, Ar-*H*), 6.68 (1 H, s, NH), 5.66 (1H, s, CH), 5.62 (2 H, d,  $^2J_{\text{HH}} = 1.02$  Hz, C=CH<sub>2</sub>), 5.34 (2 H, d,  $^2J_{\text{HH}} = 1.02$  Hz, C=CH<sub>2</sub>), 2.42 (3 H, s, CH<sub>3</sub>), 1.61 (3 H, s, CH<sub>3</sub>);  $^{13}\text{C}$  NMR (75 MHz,  $\text{CDCl}_3$ ):  $\delta$  167.85, 165.70, 146.96, 140.48, 140.22, 137.75, 135.35, 131.22, 128.43, 128.21, 127.62, 127.43, 126.15, 166.32, 74.48, 21.01, 20.60.

**General procedure for preparation of 42 and 43.** To a solution of **40** or **41** dissolved in ethanol (5 mL) was added 10 % wt Pd-C (20 % wt/wt of **40** or **41**). The solution was stirred vigorously under a atmosphere of hydrogen overnight at room temperature. The solution was filtered through Celite and analyzed by GC-MS to determine diastereomeric ratios without further purification (Figure 4.5).  $^1\text{H}$  NMR were consistent with full

hydrogenation of the alkene functionality; however, the mixture was too complex to assign individual resonances. Compound **42**: MS (ESI):  $m/z$  528 ( $M^+ + 1$ ), 550 ( $M^+ + Na$ ). Compound **43**: MS (ESI):  $m/z$  514 ( $M^+ + Na$ ). See Figure 4.5 for GC-MS chromatogram.

## Bibliography

---

- (1) Bytschkov, I.; Doye, S. *Eur. J. of Org. Chem.* **2003**, 935-946.
- (2) Walsh, P. J.; Baranger, A. M.; Bergman, R. G. *J. Am. Chem. Soc.* **1992**, *114*, 1708-19.
- (3) Muller, T. E.; Beller, M. *Chem. Rev.* **1998**, *98*, 675.
- (4) Seayad, J.; Tillack, A.; Hartung, C. G.; Beller, M. *Adv. Synth. Catal.* **2002**, *344*, 795-813.
- (5) a) Hong, S.; Marks, T. J. *Acc. Chem. Res.* **2004**, *37*, 673-686. b) Struab, T.; Haskel, A.; Neyroud, T. G.; Kapon, M.; Botoshansky, M.; Eisen, M. S. *Organometallics* **2001**, *20*, 5017-5035.
- (6) Hultzs, K. C. *Adv. Synth. Catal.* **2005**, *347*, 367-391.
- (7) Nobis, M.; Driessen-Holscher, B. *Angew. Chem., Int. Ed.* **2001**, *40*, 3983-3985.
- (8) Ki, Y.; Marks, T. J. *J. Am. Chem. Soc.* **1996**, *118*, 9295-9306.
- (9) Arredondo, V. M.; McDonald, F. E.; Marks, T. J. *J. Am. Chem. Soc.* **1998**, *120*, 4871-4872.
- (10) Arredondo, V. M.; McDonald, F. E.; Marks, T. J. *Organometallics* **1999**, *18*, 1949-1960.
- (11) Ryu, J.-S.; Marks, T. J.; McDonald, F. E. *Org. Lett.* **2001**, *3*, 3091-3094.
- (12) Douglass, M. R.; Ogasawara, M.; Hong, S.; Metz, M. V.; Marks, T. J. *Organometallics* **2002**, *21*, 283-292.
- (13) Tokunaga, M.; Eckert, M.; Wakatsuki, Y. *Angew. Chem., Int. Ed.* **1999**, *38*, 3222-3225.
- (14) Hartung, C. G.; Tillack, A.; Trauthwein, H.; Beller, M. *J. Org. Chem.* **2001**, *66*, 6339-6343.
- (15) Kadota, I.; Shibuya, A.; Lutete, L. M.; Yamamoto, Y. *J. Org. Chem.* **1999**, *64*, 4570-4571.
- (16) Straub, T.; Haskel, A.; Neyroud, T. G.; Kapon, M.; Botoshansky, M.; Eisen, M. S. *Organometallics* **2001**, *20*, 5017-5035.
- (17) Lauterwasser, F.; Hayes, P. G.; Braese, S.; Piers, W. E.; Schafer, L. L. *Organometallics* **2004**, *23*, 2234-2237.
- (18) Hartwig, J. F. *Pure and Appl. Chem.* **2004**, *76*, 507-516.
- (19) Beller, M.; Trauthwein, H.; Eichberger, M.; Breindl, C.; Muller, T. E. *Eur. J. Inorg. Chem.* **1999**, 1121-1132.
- (20) Beller, M.; Trauthwein, H.; Eichberger, M.; Breindl, C.; Herwig, J.; Muller, T. E.; Thiel, O. R. *Chem. Eur. J.* **1999**, *5*, 1306-1319.
- (21) Brunet, J.-J.; Commenges, G.; Neibecker, D.; Philippot, K. *J. Organomet. Chem.* **1994**, *469*, 221-8.
- (22) Brunet, J. J.; Neibecker, D.; Philippot, K. *Tetrahedron Lett.* **1993**, *34*, 3877-80.
- (23) Brunet, J. J.; Neibecker, D.; Philippot, K. *J. Chem. Soc., Chem. Comm.* **1992**, 1215-16.
- (24) Dorta, R.; Egli, P.; Zuercher, F.; Togni, A. *J. Am. Chem. Soc.* **1997**, *119*, 10857-10858.
- (25) Schlummer, B.; Hartwig, J. F. *Org. Lett.* **2002**, *4*, 1471-1474.
- (26) Gribkov, D. V.; Hultzs, K. C. *Angew. Chem., Int. Ed.* **2004**, *43*, 5542-5546.

- (27) Collin, J.; Daran, J.-C.; Jacquet, O.; Schulz, E.; Trifonov, A. *Chem. Eur. J.* **2005**, *11*, 3455-3462.
- (28) Riegert, D.; Collin, J.; Meddour, A.; Schulz, E.; Trifonov, A. *J. Org. Chem.* **2006**, *71*, 2514-2517.
- (29) Gagne, M. R.; Brard, L.; Conticello, V. P.; Giardello, M. A.; Stern, C. L.; Marks, T. J. *Organometallics* **1992**, *11*, 2003-2005.
- (30) Roesky, P. W.; Mueller, T. E. *Angew. Chem., Int. Ed.* **2003**, *42*, 2708-2710.
- (31) Hultzs, K. C. *Org. Biomol. Chem.* **2005**, *3*, 1819-1824.
- (32) Gribkov, D. V.; Hultzs, K. C.; Hampel, F. *J. Am. Chem. Soc.* **2006**, *128*, 3748-3759.
- (33) Kim, J. Y.; Livinghouse, T. *Org. Lett.* **2005**, *7*, 4391-4393.
- (34) Loeber, O.; Kawatsura, M.; Hartwig, J. F. *J. Am. Chem. Soc.* **2001**, *123*, 4366-4367.
- (35) Patil, N. T.; Lutete, L. M.; Wu, H.; Pahadi, N. K.; Gridnev, I. D.; Yamamoto, Y. *J. Org. Chem.* **2006**, *71*, 4270-4279.
- (36) Knight, P. D.; Munslow, I.; O'Shaughnessy, P. N.; Scott, P. *Chem. Commun.* **2004**, 894-895.
- (37) Martinez, P. H.; Hultzs, K. C.; Hampel, F. *Chem. Commun.* **2006**, 2221-2223.
- (38) Giardello, M. A.; Conticello, V. P.; Brard, L.; Gagne, M. R.; Marks, T. J. *J. Am. Chem. Soc.* **1994**, *116*, 10241-54.
- (39) Hong, S.; Tian, S.; Metz, M. V.; Marks, T. J. *J. Am. Chem. Soc.* **2003**, *125*, 14768-14783.
- (40) Gribkov, D. V.; Hultzs, K. C.; Hampel, F. *Chem. Eur. J.* **2003**, *9*, 4796-4810.
- (41) Gribkov, D. V.; Hultzs, K. C. *Chem. Commun.* **2004**, 730-731.
- (42) Kim, J. Y.; Livinghouse, T. *Org. Lett.* **2005**, *7*, 1737-1739.
- (43) O'Shaughnessy, P. N.; Knight, P. D.; Morton, C.; Gillespie, K. M.; Scott, P. *Chem. Commun.* **2003**, 1770-1771.
- (44) *CRC Handbook of Chemistry and Physics, 85th Edition*, 4-32,33.
- (45) McGrane, P. L.; Jensen, M.; Livinghouse, T. *J. Am. Chem. Soc.* **1992**, *114*, 5459-5460.
- (46) Haak, E.; Siebeneicher, H.; Doye, S. *Org. Lett.* **2000**, *2*, 1935-1937.
- (47) Pohlki, F.; Doye, S. *Angew. Chem., Int. Ed.* **2001**, *40*, 2305-2308.
- (48) Bytschkov, I.; Doye, S. *Tetrahedron Lett.* **2002**, *43*, 3715-3718.
- (49) Odom, A. L. *Dalt. Trans.* **2005**, 225-233.
- (50) Tillack, A.; Jiao, H.; Castro, I. G.; Hartung, C. G.; Beller, M. *Chem. Eur. J.* **2004**, *10*, 2409-2420.
- (51) Li, Y.; Shi, Y.; Odom, A. L. *J. Am. Chem. Soc.* **2004**, *126*, 1794-1803.
- (52) Johnson, J. S.; Bergman, R. G. *J. Am. Chem. Soc.* **2001**, *123*, 2923-2924.
- (53) Thomson, R. K.; Bexrud, J. A.; Schafer, L. L. *Organometallics* **2006**, *25*, 4069-4071.
- (54) Kim, H.; Lee, P. H.; Livinghouse, T. *Chem. Commun.* **2005**, 5205-5207.
- (55) Bexrud, J. A.; Beard, J. D.; Leitch, D. C.; Schafer, L. L. *Org. Lett.* **2005**, *7*, 1959-1962.
- (56) Mueller, C.; Loos, C.; Schulenberg, N.; Doye, S. *Eur. J. Org. Chem.* **2006**, 2499-2503.

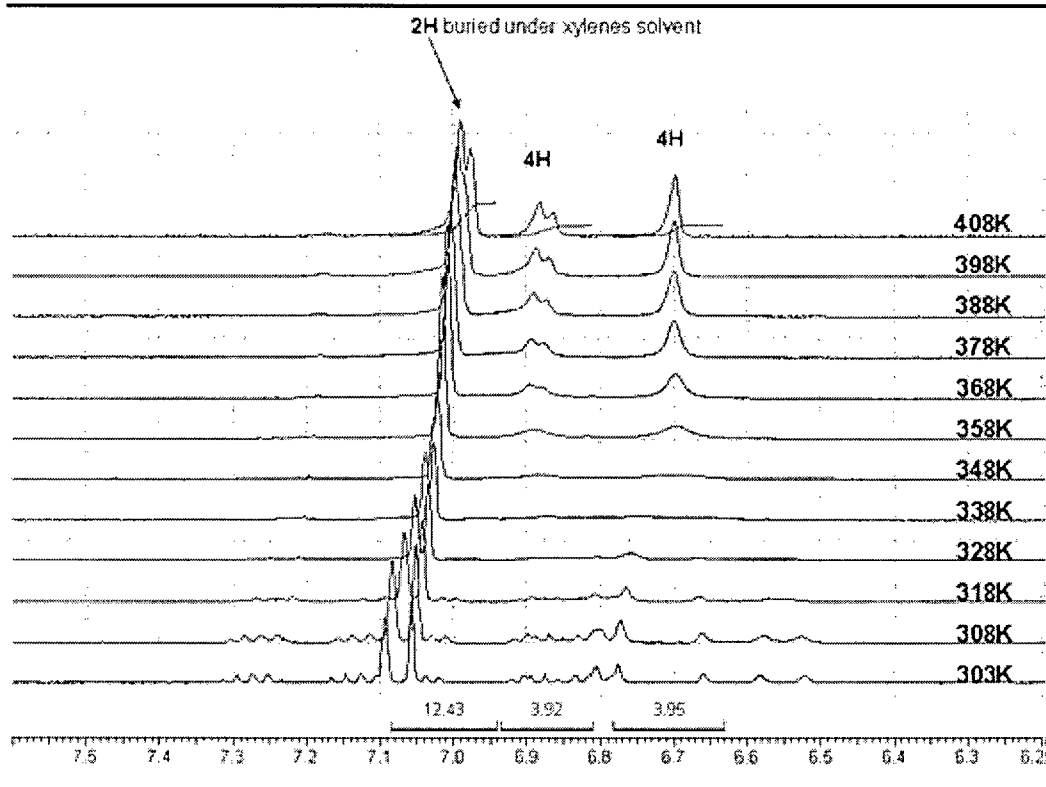
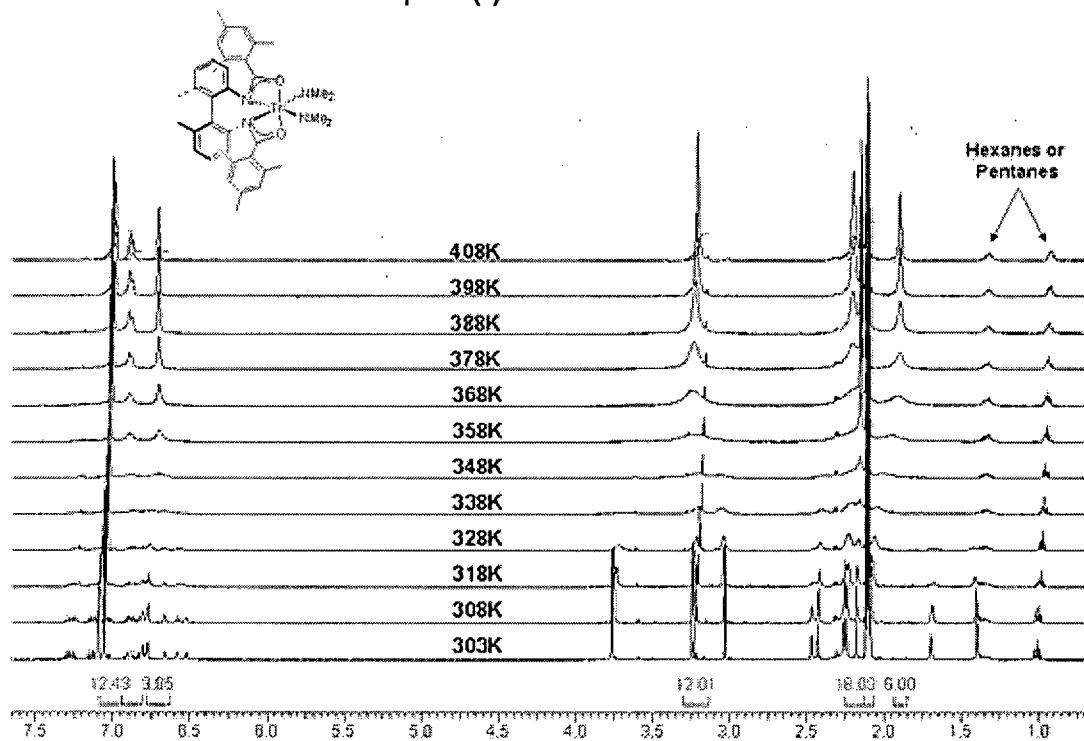
- (57) Wood, M. C.; Leitch, D. C.; Yeung, C. S.; Kozak, J. A.; Schafer, L. L. *Angew. Chem., Int. Ed.* **2006**, In Press.
- (58) Watson, D. A.; Chiu, M.; Bergman, R. G. *Organometallics* **2006**, *25*, 4731-4733.
- (59) Ackermann, L.; Kaspar, L. T.; Gschrei, C. J. *Org. Lett.* **2004**, *6*, 2515-2518.
- (60) Kaspar, L. T.; Fingerhut, B.; Ackermann, L. *Angew. Chem., Int. Ed.* **2005**, *44*, 5972-5974.
- (61) Anderson, L. L.; Arnold, J.; Bergman, R. G. *J. Am. Chem. Soc.* **2005**, *127*, 14542-14543.
- (62) Geisbrecht, G. R.; Shafir, A.; Arnold, J. *Inorg. Chem.* **2001**, *127*.
- (63) Thomson, R. K.; Patrick, B. O.; Schafer, L. L. *Can. J. Chem.* **2005**, *83*, 1037-1042.
- (64) Thomson, R. K.; Zahariev, F. E.; Zhang, Z.; Patrick, B. O.; Wang, Y. A.; Schafer, L. L. *Inorg. Chem.* **2005**, *44*, 8680-8689.
- (65) Li, C.; Thomson, R. K.; Gillon, B.; Patrick, B. O.; Schafer, L. L. *Chem. Commun.* **2003**, 2462-2463.
- (66) Zhang, Z.; Leitch, D. C.; Lu, M.; Patrick, B. O.; Schafer, L. L. *Chem. Eur. J.* **2006**, In Press.
- (67) Ong, T.-G.; Yap, G. P. A.; Richeson, D. S. *Organometallics* **2002**, *21*, 2839-2841.
- (68) Morton, C.; O'Shaughnessy, P.; Scott, P. *Chem. Commun.* **2000**, 2099-2100.
- (69) Hagadorn, J. R.; Arnold, J. *Angew. Chem., Int. Ed.* **1998**, *37*, 1729-1731.
- (70) Stewart, P. J.; Blake, A. J.; Mountford, P. *Organometallics* **1998**, *17*, 3271-3281.
- (71) Guiducci, A. E.; Boyd, C. L.; Mountford, P. *Organometallics* **2006**, *25*, 1167-1187.
- (72) Mijatovic, I.; Kickelbick, G.; Schubert, U. *Eur. J. Inorg. Chem.* **2001**, 1933-1935.
- (73) Zhang, Z.; Schafer, L. L. *Org. Lett.* **2003**, *5*, 4733-4736.
- (74) Ayinla, R. O.; Schafer, L. L. *Inorg. Chim. Acta* **2006**, *359*, 3097-3102.
- (75) Chen, Y.; Yekta, S.; Yudin, A. K. *Chem. Rev.* **2003**, *103*, 3155 - 3211.
- (76) Bringmann, G.; Mortimer, A. J. P.; Keller, P. A.; Gresser, M. J.; Garner, J.; Breuning, M. *Angew. Chem., Int. Ed.* **2005**, *44*, 5384-5427.
- (77) O'Shaughnessy, P. N.; Scott, P. *Tetrahedron: Asymmetry* **2003**, *14*, 1979-1983.
- (78) O'Shaughnessy, P. N.; Gillespie, K. M.; Knight, P. D.; Munslow, I. J.; Scott, P. *Dalt. Trans.* **2004**, 2251-2256.
- (79) Gribkov, D. V.; Hampel, F.; Hultzs, K. C. *Eur. J. Inorg. Chem.* **2004**, 4091-4101.
- (80) Collin, J.; Daran, J.-C.; Schulz, E.; Trifonov, A. *Chem. Commun.* **2003**, 3048-3049.
- (81) Marxen, T. L.; Johnson, B. J.; Nilsson, P. V.; Pignolet, L. H. *Inorg. Chem.* **1984**, *23*, 4663-70.
- (82) Gillespie, K. M.; Sanders, C. J.; O'Shaughnessy, P.; Westmoreland, I.; Thickitt, C. P.; Scott, P. *J. Org. Chem.* **2002**, *67*, 3450-3458.
- (83) Gostan, T.; Brun, E.; Tramesel, D.; Prigent, Y.; Delsuc, M. *Bruker Spin Report* **2005**, *154/155*, 18 - 25, <http://www.bruker-biospin.de/NMR/nmrsoftw/news/report/154/pdf/18-25.pdf> (accessed Dec 5, 2006)
- (84) Shi, Y.; Cao, C.; Odom, A. *Inorg. Chem.* **2004**, *43*, 275-281.
- (85) Turculet, L.; Tilley, T. D. *Organometallics* **2002**, *21*, 3961-3972.
- (86) Scollard, J. D.; McConville, D. H.; Vittal, J. J. *Organometallics* **1997**, *16*, 4415-4420.

- (87) Li, Y.; Shi, Y.; Odom, A. L. *J. Am. Chem. Soc.* **2004**, *126*, 1794-1803.
- (88) Ackermann, L.; Bergman, R. G.; Loy, R. N. *J. Am. Chem. Soc.* **2003**, *125*, 11956-11963.
- (89) Timperley, C. M.; White, W. E. *J. F. Chem.* **2003**, *123*, 65-70.
- (90) Beard, J. D. *M. Sc. Thesis* **2005**.
- (91) Leitch, D. C. *B. Sc. Thesis* **2004**.
- (92) Lee, A. V.; Schafer, L. L. *Organometallics* **2006**, *25*, 5249-5254.
- (93) Eldred Sarah, E.; Stone David, A.; Gellman Samuel, H.; Stahl Shannon, S. *J. Am. Chem. Soc.* **2003**, *125*, 3422-3.
- (94) Hong, S.; Kawaoka, A. M.; Marks, T. J. *J. Am. Chem. Soc.* **2003**, *125*, 15878-15892.
- (95) Thomson, R. K.; Schafer, L. L. **2006**, unpublished result.
- (96) Beesley, R. M.; Ingold, C. K.; Thorpe, J. F. *J. Chem. Soc.* **1915**, *107*, 1080.
- (97) Brown, R. F.; Van Gulick, N. M. *J. Org. Chem.* **1956**, *21*, 1046-1049.
- (98) Nicolaou, K. C.; Roecker, A. J.; Pfefferkorn, J. A.; Cao, G. *J. Am. Chem. Soc.* **2000**, *122*, 2966-2967.
- (99) Liang, Y.; Gao, S.; Wan, H.; Wang, J.; Chen, H.; Zheng, Z.; Hu, X. *Tetrahedron: Asymmetry* **2003**, *14*, 1267-1273.
- (100) Cherian, A. E.; Lobkovsky, E. B.; Coates, G. W. *Chem. Commun.* **2003**, 2566-2567.
- (101) Arienti, A.; Bigi, F.; Maggi, R.; Marzi, E.; Moggi, P.; Rastelli, M.; Sartori, G.; Tarantola, F. *Tetrahedron* **1997**, *53*, 3795-3804.
- (102) Cherian, A. E.; Domski, G. J.; Rose, J. M.; Lobkovsky, E. B.; Coates, G. W. *Org. Lett.* **2005**, *7*, 5135-5137.
- (103) Cui, X.; Burgess, K. *Chem. Rev.* **2005**, *105*, 3272-3296.
- (104) Buchwald, S. L.; Broene, R. D. *J. Am. Chem. Soc.* **1993**, *115*, 12569-12570.
- (105) Pfaltz, A.; Blankenstein, J.; Hilgraf, R.; Hörmann, E.; McIntyre, S.; Menges, F.; Schönleber, M.; Smidt, S. P.; Wüstenberg, B.; Zimmermann, N. *Adv. Synth. Catal.* **2003**, 33-44.
- (106) Bell, S.; Wustenberg, B.; Kaiser, S.; Menges, F.; Netscher, T.; Pfaltz, A. *Science* **Feb. 2006**, *311*, 642-644, and references therein.
- (107) Gagne, M. R.; Marks, T. J. *J. Am. Chem. Soc.* **1989**, *111*, 4108-9.



## Appendix

### Appendix I Variable Temperature $^1\text{H}$ NMR Spectroscopic Analysis of Complex (-)-13a



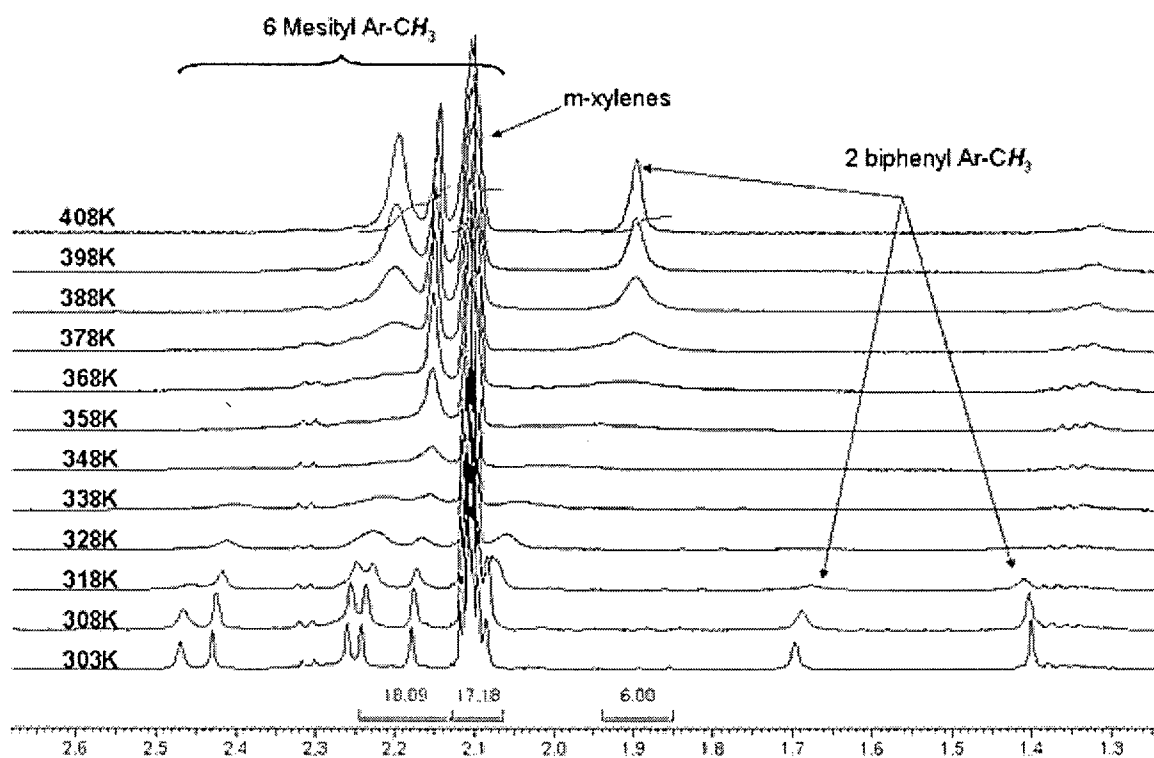
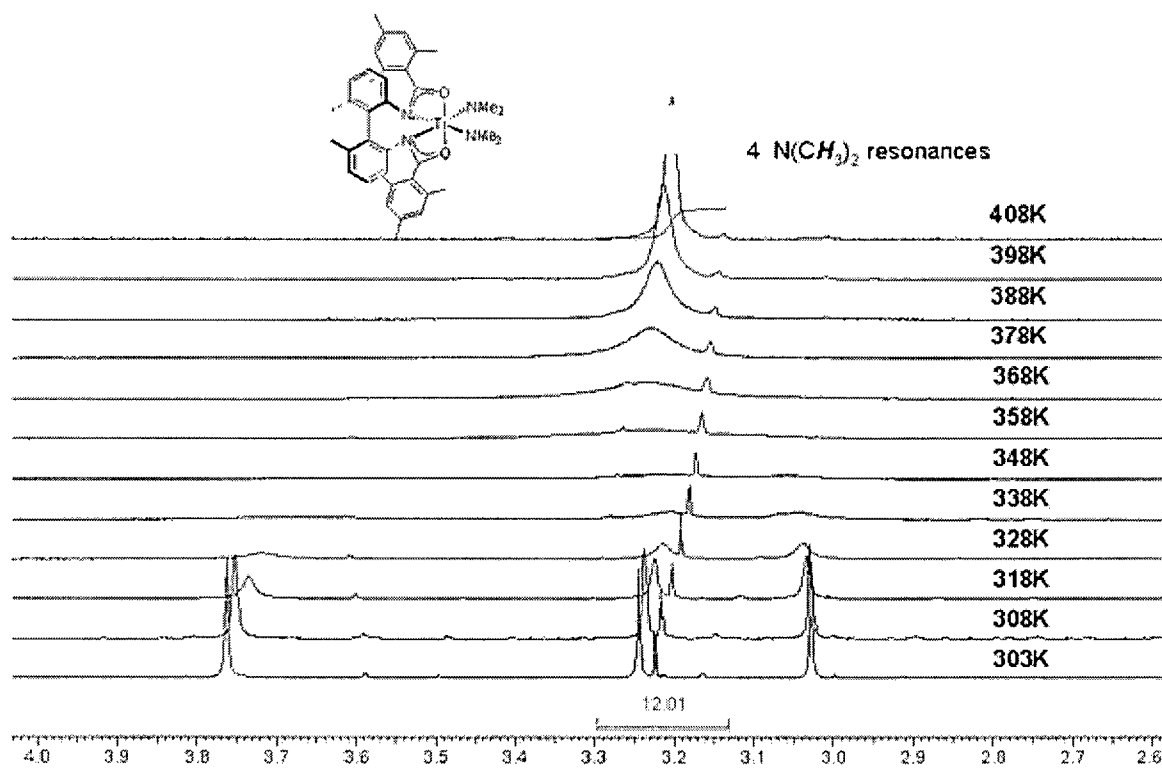
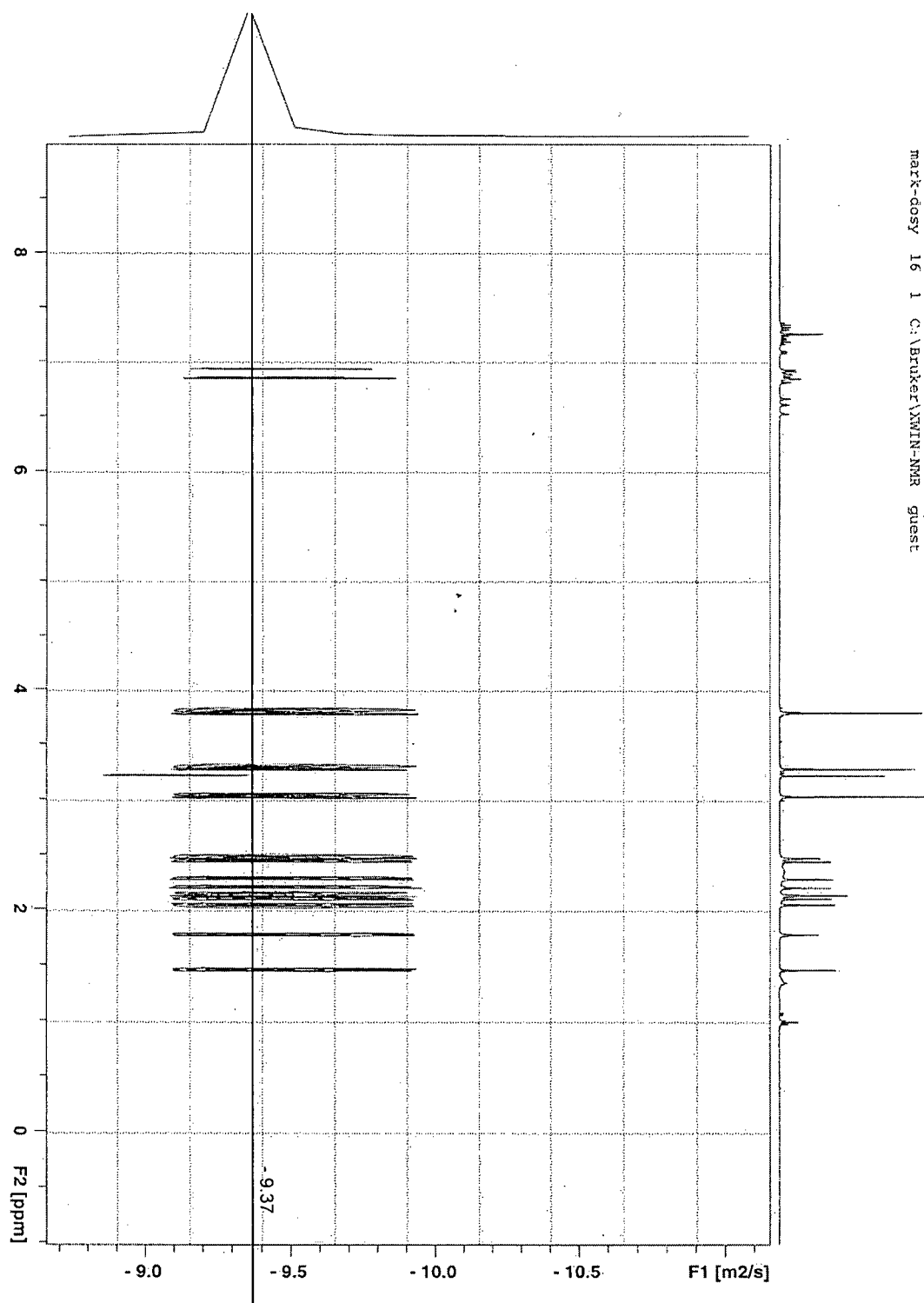


Figure A-1: Variable temperature <sup>1</sup>H NMR of complex (-)-13c

Figure A-1 illustrates the high temperature VT  $^1\text{H}$  NMR spectrum of (-)-**13a** that was conducted to improve our understanding of the structure, and explain why poor reactivity was observed for alkene hydroamination (Chapter 3). There are a number of structural isomers that could exist in solution. The first possibility is that the complex is a low symmetry oligomer at room temperature, but converts to a monomeric species at higher temperatures. Secondly, the amidate ligands may be fluxional going from monodentate ( $\kappa^1$  or  $\kappa^2$ ) at room temperature to bidentate ( $\kappa^2$  or  $\kappa^4$ ) to when heated. This process is less likely for a rigid tethered system, however, it cannot be eliminated as a possible solution structure. The third possibility is that the complex is not only oligomeric at room temperature, but also contains localized hindered rotation (ie: hindered mesityl or dimethylamido rotation). This would remove symmetry in the oligomer making the NMR spectrum more complicated. If so, when the complex is heated, you may observe two mechanisms intertwined where the complex is converting to a monomer in solution as well as overcoming the energy barrier for localized hindered rotation. Closer examination of the  $^1\text{H}$  NMR integrations suggests that the third mechanism proposed is the closest approximation. The number of hydrogens does not correspond to a monomeric species at room temperature, but as the temperature was increased, the aromatic and aliphatic hydrogen resonances coalesce into a simple spectrum. The relative integration of the complex at 408 K is more indicative of a monomeric species. In the high temperature NMR spectra, the three resonances for the dimethylamido ligands coalesce into one signal that integrates to 12 hydrogens. The mesityl methyl substituents on the amidate ligand coalesce from 6 singlets into two broad singlets integrating to 18 hydrogens, and the two methyl groups on the biphenyl coalesce from 2 singlets to one singlet. When the temperature is lowered back to room temperature, the  $^1\text{H}$  NMR spectra returns to its original state confirming that an equilibrium is taking place without decomposition or isomerisation to a thermodynamic minimum. The fact that the signals observed at high temperatures do not coalesce into a single peaks equidistant from the two at room temperature, suggests a monomer/oligomer equilibrium combined with isolated hindered rotation may be taking place. Further structural investigations by DOSY NMR spectroscopy are discussed in Chapter 2.

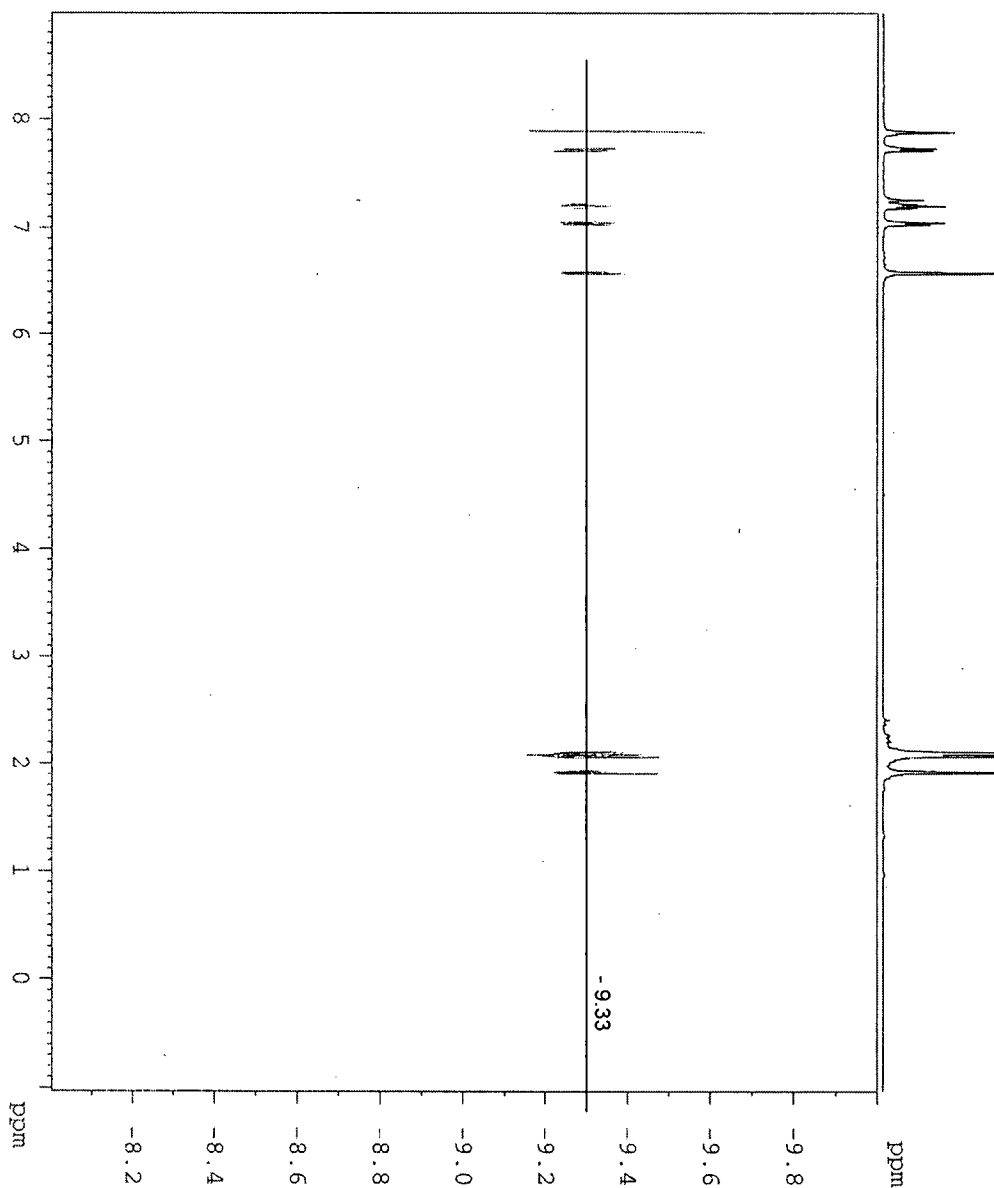
# Appendix II

## DOSY NMR spectroscopy for complex (-)-13a



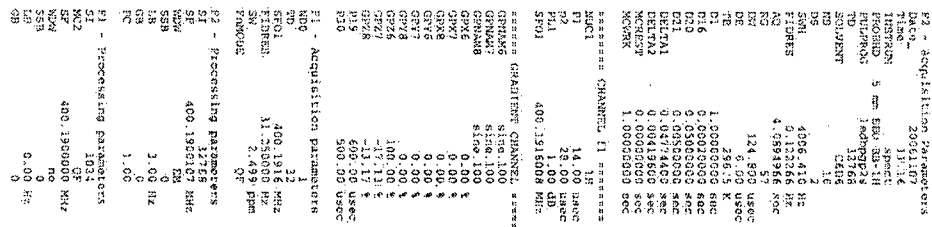
Mark Wood MW-01-95

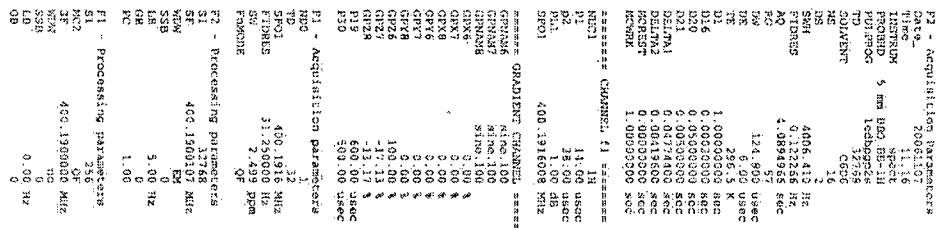
C6D5/CDC13

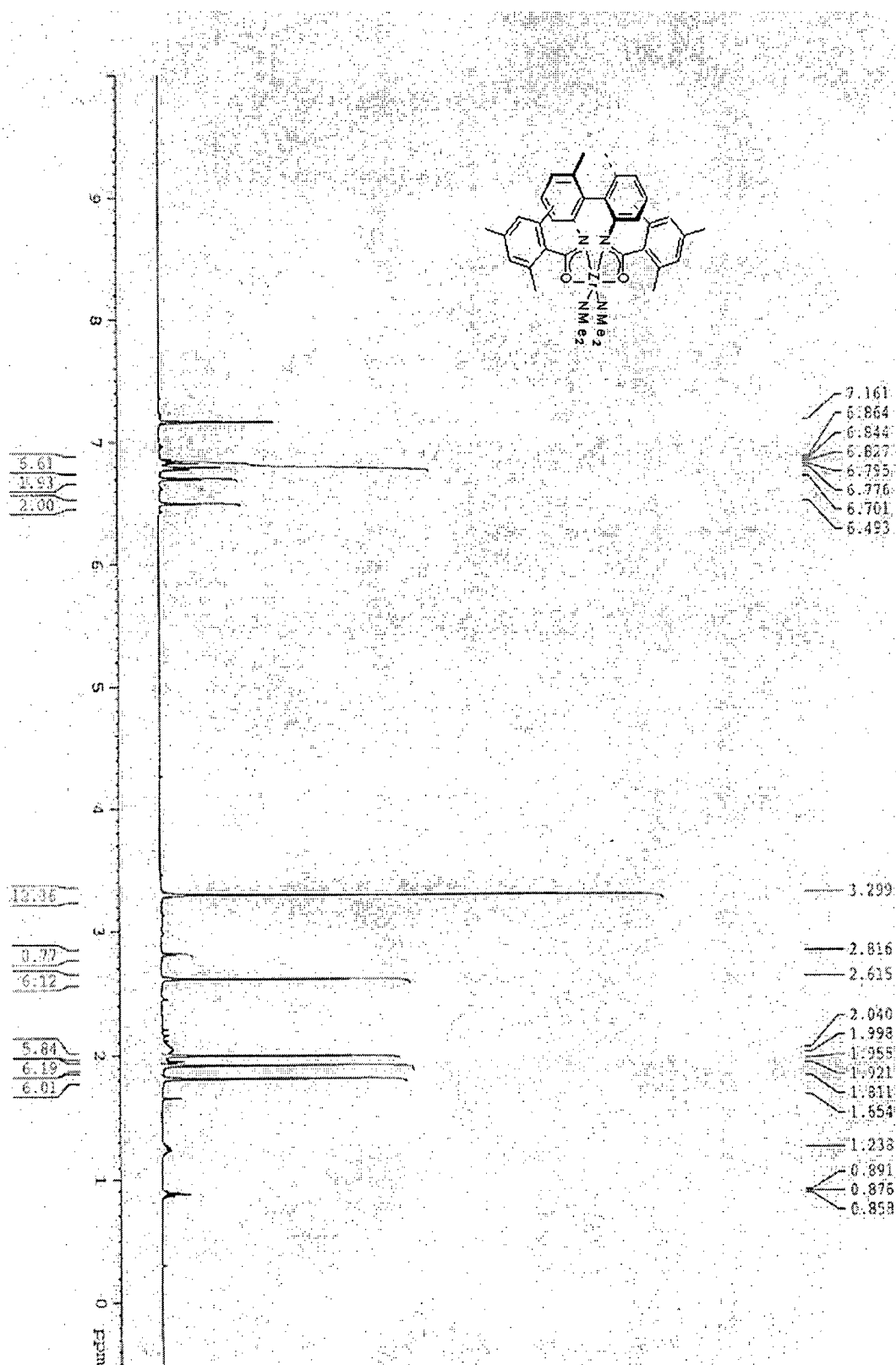


Current Data		Parameters	
NAME	mark-day		
EXPNO	1		
PROCNO	1		
F2 - Acquisition Parameters			
Date_	20061107		
Time	11:16		
PROBHD	5 mm BBO HD		
PULPROG	zgpg30		
TD	32768		
SOLVENT	C6D6		
D5	1		
SWH	4006.410 Hz		
F1FREQ	0.122266 Hz		
	4.0051916 sec		
DE	6.00 umsec		
TE	296.5 K		
NUC1	13C		
NUC2	1H		
PC	1.00 dB		
FL1	400.1315008 Hz		
***** CHANNEL f1 *****			
NAME	EXH1PT		
PROBHD	5 mm BBO HD		
PULPROG	zgpg30		
TD	32768		
SOLVENT	C6D6		
D5	1		
SWH	4006.410 Hz		
F1FREQ	0.122266 Hz		
	4.0051916 sec		
DE	6.00 umsec		
TE	296.5 K		
NUC1	13C		
NUC2	1H		
PC	1.00 dB		
FL1	400.1315008 Hz		
***** CHANNEL f2 *****			
NAME	EXH2PT		
PROBHD	5 mm BBO HD		
PULPROG	zgpg30		
TD	32768		
SOLVENT	C6D6		
D5	1		
SWH	4006.410 Hz		
F1FREQ	0.122266 Hz		
	4.0051916 sec		
DE	6.00 umsec		
TE	296.5 K		
NUC1	13C		
NUC2	1H		
PC	1.00 dB		
FL1	400.1315008 Hz		
***** CHANNEL f3 *****			
NAME	EXH3PT		
PROBHD	5 mm BBO HD		
PULPROG	zgpg30		
TD	32768		
SOLVENT	C6D6		
D5	1		
SWH	4006.410 Hz		
F1FREQ	0.122266 Hz		
	4.0051916 sec		
DE	6.00 umsec		
TE	296.5 K		
NUC1	13C		
NUC2	1H		
PC	1.00 dB		
FL1	400.1315008 Hz		
***** CHANNEL f4 *****			
NAME	EXH4PT		
PROBHD	5 mm BBO HD		
PULPROG	zgpg30		
TD	32768		
SOLVENT	C6D6		
D5	1		
SWH	4006.410 Hz		
F1FREQ	0.122266 Hz		
	4.0051916 sec		
DE	6.00 umsec		
TE	296.5 K		
NUC1	13C		
NUC2	1H		
PC	1.00 dB		
FL1	400.1315008 Hz		
***** CHANNEL f5 *****			
NAME	EXH5PT		
PROBHD	5 mm BBO HD		
PULPROG	zgpg30		
TD	32768		
SOLVENT	C6D6		
D5	1		
SWH	4006.410 Hz		
F1FREQ	0.122266 Hz		
	4.0051916 sec		
DE	6.00 umsec		
TE	296.5 K		
NUC1	13C		
NUC2	1H		
PC	1.00 dB		
FL1	400.1315008 Hz		
***** CHANNEL f6 *****			
NAME	EXH6PT		
PROBHD	5 mm BBO HD		
PULPROG	zgpg30		
TD	32768		
SOLVENT	C6D6		
D5	1		
SWH	4006.410 Hz		
F1FREQ	0.122266 Hz		
	4.0051916 sec		
DE	6.00 umsec		
TE	296.5 K		
NUC1	13C		
NUC2	1H		
PC	1.00 dB		

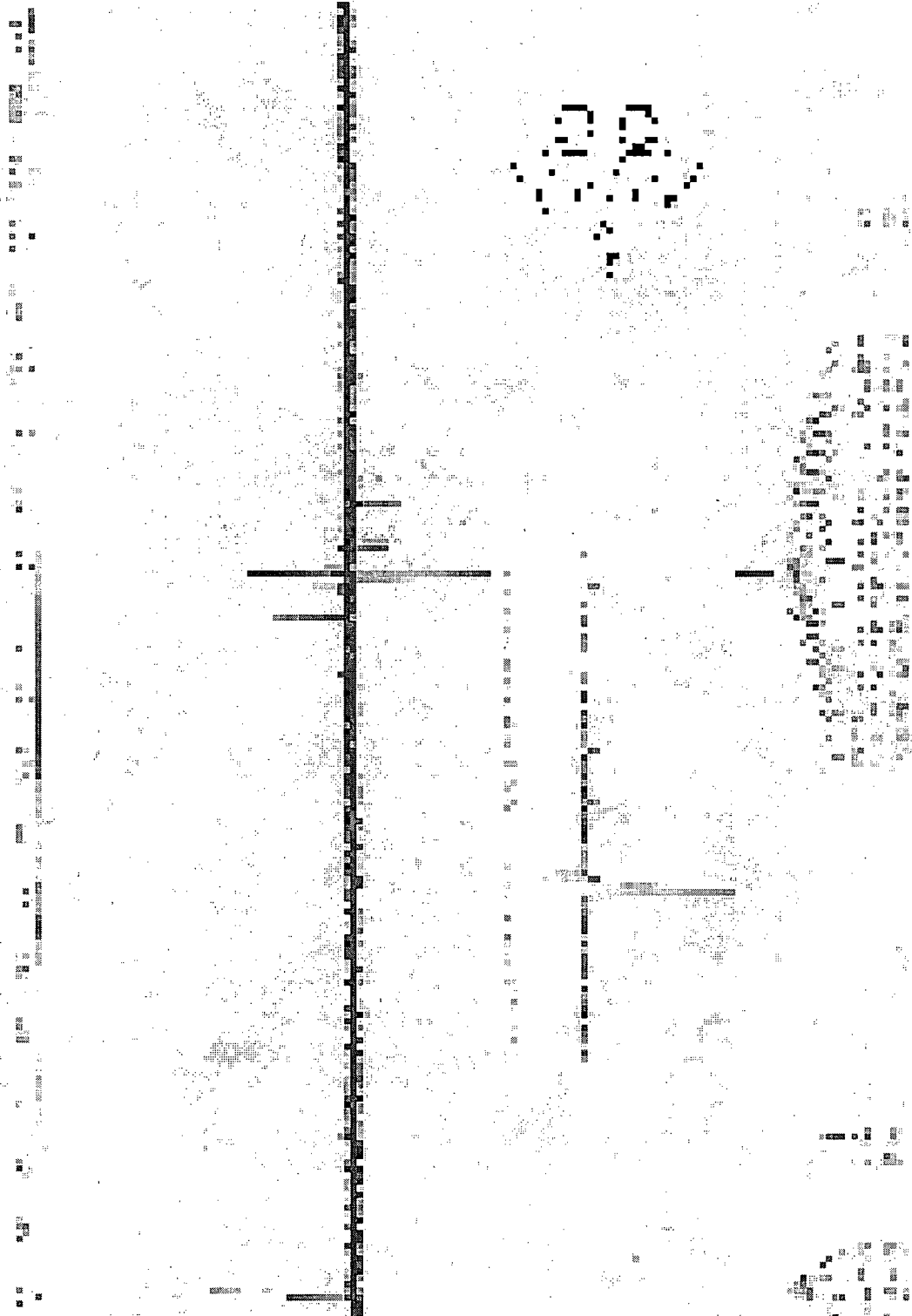
Component	Data	Parameters
NAME		mark-dosy
EXPNO		3
PROCNO		1











## Appendix V

## X-ray Crystallographic Data for Complex (+)-13c

**Table A-1.** Crystal data and structure refinement for dimethylamine adduct of (+)-13c.

Identification code	Is065
Empirical formula	C <sub>40</sub> H <sub>53</sub> N <sub>5</sub> O <sub>2</sub> Zr
Formula weight	727.09
Temperature	293(2) K
Wavelength	0.71073 Å
Crystal system, space group	Triclinic, <i>p</i> -1
Unit cell dimensions	<i>a</i> = 10.3739(18) Å <i>alpha</i> = 76.0480(10) deg. <i>b</i> = 11.975(2) Å <i>beta</i> = 73.900(12) deg. <i>c</i> = 16.814(3) Å <i>gamma</i> = 73.903(12) deg.
Volume	1897.4(6) Å <sup>3</sup>
Z, Calculated density	2, 1.273 Mg/m <sup>3</sup>
Absorption coefficient	0.330 mm <sup>-1</sup>
F(000)	768
Crystal size	0.3 x 0.25 x 0.2 mm
Theta range for data collection	2.39 to 25.05 deg.
Limiting indices	-10 ≤ <i>h</i> ≤ 12, -14 ≤ <i>k</i> ≤ 14, -19 ≤ <i>l</i> ≤ 19
Reflections collected / unique	12020 / 6349 [ <i>R</i> (int) = 0.0623]
Completeness to theta = 25.05	94.4 %
Absorption correction	Semi-empirical from equivalents
Max. and min. transmission	1.1237 and 1.07
Refinement method	Full-matrix least-squares on <i>F</i> <sup>2</sup>
Data / restraints / parameters	6349 / 0 / 437
Goodness-of-fit on <i>F</i> <sup>2</sup>	1.051
Final <i>R</i> indices [ <i>I</i> > 2σ( <i>I</i> )]	<i>R</i> 1 = 0.0561, <i>wR</i> 2 = 0.1172
<i>R</i> indices (all data)	<i>R</i> 1 = 0.0954, <i>wR</i> 2 = 0.1274
Largest diff. peak and hole	0.447 and -0.626 e.Å <sup>-3</sup>

**Table A-2** Atomic coordinates ( $\times 10^4$ ) and equivalent isotropic displacement parameters ( $\text{\AA}^2 \times 10^3$ ) for (+)-**13c**. U(eq) is defined as one third of the trace of the orthogonalized Uij tensor.

	x	y	z	U(eq)
Zr(1)	-1033(1)	2916(1)	3319(1)	16(1)
O(1)	-1526(3)	1134(3)	3981(2)	22(1)
O(2)	-263(3)	4629(3)	2892(2)	23(1)
N(1)	-556(4)	1334(3)	2639(2)	17(1)
N(2)	829(3)	3206(3)	2182(2)	16(1)
C(26)	1772(4)	5027(4)	1841(3)	16(1)
N(3)	-2705(4)	3684(4)	2779(3)	23(1)
N(5)	1076(5)	1970(5)	3929(3)	37(1)
C(1)	-1280(4)	745(4)	3298(3)	19(1)
C(3)	-492(4)	1349(4)	1779(3)	17(1)
C(28)	3099(5)	5854(4)	538(3)	23(1)
C(9)	2050(4)	2408(4)	1847(3)	17(1)
C(27)	2058(4)	5274(4)	966(3)	19(1)
N(4)	-2035(4)	3412(4)	4471(3)	34(1)
C(10)	1989(4)	1543(4)	1434(3)	19(1)
C(33)	2179(5)	5178(5)	3236(3)	31(1)
C(29)	3870(5)	6208(4)	962(3)	23(1)
C(6)	-444(5)	1635(5)	83(3)	29(1)
C(31)	2478(5)	5418(4)	2282(3)	21(1)
C(18)	-955(5)	-1268(4)	2974(3)	26(1)
C(7)	-1598(5)	1393(5)	681(3)	28(1)
C(22)	-3268(5)	-184(5)	3541(3)	27(1)
C(4)	701(4)	1562(4)	1170(3)	18(1)
C(14)	3312(4)	2383(5)	2029(3)	23(1)
C(11)	3154(5)	624(5)	1259(3)	26(1)
C(5)	699(5)	1731(4)	316(3)	21(1)
C(17)	-1837(5)	-276(4)	3283(3)	23(1)
C(16)	144(5)	-392(5)	879(4)	38(1)
C(30)	3520(5)	5996(4)	1826(3)	23(1)
C(15)	1905(5)	2022(5)	-386(3)	34(1)
C(19)	-1528(5)	-2154(5)	2882(4)	37(1)
C(2)	770(4)	4271(4)	2309(3)	17(1)
C(13)	4454(5)	1499(5)	1837(3)	30(1)
C(24)	-4252(5)	865(5)	3888(4)	33(1)
C(12)	4362(5)	619(5)	1472(3)	32(1)
C(36)	-4129(5)	4065(5)	3209(4)	33(1)
C(8)	-1623(5)	1258(5)	1521(3)	25(1)
C(32)	1245(5)	4960(5)	474(3)	29(1)
C(35)	-2567(5)	4056(5)	1877(3)	31(1)
C(34)	5073(5)	6759(5)	474(4)	35(1)
C(21)	-3798(6)	-1091(5)	3436(4)	37(1)
C(20)	-2937(6)	-2064(5)	3099(4)	39(2)
C(23)	588(5)	-1428(5)	2717(4)	40(2)
C(39)	1614(6)	707(5)	3921(4)	48(2)
C(37)	2794(6)	2769(6)	5220(4)	52(2)
C(25)	-3559(7)	-2986(6)	2955(5)	60(2)
C(40)	1003(7)	2257(7)	4740(4)	65(2)
C(38)	-2143(8)	4594(6)	4627(4)	68(2)

**Table A-3** Selected bond lengths and bond angles for (+)-13c

Bond	lengths [Å]
Zr(1)-N(3)	2.065(4)
Zr(1)-N(4)	2.069(4)
Zr(1)-O(1)	2.280(3)
Zr(1)-O(2)	2.289(3)
Zr(1)-N(1)	2.313(4)
Zr(1)-N(2)	2.347(4)
Zr(1)-N(5)	2.536(4)
Zr(1)-C(1)	2.692(5)
Zr(1)-C(2)	2.757(5)
O(1)-C(1)	1.278(6)
O(2)-C(2)	1.287(5)
N(1)-C(1)	1.320(6)
N(1)-C(3)	1.425(6)
N(2)-C(2)	1.325(6)
N(2)-C(9)	1.424(6)
C(26)-C(27)	1.392(6)
C(26)-C(31)	1.401(6)
C(26)-C(2)	1.498(6)
N(3)-C(36)	1.451(6)
N(3)-C(35)	1.453(6)
N(5)-C(39)	1.462(8)
N(5)-C(40)	1.463(8)
C(1)-C(17)	1.498(7)
C(3)-C(8)	1.398(6)
C(3)-C(4)	1.411(6)
C(28)-C(27)	1.382(6)
C(28)-C(29)	1.406(7)
C(9)-C(10)	1.402(7)
C(9)-C(14)	1.415(6)
C(27)-C(32)	1.500(6)
N(4)-C(37)	1.455(7)
N(4)-C(38)	1.469(8)
C(10)-C(11)	1.407(7)
C(10)-C(4)	1.515(6)
C(33)-C(31)	1.518(7)
C(29)-C(30)	1.375(7)
C(29)-C(34)	1.513(6)
C(6)-C(7)	1.383(7)
C(6)-C(5)	1.388(7)
C(31)-C(30)	1.391(6)
C(18)-C(17)	1.396(7)
C(18)-C(19)	1.409(7)
C(18)-C(23)	1.507(7)
C(7)-C(8)	1.376(7)
C(22)-C(17)	1.407(6)
C(22)-C(21)	1.410(7)
C(22)-C(24)	1.508(7)
C(4)-C(5)	1.402(7)
C(14)-C(13)	1.373(7)
C(11)-C(12)	1.394(7)
C(11)-C(16)	1.507(7)
C(5)-C(15)	1.517(6)
C(19)-C(20)	1.385(7)

C(13)-C(12)	1.377(7)
C(21)-C(20)	1.392(8)
C(20)-C(25)	1.518(7)

Bond	Angles [deg]
N(3)-Zr(1)-N(4)	94.40(17)
N(3)-Zr(1)-O(1)	100.81(14)
N(4)-Zr(1)-O(1)	83.64(16)
N(3)-Zr(1)-O(2)	91.14(14)
N(4)-Zr(1)-O(2)	89.65(15)
O(1)-Zr(1)-O(2)	166.68(11)
N(3)-Zr(1)-N(1)	89.30(15)
N(4)-Zr(1)-N(1)	140.20(16)
O(1)-Zr(1)-N(1)	56.81(12)
O(2)-Zr(1)-N(1)	129.94(12)
N(3)-Zr(1)-N(2)	102.39(14)
N(4)-Zr(1)-N(2)	141.67(16)
O(1)-Zr(1)-N(2)	125.49(13)
O(2)-Zr(1)-N(2)	56.21(12)
N(1)-Zr(1)-N(2)	74.88(13)
N(3)-Zr(1)-N(5)	177.96(17)
N(4)-Zr(1)-N(5)	87.56(17)
O(1)-Zr(1)-N(5)	79.99(14)
O(2)-Zr(1)-N(5)	88.26(14)
N(1)-Zr(1)-N(5)	89.59(15)
N(2)-Zr(1)-N(5)	75.67(15)
N(3)-Zr(1)-C(1)	90.91(15)
N(4)-Zr(1)-C(1)	110.87(17)
O(1)-Zr(1)-C(1)	28.27(12)
O(2)-Zr(1)-C(1)	159.15(13)
N(1)-Zr(1)-C(1)	29.36(13)
N(2)-Zr(1)-C(1)	103.14(14)
N(5)-Zr(1)-C(1)	88.96(15)
N(3)-Zr(1)-C(2)	99.10(14)
N(4)-Zr(1)-C(2)	115.10(16)
O(1)-Zr(1)-C(2)	151.37(13)
O(2)-Zr(1)-C(2)	27.61(12)
N(1)-Zr(1)-C(2)	103.31(14)
N(2)-Zr(1)-C(2)	28.68(13)
N(5)-Zr(1)-C(2)	79.49(15)
C(1)-Zr(1)-C(2)	131.82(14)
C(1)-O(1)-Zr(1)	94.1(3)
C(2)-O(2)-Zr(1)	96.9(3)
C(1)-N(1)-C(3)	126.1(4)
C(1)-N(1)-Zr(1)	91.4(3)
C(3)-N(1)-Zr(1)	128.5(3)
C(2)-N(2)-C(9)	125.3(4)
C(2)-N(2)-Zr(1)	93.1(3)
C(9)-N(2)-Zr(1)	131.7(3)
C(27)-C(26)-C(31)	120.4(4)
C(27)-C(26)-C(2)	119.6(4)
C(31)-C(26)-C(2)	119.9(4)
C(36)-N(3)-C(35)	109.6(4)
C(36)-N(3)-Zr(1)	127.3(3)
C(35)-N(3)-Zr(1)	122.7(3)
C(39)-N(5)-C(40)	111.5(5)

C(39)-N(5)-Zr(1)	115.7(3)
C(40)-N(5)-Zr(1)	115.5(4)
O(1)-C(1)-N(1)	114.5(4)
O(1)-C(1)-C(17)	120.2(4)
N(1)-C(1)-C(17)	125.2(4)
O(1)-C(1)-Zr(1)	57.7(2)
N(1)-C(1)-Zr(1)	59.2(3)
C(17)-C(1)-Zr(1)	163.4(3)
C(8)-C(3)-C(4)	119.5(4)
C(8)-C(3)-N(1)	121.5(4)
C(4)-C(3)-N(1)	118.8(4)
C(27)-C(28)-C(29)	121.9(5)
C(10)-C(9)-C(14)	119.2(4)
C(10)-C(9)-N(2)	120.7(4)
C(14)-C(9)-N(2)	119.5(4)
C(28)-C(27)-C(26)	119.0(4)
C(28)-C(27)-C(32)	119.0(4)
C(26)-C(27)-C(32)	121.9(4)
C(37)-N(4)-C(38)	108.2(5)
C(37)-N(4)-Zr(1)	129.9(4)
C(38)-N(4)-Zr(1)	121.8(4)
C(9)-C(10)-C(11)	119.5(4)
C(9)-C(10)-C(4)	122.0(4)
C(11)-C(10)-C(4)	118.5(4)
C(30)-C(29)-C(28)	117.5(4)
C(30)-C(29)-C(34)	121.9(4)
C(28)-C(29)-C(34)	120.5(5)
C(7)-C(6)-C(5)	121.2(5)
C(30)-C(31)-C(26)	118.6(4)
C(30)-C(31)-C(33)	119.5(4)
C(26)-C(31)-C(33)	121.8(4)
C(17)-C(18)-C(19)	118.8(4)
C(17)-C(18)-C(23)	123.1(5)
C(19)-C(18)-C(23)	118.1(5)
C(8)-C(7)-C(6)	119.6(4)
C(17)-C(22)-C(21)	118.2(5)
C(17)-C(22)-C(24)	122.6(4)
C(21)-C(22)-C(24)	119.1(4)
C(5)-C(4)-C(3)	119.0(4)
C(5)-C(4)-C(10)	120.3(4)
C(3)-C(4)-C(10)	120.5(4)
C(13)-C(14)-C(9)	120.9(5)
C(12)-C(11)-C(10)	119.1(5)
C(12)-C(11)-C(16)	117.9(5)
C(10)-C(11)-C(16)	123.0(4)
C(6)-C(5)-C(4)	119.8(4)
C(6)-C(5)-C(15)	117.2(4)
C(4)-C(5)-C(15)	123.0(4)
C(18)-C(17)-C(22)	121.0(4)
C(18)-C(17)-C(1)	120.2(4)
C(22)-C(17)-C(1)	118.7(4)
C(29)-C(30)-C(31)	122.4(4)
C(20)-C(19)-C(18)	121.4(5)
O(2)-C(2)-N(2)	113.5(4)
O(2)-C(2)-C(26)	121.0(4)
N(2)-C(2)-C(26)	125.5(4)
O(2)-C(2)-Zr(1)	55.5(2)

N(2)-C(2)-Zr(1)	58.2(2)
C(26)-C(2)-Zr(1)	174.2(3)
C(14)-C(13)-C(12)	119.4(5)
C(13)-C(12)-C(11)	121.8(5)
C(7)-C(8)-C(3)	120.9(5)
C(20)-C(21)-C(22)	121.5(5)
C(19)-C(20)-C(21)	119.0(5)
C(19)-C(20)-C(25)	121.3(6)
C(21)-C(20)-C(25)	119.6(5)

**Table A-4** Anisotropic displacement parameters ( $\text{\AA}^2 \times 10^3$ ) for **(+)-13c**. The anisotropic displacement factor exponent takes the form:  $-2 \pi^2 [h^2 a^{*2} U_{11} + \dots + 2 h k a^* b^* U_{12}]$

	U11	U22	U33	U23	U13	U12
Zr(1)	16(1)	18(1)	12(1)	-2(1)	-2(1)	-4(1)
O(1)	24(2)	25(2)	16(2)	0(2)	-2(1)	-9(2)
O(2)	21(2)	25(2)	25(2)	-11(2)	0(2)	-6(2)
N(1)	17(2)	14(2)	16(2)	-2(2)	-1(2)	-2(2)
N(2)	14(2)	15(2)	19(2)	-6(2)	-6(2)	-2(2)
C(26)	19(2)	10(3)	19(3)	-4(2)	-4(2)	-2(2)
N(3)	22(2)	20(2)	24(2)	2(2)	-9(2)	-1(2)
N(5)	33(3)	40(3)	38(3)	0(3)	-18(2)	-4(2)
C(1)	14(2)	20(3)	20(3)	-3(2)	-6(2)	2(2)
C(3)	20(2)	10(3)	20(3)	-2(2)	-3(2)	-3(2)
C(28)	26(3)	21(3)	18(3)	2(2)	-4(2)	-5(2)
C(9)	15(2)	21(3)	14(3)	-1(2)	-1(2)	-6(2)
C(27)	19(2)	13(3)	25(3)	-4(2)	-7(2)	-2(2)
N(4)	42(3)	38(3)	15(2)	-7(2)	2(2)	-5(2)
C(10)	17(2)	21(3)	17(3)	-4(2)	1(2)	-4(2)
C(33)	34(3)	42(4)	27(3)	-17(3)	-7(2)	-13(3)
C(29)	20(2)	17(3)	26(3)	-1(2)	-2(2)	-2(2)
C(6)	43(3)	28(3)	21(3)	-8(2)	-10(2)	-9(3)
C(31)	25(3)	15(3)	21(3)	-4(2)	-9(2)	0(2)
C(18)	26(3)	16(3)	36(3)	-2(2)	-5(2)	-6(2)
C(7)	30(3)	32(3)	29(3)	-6(3)	-13(2)	-8(2)
C(22)	29(3)	23(3)	25(3)	-3(2)	1(2)	-10(2)
C(4)	19(2)	11(3)	21(3)	-7(2)	0(2)	-1(2)
C(14)	17(3)	27(3)	24(3)	-2(2)	-3(2)	-6(2)
C(11)	22(3)	25(3)	24(3)	-4(2)	4(2)	-5(2)
C(5)	25(3)	18(3)	21(3)	-6(2)	0(2)	-8(2)
C(17)	24(3)	22(3)	19(3)	5(2)	-1(2)	-11(2)
C(16)	38(3)	30(4)	39(4)	-17(3)	5(3)	0(3)
C(30)	20(2)	17(3)	36(3)	-7(2)	-11(2)	-5(2)
C(15)	36(3)	40(4)	25(3)	-10(3)	6(2)	-17(3)
C(19)	39(3)	31(4)	37(4)	-8(3)	1(3)	-10(3)
C(2)	20(2)	19(3)	14(3)	-1(2)	-7(2)	-5(2)
C(13)	19(3)	38(4)	32(3)	-4(3)	-8(2)	-4(2)
C(24)	24(3)	29(3)	44(4)	-10(3)	2(2)	-8(2)
C(12)	19(3)	30(3)	34(3)	-5(3)	0(2)	6(2)
C(36)	23(3)	25(3)	48(4)	-6(3)	-7(3)	-2(2)
C(8)	24(3)	27(3)	24(3)	-3(2)	-4(2)	-9(2)
C(32)	34(3)	39(4)	20(3)	2(3)	-11(2)	-16(3)
C(35)	37(3)	21(3)	31(3)	1(3)	-17(3)	3(2)
C(34)	32(3)	23(3)	51(4)	-11(3)	4(3)	-15(2)

C(21)	34(3)	35(4)	44(4)	-2(3)	-4(3)	-21(3)
C(20)	52(4)	28(4)	39(4)	0(3)	-6(3)	-22(3)
C(23)	31(3)	31(4)	50(4)	-9(3)	-5(3)	0(3)
C(39)	36(3)	42(4)	64(5)	17(3)	-23(3)	-13(3)
C(37)	66(4)	52(5)	28(4)	-11(3)	6(3)	-9(4)
C(25)	59(4)	44(4)	91(6)	-29(4)	-6(4)	-29(4)
C(40)	66(5)	92(6)	41(4)	-6(4)	-33(4)	-10(4)
C(38)	104(6)	56(5)	38(4)	-19(4)	10(4)	-24(4)